



## AVERTISSEMENT

Ce document est le fruit d'un long travail approuvé par le jury de soutenance et mis à disposition de l'ensemble de la communauté universitaire élargie.

Il est soumis à la propriété intellectuelle de l'auteur. Ceci implique une obligation de citation et de référencement lors de l'utilisation de ce document.

D'autre part, toute contrefaçon, plagiat, reproduction illicite encourt une poursuite pénale.

Contact : [ddoc-theses-contact@univ-lorraine.fr](mailto:ddoc-theses-contact@univ-lorraine.fr)

## LIENS

Code de la Propriété Intellectuelle. articles L 122. 4

Code de la Propriété Intellectuelle. articles L 335.2- L 335.10

[http://www.cfcopies.com/V2/leg/leg\\_droi.php](http://www.cfcopies.com/V2/leg/leg_droi.php)

<http://www.culture.gouv.fr/culture/infos-pratiques/droits/protection.htm>



UNIVERSITÉ DE LORRAINE  
GEORESSOURCES - RP2E

# THÈSE

Présentée en vue d'obtenir le grade de

**DOCTEUR DE L'UNIVERSITÉ DE LORRAINE**

spécialité “**Géosciences**”

par

**Andrey MYAGKIY**

---

## MINERALIZATION OF NICKEL IN SAPROLITIC ORE OF NEW CALEDONIA: DYNAMICS OF METAL TRANSFER AND MODELING OF COUPLED GEOCHEMICAL AND HYDRODYNAMIC PROCESSES

---

Thèse soutenue publiquement le 08/12/2017 devant le jury composé de :

|                           |  |              |
|---------------------------|--|--------------|
| Mme. CÉCILE QUANTIN       | Professeur, Université Paris-Sud               | Rapporteur   |
| M. VINCENT LAGNEAU        | Professeur, MINES ParisTech                    | Rapporteur   |
| Mme. MARTINE BUATIER      | Professeur, Université de Franche-Comté        | Examinatrice |
| M. JEAN-PAUL AMBROSI      | Chargé de recherche, CEREGE                    | Examinateur  |
| Mme. MARIE-ODILE SIMONNOT | Professeur, LRGP                               | Examinatrice |
| vM. FABRICE GOLFIER       | Maître de conférences, Université de Lorraine  | Directeur    |
| M. LAURENT TRUCHE         | Professeur, Université Grenoble Alpes          | Co-directeur |
| M. MICHEL CATHELINEAU     | Directeur de recherche, Université de Lorraine | Co-directeur |

Laboratoire GeoRessources - ENSG,  
Rue du Doyen Marcel Roubault,  
54518 VANDOEUVRE-LES-NANCY CEDEX.



# ACKNOWLEDGEMENTS

First and foremost, I would like to express my sincere gratitude to my three directors - Fabrice GOLFIER, Laurent TRUCHE and Michel CATHELINEAU for motivation, for our friendship, and for all that work we made together. You were my mentors, my guides and provided me with everything for my scientific and personal growth. I couldn't have done it without you.

I would also like to thank my jury - Cécile Quantin, Vincent Lagneau, Martine Buatier, Jean-Paul Ambrosi and Marie-Odile Simonnot for accepting to evaluate my work, for your valuable comments and suggestions, and fruitful discussion. I am very grateful to you.

I should also note that this work would not be possible without financial support of the French National Research Agency through the national program "Investissements d'avenir" with the reference ANR-10-LABX-21-01 / LABEX RESSOURCES21.

Last but not least, I would like to thank my parents, my sister and all my good friends. Words can not express how grateful I am to my mom and my dad for all their sacrifices that they have made sending me first to Moscow from a little town in the south of Russia, and then to France.

Thank you to you all!

Yours sincerely,

Andrey

February 2, 2018.



# RÉSUMÉ

DE nombreux travaux récents ont enrichi la connaissance des conditions de formations d'enrichissement en Ni des latérites développées sur roches ultrabasique (Golightly, 2010; Butt and Cluzel, 2013; Freyssinet et al., 2005; Cluzel and Vigier, 2008; Cathelineau et al., 2016b,a; Villanova-de-Benavent et al., 2014; Quesnel et al., 2017). Dans le cas de la Nouvelle Calédonie, comme dans le cas de gisements équivalents à l'échelle mondiale (Cuba, République Dominicaine, Indonésie) (Fig. 1), le modèle principal de genèse des enrichissements en Ni est basé sur le concept de développement de la latérite, où les éléments comme Si, Mg sont expulsés et lixiviés, tandis que le sol résiduel est enrichi dans tous les métaux insolubles (Fe, Al, Cr). L'enrichissement en Ni est beaucoup plus complexe à interpréter car il ne correspond pas à un enrichissement résiduel s.s., le niveau enrichi n'étant pas situé dans les latérites jaunes et rouges (soit les principaux horizons résiduels), mais dans la saprolite surmontant le bedrock.

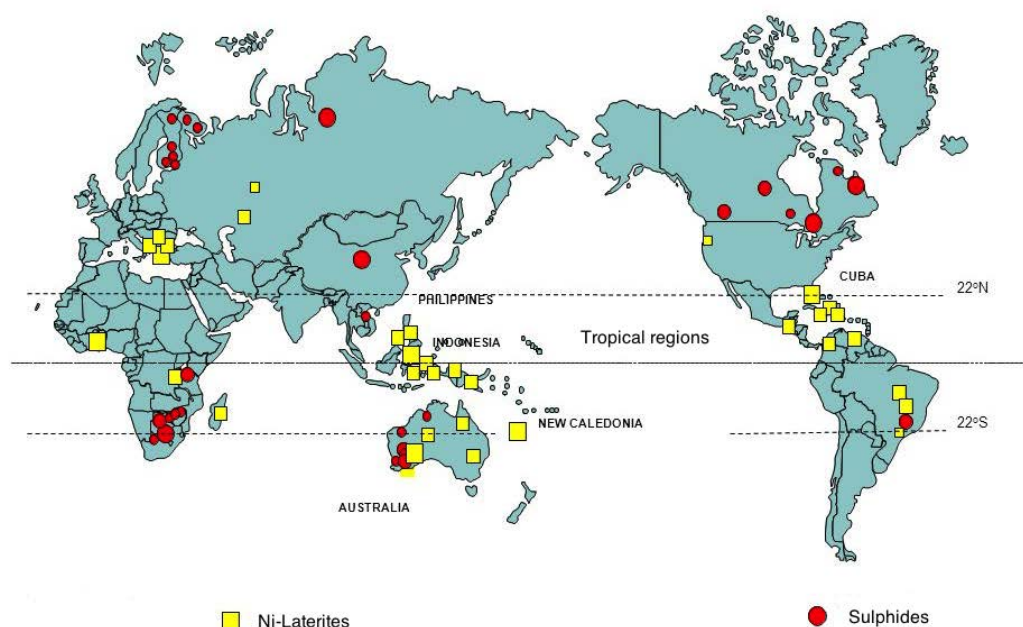


Figure 1 – *Global distribution of Ni resources (Butt, 2007). Laterite-Nickel Ore deposits are presented in Cuba, New Caledonia, Indonesia, Philippines, Burma, Vietnam, Brazil and Nickel Sulphide Ore deposits - in Canada, Russia, Australia, China, South Africa, etc.*

L'objectif principal de ce travail est de proposer et tester un modèle conceptuel qui tient

compte des observations les plus récentes des différents types de minerais. La thèse cherche à détailler le rôle relatif des paramètres physico-chimiques qui régissent les principaux processus de dissolution-reprécipitation et d'adsorption qui contrôlent les enrichissements en Ni. Il a été réalisé dans le cadre des actions de modélisation du transport - réactif mené dans le cadre du labex Ressources 21.

## CONTEXTE ET APPROCHE

Les travaux menés partent sur la modélisation du transport réactif dans le contexte de la formation d'un profil latéritique se développant sur roche ultra-basique. Un des premiers travaux publiés dans ce domaine est celui de Domenech et al (2017), mais il est restreint au rôle de l'adsorption, et de la formation des oxy-hydroxydes. Le concept des modélisations réalisées dans le cadre de la thèse est basé sur le développement: i) d'un modèle 1D puissant dont l'objectif est de traiter le comportement géochimique du Nickel au cours de l'altération progressive de la péridotite, en comparant les évolutions modélisées avec celles observées sur le terrain, et s'intéressant en particulier à la mobilité spécifique et relative des éléments en traces comme les métaux, et ii) d'un modèle 2D thermo-hydro-chimique qui donne un nouvel éclairage sur le rôle des discontinuités et les différents paramètres contrôlant l'hydrodynamique des aquifères situés au dessus du bedrock (rôle du relief, topographie de l'interface saprolite-bedrock, impact des fractures et des réseaux de discontinuités).

Les minerais en Nouvelle Calédonie peuvent se classer en deux grands types distincts : les minerais oxydés constitués essentiellement d'oxy-hydroxydes de fer, de chromites résiduelles et de faibles quantités d'argiles , et les minéraux silicates constitués principalement de silicates résiduels non encore totalement dissous (olivine , pyroxène, serpentine) et de silicates néoformés (talc-like ou kérolite, rarement de la sépiolite, des smectites de type nontronite dans certains profils particuliers). Le nickel peut être présent sous différentes formes : i) adsorbé sur des sites faibles ou forts sur la goethite, ii) incorporé dans le réseau cristallin de la goethite (Fe, Ni) O-OH, ou encore précipité dans des silicates néoformés. Les simulations ont été réalisées en utilisant le code géochimique PHREEQC et la base de données thermodynamique de LLNL (llnl.dat) , avec des calculs spécifiques réalisés afin de disposer de données sur la "garniérine", soit les silicates composés potentiellement de talc-like (série kérolite-pimélite), et localement de sépiolite. Le modèle 2D a été réalisé en utilisant une interface, nommée iCP, qui permet de coupler les processus physiques dans COMSOL avec des calculs géochimiques dans PHREEQC, ceci permettant de fusionner les capacités des deux codes dans un seul.

## RÉSULTATS

### **Modèle 1D de transport-réactif.**

Le premier modèle développé consiste en une étude détaillée de la formation des minéraux néoformés le long du profil d'altération, en particulier en fonction de la migration vers le bas du front de dissolution et d'altération des minéraux de la péridotite. Le travail a consisté à calculer et représenter : i) la formation d'une latérite sur une longue période de temps (10 Ma), ii) la mobilité des éléments et évaluer les facteurs qui contrôlent cette mobilité, iii) comparer les profils modélisés avec ceux rencontrés sur les sites naturels, iv) les processus de rétention. Le mécanisme principal de transfert puis de rétention du Nickel s'avère contrôlé par la compétition entre les processus d'adsorption et d'incorporation dans le réseau de la goethite, puis la formation des silicates nickélifères (kérolite/ sépiolite). Cette modélisation tient compte de l'ensemble des principaux processus de rétention du Nickel et démontre que la formation et l'épaississement de la zone enrichie en Ni est gouvernée par la progression du front pH. Le mécanisme principal de rétention du nickel dans la zone limonitique (latérite jaune des mineurs) est son incorporation dans le réseau de la goethite, les mécanismes d'adsorption n'étant que transitoires. Il est à noter que les travaux de lixiviation menés au CEREGE (JP Ambrosi, travaux du CNRT) confirment que le nickel est majoritairement non désorbable dans les latérites jaunes et bien incorporé dans le réseau de la goethite. Les horizons où les silicates sont entièrement dissous sont caractérisés par la présence de goethite-Ni, tandis que les niveaux où subsistent des reliques d'olivine se caractérisent par la présence de manière transitoire de Ni adsorbé et de Ni intra-cristallin. Cette distribution est aussi en accord avec les travaux EXAFS de Dublet et al (2012). Ces modélisations sont donc en accord avec les observations, et sont d'importance pour les procédés de traitement de minerais, ainsi que pour les techniques d'agromining qui doivent choisir les plantes hyper-accumulatrices les plus appropriées. De plus, la modélisation des mécanismes compétitifs d'occupation des sites de sorption de la goethite, a montré que les autres cations, en particulier le magnésium pouvait avoir un rôle non négligeable. L'adsorption du Ni est ainsi importante dans une gamme restreinte de pH autour de 8, tandis qu'à pH neutre, la compétition avec le magnésium intervient ce qui entraîne le relâchement du nickel dans les eaux porales.

### **Modèle 2D hydro-géochimique couplé avec une description réaliste du comportement hydrogéologique.**

Après l'étude détaillée des processus géochimiques à l'origine de la formation du minerai de nickel et l'identification des principaux paramètres de contrôle, le modèle géochimique a



été couplé au comportement hydrodynamique du système. Les résultats de simulation 2D sont discutés au travers d’une analyse de l’impact structurel et hydrodynamique sur les profils d’altération et les facies de minéralisation nickelifère. Une telle étude visait à proposer un nouveau modèle de minéralisation conceptuelle de la redistribution du Ni dans des environnements complexes et surélevés avec un intérêt particulier sur la compréhension des phénomènes de sur-enrichissement locaux en Ni, à savoir: i) l’augmentation induite par la topographie de la teneur en Ni dans les zones à faible relief, comme ceux décrits par Quesnel et al. (2017), ii) la précipitation de pimélite porteuse de Ni à l’intérieur des fractures, et iii) la formation de minerai concentrique de silicate nickelifère dans les réseaux de fractures. Le modèle numérique développé permet de décrire la mobilité des métaux et les réactions chimiques associées dans les milieux poreux fracturés. L’impact des fractures, de leur orientation et de leur connectivité ainsi que de la topographie générale du milieu sur la distribution des métaux a été étudié. Les résultats du modèle ont révélé un contrôle prédominant de la topographie et de la canalisations de l’écoulement sur la redistribution et la localisation future des gisements de Ni. Le nickel, tout d’abord remobilisé dans les horizons supérieurs, se concentre dans les silicates néo-formés dans le bas de la formation saprolitique. En outre, les simulations ont révélé une contribution mineure de l’horizon latéritique (Ni-oxi-hydroxydes) dans la remobilisation du Ni. Le Nickel remobilisé semble provenir principalement de la saprolite en raison de la redissolution des silicates porteurs de Ni précédemment formés et de l’olivine qui persiste encore dans cette zone. Ce comportement est expliqué par la migration latérale du front de pH au sein de la formation saprolitique qui déclenche la dissolution des silicates accompagné d’une lixiviation subséquente des composants minéralisateurs (Ni, Mg et Si) dans le sens du gradient hydraulique. L’infiltration latérale de l’eau transportant le Ni remobilisé à partir des zones telles que les hauts topographiques vers les zones de talus en aval entraîne la formation des facies de dépôts les plus riches dans cette partie inférieure du profil. Le mode de redistribution est entièrement régi par les caractéristiques topographiques locales, telles que la pente, le contact avec le substrat rocheux et la localisation des chemins d’écoulement préférentiels. Il a également été établi que la migration des composants minéralisateurs de la saprolite dans les fractures est encore renforcée par les processus de dissolution qui se produisent dans le bedrock fracturé. Ces deux processus entraînent la formation d’enrichissement exceptionnel en Ni dans la zone fracturée. Une étude complémentaire de l’impact induit par le réseau régulier de fractures nous a permis d’expliquer les processus d’altération qui se produisent dans les blocs rocheux.

Le modèle conceptuel de genèse des gisements de nickel proposé dans ce travail et visant à expliquer l’enrichissement en métaux dans les saprolites, latérites et zones fracturées du

substratum tient également compte de l'histoire «hydrothermal» à basse température liée aux stades précoces de déformation (Ni syntectonique et silicates associés). Sur la base des analyses quantitatives des échantillons de brèches trouvées dans les failles des roches ultrabasiques de Nouvelle-Calédonie ainsi que de la composition isotopique en oxygène du quartz microcristallin qui termine l'étape principale de formation de la kérolite Ni-Mg, nous en avons conclu qu'une grande partie du remplissage des fractures par ces phases silicatées nickélifères s'est formée au cours d'une série de processus de fracturation et de bréchification hydraulique. Il est supposé que la plage de température requise pour une telle formation se situe entre 50 et 90 °C (Quesnel, 2016), ce qui est en accord avec l'absence de minéraux de type sépiolite dans les fractures à kérolite-quartz. En effet, les sépiolites disparaissent complètement du diagramme de stabilité à des températures supérieures à 50 °C, excluant ainsi leur précipitation. Par conséquent, la séquence des remplissages de fractures a été interprétée comme le résultat d'une évolution du système hydrothermal en condition de moyenne à basse température et sous une pression de fluide fluctuante. Les conséquences de ces observations sont très importantes pour les modèles proposés de circulation des fluides minéralisateurs. Un tel modèle complète notre compréhension du développement des gisements néo-calédoniens qui apparaît donc comme le résultat d'une superposition complexe des processus hydrothermaux et supergènes et ne peut être interprété par simple migration gravitaire d'un front de précipitation de nickel au cours de la formation des latérites.

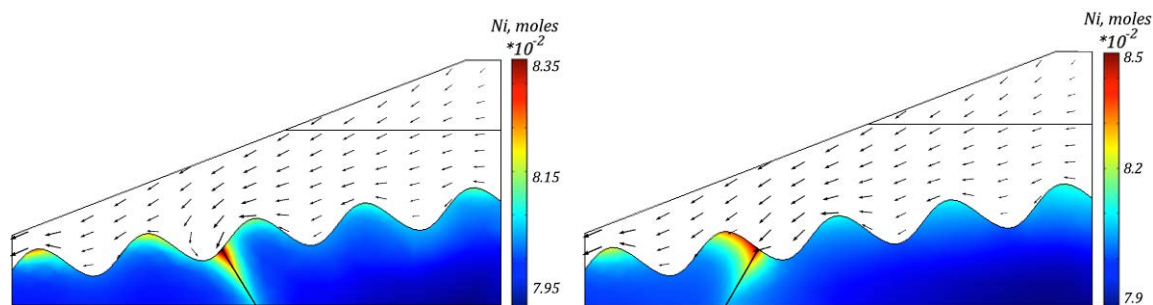


Figure 2 – *Development of secondary nickel ores within the bedrock zone with two contrasting positions of the fracture*

Les modèles présentés dans ce travail couvrent donc la formation de toutes les principales étapes de distribution des minéralisations de Ni observées en Nouvelle-Calédonie et révèlent les principales clés pour comprendre le contrôle topographique et géochimique de la mobilité des éléments traces dans un environnement ultramafique. Le modèle développé permet désormais la simulation numérique de la dynamique des métaux et des réactions chimiques dans les milieux poreux fracturés. Il fournit un éclairage nouveau sur la distribution des ressources minérales et peut être d'une grande aide dans l'industrie pour la prospection minérale future.



# CONTENTS

|  |      |
|--|------|
| RÉSUMÉ   | v    |
| CONTENTS   | xi   |
| LIST OF FIGURES  | xiii |
| INTRODUCTION   | 1    |
| 1 GEOLOGICAL CONTEXT AND FORMATION OF NI LATERITE DEPOSITS IN<br>NEW CALEDONIA   | 5    |
| 1.1 OVERVIEW . . . . .   | 6    |
| 1.2 GEOLOGICAL FORMATION . . . . .   | 7    |
| 1.2.1 Geodynamic evolution of the SW Pacific . . . . .   | 7    |
| 1.2.2 Peridotite nappe . . . . .   | 10   |
| 1.3 NICKEL LATERITE FORMATION . . . . .  | 11   |
| 1.3.1 Typical laterite profile in New Caledonia . . . . .  | 11   |
| 1.3.2 Direct laterite formation . . . . .  | 13   |
| 1.3.3 Multi-stage formation . . . . .  | 14   |
| 1.4 DEPOSIT MODEL . . . . .  | 15   |
| 1.4.1 Per-descensum formation . . . . .  | 15   |
| 1.4.2 Relations of the Deposits to Structures . . . . .  | 17   |
| 1.5 DESCRIPTION AND OBJECTIVES OF THE THESIS . . . . .   | 18   |
| 2 REACTIVE GEOCHEMICAL TRANSPORT MODEL OF THE FORMATION OF<br>NICKEL LATERITE PROFILE  | 21   |
| 2.1 INTRODUCTION . . . . .   | 22   |
| 2.2 ARTICLE 1. REVEALING THE CONDITIONS OF NI MINERALIZATION IN LAT-<br>ERITE PROFILE OF NEW CALEDONIA: INSIGHTS FROM REACTIVE GEOCHEM-<br>ICAL TRANSPORT MODELLING. . . . . | 23   |

|       |   |     |
|-------|---|-----|
| 2.3   | CONDITIONS FOR PRECIPITATION OF TALC-LIKE AND SEPIOLITE-LIKE MIN-<br>ERALS . . . . .  | 59  |
| 3     | REACTIVE TRANSPORT MODELLING APPLIED TO NI ORE DEPOSITS IN<br>NEW CALEDONIA: ROLE OF HYDRODYNAMIC FACTORS AND GEOLOGICAL<br>STRUCTURES ON NI MINERALIZATION.  | 63  |
| 3.1   | INTRODUCTION . . . . .  | 64  |
| 3.2   | MATERIALS AND METHODS . . . . .   | 66  |
| 3.2.1 | Conceptual model of Saprolitic nickel-ore formation in New Caledonia . . .  | 66  |
| 3.2.2 | Physical assumptions and equations governing hydrodynamic system . . . .  | 68  |
| 3.2.3 | Geochemical system . . . . .  | 70  |
| 3.3   | NUMERICAL MODEL AND VALIDATION . . . . .  | 72  |
| 3.4   | RESULTS AND DISCUSSION . . . . .  | 74  |
| 3.4.1 | 2D reactive transport model of saprolitic deposits formation . . . . .  | 74  |
| 3.4.2 | Impact of fractures on redistribution of ore deposits . . . . .   | 77  |
| 3.4.3 | Weathering of peridotite corestone within the set of fractures. Target-like ore   | 81  |
| 3.5   | CONCLUSIONS . . . . .   | 83  |
| 4     | CONCEPTUAL MODEL OF MULTISTAGE FRACTURE FILLING DUE TO THE<br>FLUID OVERPRESSURE. EVIDENCES OF LOW-TO-MEDIUM-TEMPERATURE<br>HYDROTHERMAL FLUID CIRCULATION DURING THE FORMATION OF THE<br>NI SILICATE VEINS | 85  |
| 4.1   | ARTICLE 3. MULTISTAGE CRACK SEAL VEIN AND HYDROTHERMAL NI EN-<br>RICHMENT IN SERPENTINIZED ULTRAMAFIC ROCKS (KONIAMBO MASSIF,<br>NEW CALEDONIA) . . . . .   | 86  |
|       | CONCLUSIONS   | 103 |
|       | BIBLIOGRAPHY  | 109 |

# LIST OF FIGURES

|     |  |    |
|-----|--|----|
| 1   | Global distribution of Ni resources (Butt, 2007). Laterite-Nickel Ore deposits are presented in Cuba, New Caledonia, Indonesia, Philippines, Burma, Vietnam, Brazil and Nickel Sulphide Ore deposits - in Canada, Russia, Australia, China, South Africa, etc. . . . . | v  |
| 2   | Development of secondary nickel ores within the bedrock zone with two contrasting positions of the fracture . . . . .  | ix |
| 3   | Global distribution of Ni resources (Butt, 2007). Laterite-Nickel Ore deposits are presented in Cuba, New Caledonia, Indonesia, Philippines, Burma, Vietnam, Brazil and Nickel Sulphide Ore deposits - in Canada, Russia, Australia, China, South Africa, etc. . . . . | 1  |
| 1.1 | Physical map of New Caledonia (From GEOATLAS.com). . . . .   | 6  |
| 1.2 | Structural map of the SW Pacific. <b>NC</b> stands for New Caledonia. (Modified from Cluzel et al., 2001). . . . .   | 8  |
| 1.3 | Geodynamic evolution model for New Caledonia from 65 Ma to 35 Ma. (Modified from Whattam et al., 2008). . . . .  | 9  |
| 1.4 | Simplified geological map of New Caledonia. Types of Ni ores and investigated mining sites.(Modified from Fritsch et al., 2016). . . . .   | 10 |
| 1.5 | Classification diagram for ultramafic rocks. Location of the two main poles of compositions corresponding to the ultramafic rocks of New Caledonia. . . . .  | 12 |
| 1.6 | Typical lateritic weathering mantle over ultramafic rocks of New Caledonia correlated with Ni ore distribution in a lateritic regolith. (Modified from Troly et al., 1979; Guilbert and Park, 1986; Trescases, 1975; Pelletier, 2003). . . . .                         | 13 |

|      |  |    |
|------|--|----|
| 1.7  | Formation and evolution of oxide and hydrous Mg silicate deposits. ( <b>A</b> ) Progressive development of a well-differentiated lateritic regolith under a seasonally humid savanna climate in an area with low relief and tectonic stability. ( <b>B</b> ) With uplift and under a similar climate, leaching and reaction/exchange of Ni yield hydrous Mg silicates. ( <b>C</b> ) The profile is modified during a change to an arid climate, with precipitation of magnesite and silica (Modified from Freyssinet et al. (2005); Butt and Cluzel (2013)). . . . . | 14 |
| 1.8  | Mineral stability for idealized mineral assemblage found in the progressive weathering of nickel laterite deposits and Ni per-descensum concentration model currently proposed by most mining geologists (e.g Pelletier, 2003). (Modified from Dublet, 2013). . . . .  | 16 |
| 1.9  | Field occurrence of ores type 1 and 2 in Koniambo and their redistribution in a profile (Modified from Cathelineau et al., 2016b). . . . .   | 17 |
| 1.10 | Schematic interpretation of lateral Ni transfer from topographic highs to the zones of its subsequent reconcentration (Modified from Quesnel et al., 2017). . . . .  | 18 |
| 2.1  | Activity diagram for secondary nickel and magnesium silicates, showing their zones of stability at 25°C. Reaction path represents gradual dissolution of 10 <sup>-1</sup> mol of olivine in 8 steps. Constructed in the Geochemist's Workbench® 11 . . . . .   | 60 |
| 2.2  | Solvi for secondary nickel and magnesium silicates, showing their zones of stability at 25°C ( <b>A-B</b> ) and higher temperatures (50–60°C) ( <b>C-D</b> ). Constructed in the Geochemist's Workbench® 11 . . . . .  | 61 |
| 3.1  | Typical laterite profile of New Caledonia with different zones developed on ultramafic rocks due to the weathering processes. (Modified from Pelletier, 2003; Ulrich, 2010) . . . . .  | 64 |
| 3.2  | <b>A</b> ) Present-day unidimensional concept of redistribution of Ni deposits in uplifted profile according to Butt and Cluzel (2013), and <b>B</b> ) Proposed conceptual 2D model with formation of different Ni mineralization hotspots after tectonic uplift of regolith . . . . .   | 67 |
| 3.3  | Simplified model used for validation of iCP results. . . . .   | 73 |
| 3.4  | Comparison of the results with iCP and PHREEQC observed at the output of the column for the 1D verification case. . . . .  | 73 |
| 3.5  | Propagation of pH front in saprolitic layer after <i>A</i> ) 50 years and <i>B</i> ) 100 years. . . . .  | 75 |
| 3.6  | Ni in solution after <i>A</i> ) 50 years and <i>B</i> ) 100 years. . . . .   | 76 |

|      |   |     |
|------|---|-----|
| 3.7  | Distribution of total Ni content (in moles) within the saprolitic zone after 500 years. . . . .   | 76  |
| 3.8  | Evolution of total Ni content within the saprolite zone after <i>A)</i> 50 years and <i>B)</i> 100 years . . . . .  | 78  |
| 3.9  | <i>A)</i> Precipitation of pimelite in the bedrock zone and in the vicinity of fracture. <i>B)</i> Dissolution of olivine within the bedrock zone . . . . .   | 79  |
| 3.10 | Precipitation of pimelite within the fracture. Data is presented along the fracture length with time . . . . .  | 80  |
| 3.11 | <i>A)</i> Field occurrences of target-like ores and <i>B)</i> Representation of regular fractures network. . . . .  | 81  |
| 3.12 | <i>A)</i> Boundary conditions of modelled representative element. <i>B)</i> Weathering of peridotite corestone within the fracture network. Olivine dissolution (in moles) after 30 years. . . . .            | 82  |
| 3.13 | Simulation results after 30 years. <i>A)</i> pH values and chemical composition of the fluid along a boulder cross-section. <i>B)</i> Secondary mineral precipitations along a boulder cross-section. . . . . | 83  |
| 4.1  | Development of secondary nickel ores within the bedrock zone after 100 years with two contrasting positions of the fracture . . . . .   | 106 |
| 4.2  | Conceptual model of fractures reopening due to the circulations of ascending fluids . . . . .   | 107 |





# INTRODUCTION

NICKEL and nickel-containing materials play a major role in our everyday lives. Offering an excellent corrosion resistance and toughness they are used almost everywhere: in a food preparation equipment, mobile phones, medical equipment, transport, buildings, power generation, coins etc. - the list is almost endless. As a result, the use of nickel is growing almost exponentially since 1950 which led to it's global production of 1.9 million metric tonnes in 2013 (according to the International Nickel Study Group). The fastest growth today is seen in the rapidly industrialising countries, especially in Asia. Nickel-containing materials are needed to modernise infrastructures, in industry and to meet the material aspirations of their populations. As it reported by the U.S. Geological Survey approximately 45% of the primary nickel consumed in 2017 went into stainless and alloy steel products, 36% into nonferrous alloys and superalloys, 7% into electroplating, and 12% into other uses (Ober, 2017).

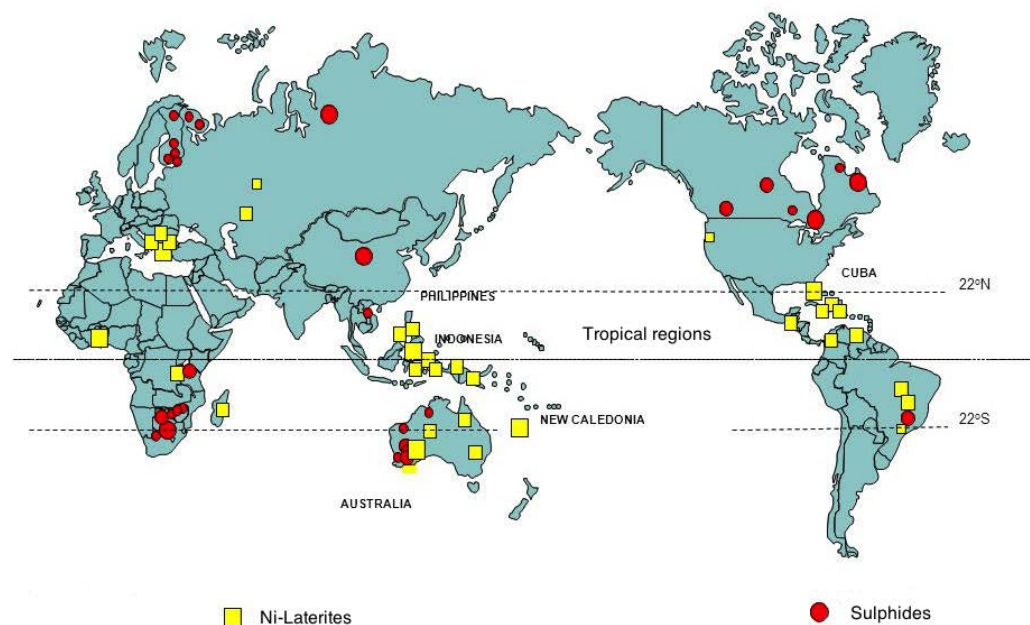


Figure 3 – *Global distribution of Ni resources (Butt, 2007). Laterite-Nickel Ore deposits are presented in Cuba, New Caledonia, Indonesia, Philippines, Burma, Vietnam, Brazil and Nickel Sulphide Ore deposits - in Canada, Russia, Australia, China, South Africa, etc.*

Economic concentrations of nickel occur in two geological environments: in magmatic sul-

phides and in laterites (Fig. 3). Sulfide ores are typically derived from volcanic or hydrothermal processes while laterite ores are formed near the surface following extensive weathering. The total known land-based resources with 1% nickel or greater contain at least 130 million tons of nickel, where laterites account for around 70% and sulfides for 30% (Mudd, 2009; Ober, 2017).

Despite the fact that the majority of nickel is contained in laterites they represent only 40% of world production. The main reason for this is the difficulty of processing nickel laterites compared to sulfides - nickel laterite operations generally require high-tonnage open-pit mining and has historically been more expensive than sulfide ores. Nevertheless, it is anticipated that increasing demand for nickel will be met largely by supply from lateritic deposits and recent metallurgical advances in processing techniques will allow more economic exploitation of these resources.

Major world nickel producers are represented by Indonesia, Russia, China, Canada, Brazil, Australia, Philippines, New Caledonia and Cuba. The table of nickel mine production reported by the United States Geological Survey (USGS) in 2017 was as follows (Tab. 1):

| <b>Mine production</b> (in metric tonnes) |             |             |
|---|-------------|-------------|
| <b>Country</b>                            | <b>2015</b> | <b>2016</b> |
| 1. Philippines                            | 554,000     | 500,000     |
| 2. Russia                                 | 269,000     | 256,000     |
| 3. Canada                                 | 235,000     | 255,000     |
| 4. Australia                              | 222,000     | 206,000     |
| 5. New Caledonia                          | 186,000     | 205,000     |
| 6. Brazil                                 | 160,000     | 142,000     |
| 7. Indonesia                              | 130,000     | 168,500     |
| 8. China                                  | 92,900      | 90,000      |
| 9. Cuba                                   | 56,400      | 56,000      |

Table 1 – *World Mine Production by the U.S. Geological Survey (Ober, 2017).*

Nickel laterite deposits are usually developed within 26 degrees of the equator with a few exceptions, such as the hydrous Mg-silicate deposit in Riddle, Oregon, and the laterite deposits in the Urals, Greece, and the Balkans (Fig. 3). The deposits are located in both presently active continental margins, in accreted terranes and obducted ophiolite sheets (New Caledonia; Moa Bay, Cuba; Falcondo, Dominican Republic) and in older accreted terranes and obducted ophiolites (Riddle, Oregon; Fifield, New South Wales; Brolga, Queensland), as well as in komatiite and cumulates that are now parts of stable cratons (Murrin Murrin, Western Australia; Goias, Brazil; Ambatovy, Madagascar) (Windley et al., 1994; Brand et al., 1998; Freyssinet et al., 2005).

Knowledge of nickeliferous laterites began with the discovery of nickel deposits in New

Caledonia by Garnier in 1863. These deposits have been mined and studied steadily since that time (Trescases, 1973, 1975; Golightly, 2010; Butt and Cluzel, 2013; Freyssinet et al., 2005; Cluzel and Vigier, 2008; Cathelineau et al., 2016b,a; Villanova-de-Benavent et al., 2014; Quesnel et al., 2017). Nonetheless, for the New Caledonian Ni laterite deposits, as for others worldwide, still a downward model of fluid circulation is classically invoked to explain the distribution of elements. Therefore, the main objective of this work is to propose and to test an integrative conceptual model for saprolitic ore formation that would in addition help to improve the exploration and our understanding of ore volumes in New Caledonia.

This manuscript consists of five chapters:

- The **first chapter** presents a brief overview of the geology of New Caledonia as well as a formation of Peridotite Nappe and its alteration through a bibliographic synthesis summarizing the current state of geological knowledge.
- The **second chapter** consists of a development of a 1D Reactive transport model with in depth understanding of Ni retention processes and the chemical parameters that govern Ni enrichment and mobility of trace elements in a laterite profile. The chapter also provides the investigations on a competitive precipitation of sepiolite/kerolite in a profile.
- The **third chapter** deals with 2D coupled model which is based on additional understanding of the hydrodynamic control on Ni laterite deposits evolution. Here we propose a new conceptual model of a laterite development influenced by the topography of a profile, as well as the modeling of remobilization of Ni from the upper zones with its subsequent redistribution at the saprolite/bedrock contact and in fractures.
- The **fourth chapter** provides a new conceptual model of formation of the Ni silicate veins in New Caledonia. This model reveals that recurrent crack and seal process in the veins may be due to the upward medium temperature fluid convection induced by hydraulic fracturing, and subsequent fluid mixing with mineral deposition.
- The **fifth chapter** presents the general conclusions and discussions, summarizing the different strengths of this study and is followed by an opening of the various perspectives of work still to be carried out in the future.



# GEOLOGICAL CONTEXT AND FORMATION OF NI LATERITE DEPOSITS IN NEW CALEDONIA

## CONTENTS

|       |   |    |
|-------|---|----|
| 1.1   | OVERVIEW . . . . .                                  | 6  |
| 1.2   | GEOLOGICAL FORMATION . . . . .                      | 7  |
| 1.2.1 | Geodynamic evolution of the SW Pacific . . . . .    | 7  |
| 1.2.2 | Peridotite nappe . . . . .                          | 10 |
| 1.3   | NICKEL LATERITE FORMATION . . . . .                 | 11 |
| 1.3.1 | Typical laterite profile in New Caledonia . . . . . | 11 |
| 1.3.2 | Direct laterite formation . . . . .                 | 13 |
| 1.3.3 | Multi-stage formation . . . . .                     | 14 |
| 1.4   | DEPOSIT MODEL . . . . .                             | 15 |
| 1.4.1 | Per-descensum formation . . . . .                   | 15 |
| 1.4.2 | Relations of the Deposits to Structures . . . . .   | 17 |
| 1.5   | DESCRIPTION AND OBJECTIVES OF THE THESIS . . . . .  | 18 |

## 1.1 OVERVIEW

New Caledonia is located in the southwest Pacific Ocean, about 1300 km east-northeast of Bundaberg ( $24^{\circ}50'S$ ,  $152^{\circ}21'E$ ), a city on the central east Australian coast and the nearest point on the Australian mainland (Fig. 1.1). The main island of New Caledonia, known as "la Grande Terre", is about 400 km long in a northwest - southeast direction and has a width of about 50 km. With a land area of  $18,576 \text{ km}^2$ , it is the third largest island in the Southwest Pacific, after Papua New Guinea and New Zealand.

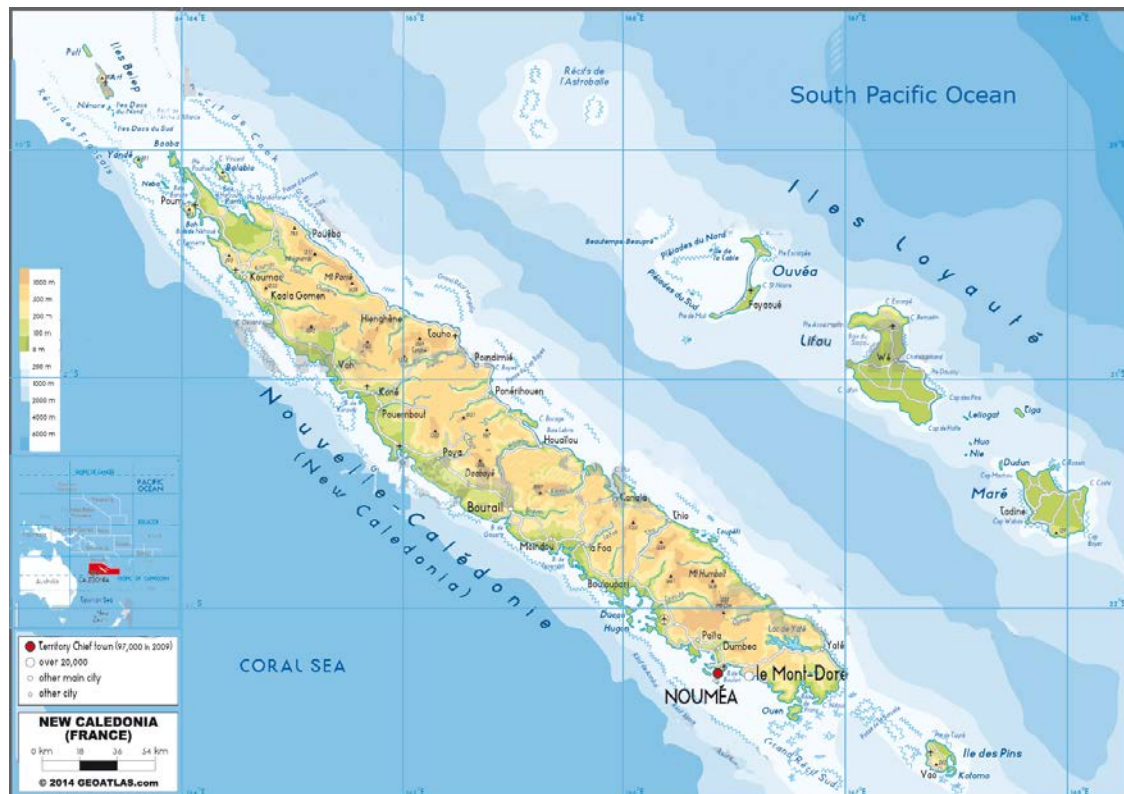


Figure 1.1 – Physical map of New Caledonia (From GEOATLAS.com).

In addition to the main island, the archipelago of New Caledonia comprises four Loyalty Islands (Ouvéa, Lifou, Tiga and Maré, located east of the Grande Terre), the Belep Islands and the Isle of Pines (to the north and to the south of the Grande Terre respectively), as well as a few more remote islands (Fig. 1.1). The island of the Grande Terre has a complex mountain relief with tablelands and peaks reaching elevations of more than 1600 meters (e.g. Mont Panié (1629 m) and Mont Humboldt (1618 m)). In the east, the relief is particularly mountainous with very steep slopes dissected by many rivers that are dipping towards the sea. In the west, the relief is characterized by the development of large coastal plains occupying the space in between the massifs. The New Caledonian barrier reef that surrounds the Grand Terre, as well as the Ile des Pins and several smaller islands, reaching

a length of 1,500 kilometres and is the second longest reef in the world, after the Australian one. On 7th July 2008 it was added to the World Heritage List of UNESCO.

Besides this, New Caledonia is well-known for its nickel deposits. Being the world's fifth largest producer, New Caledonia contains approximately one third of the world's nickel reserves (Elias, 2001). Therefore, the island represents a big interest for many mining companies that actively extract nickel from laterites nowadays. The main mining companies working here are the following: KNS, SMSP NMC, SLN, Vale Nouvelle-Calédonie, Montagnat, Ballande. The Nickel Company (SLN) is the historical minor of the island: the pyrometallurgical factory of Doniambo in Noumea has been in operation since 1910.

## 1.2 GEOLOGICAL FORMATION

### 1.2.1 Geodynamic evolution of the SW Pacific

The archipelago of New Caledonia is a part of a complex zone that consists of the oceanic and thinned continental crust basins, largely submerged continental strips, and volcanic ridges or arcs that are located between the Australian continent to the west and the broad Pacific Ocean to the east (Kroenke and Rodda, 1984; Schellart et al., 2006). New Caledonia itself represents an emerged part of the Norfolk Ridge (Fig. 1.2), which bears the Grande Terre to the north and connects southwards to the landmass of New Zealand (Klingelhoefer et al., 2007).



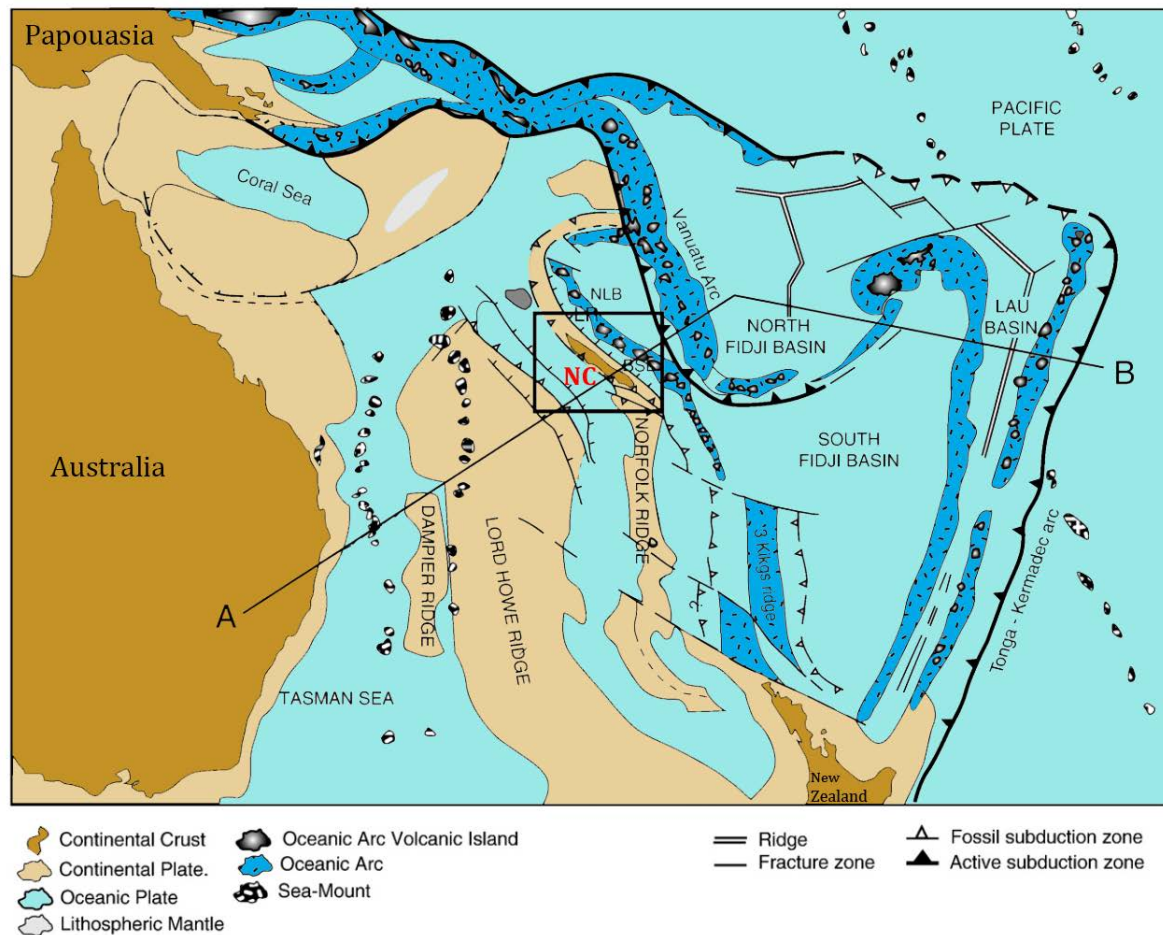


Figure 1.2 – Structural map of the SW Pacific. **NC** stands for New Caledonia. (Modified from Cluzel et al., 2001).

The complex assemblage of units on the island displays a tectonic history of the region that extends from the Permian to the Eocene. The current geodynamic model for southwestern Pacific evolution during the Upper Cretaceous to Eocene period suggests that the ophiolite was formed between 83 Ma with the opening of the South Loyalty Basin and its subsequent closing at 34 Ma (Fig. 1.3). From around 82 to 52 Ma, subduction was primarily accomplished by the east and northeast-directed rollback of the Pacific slab, accommodating the opening of the New Caledonia, South Loyalty, Coral Sea and Pocklington backarc basins and partly accommodating the spreading in the Tasman Sea (Schellart et al., 2006). The period of convergence was initiated at around 55 Ma, possibly due to a change in the relative movement between the Pacific and Australian plates (Schellart et al., 2006), leading to the gradual closure of the South Loyalty basin (Fig. 1.3 b and c). The evolution of the subduction has led to the formation of the arc of the Loyalty (Cluzel et al., 2001). The South Loyalty and Pocklington backarc basins were subducted in the Eocene to earliest Miocene along the newly formed New Caledonia and Pocklington subduction zones.

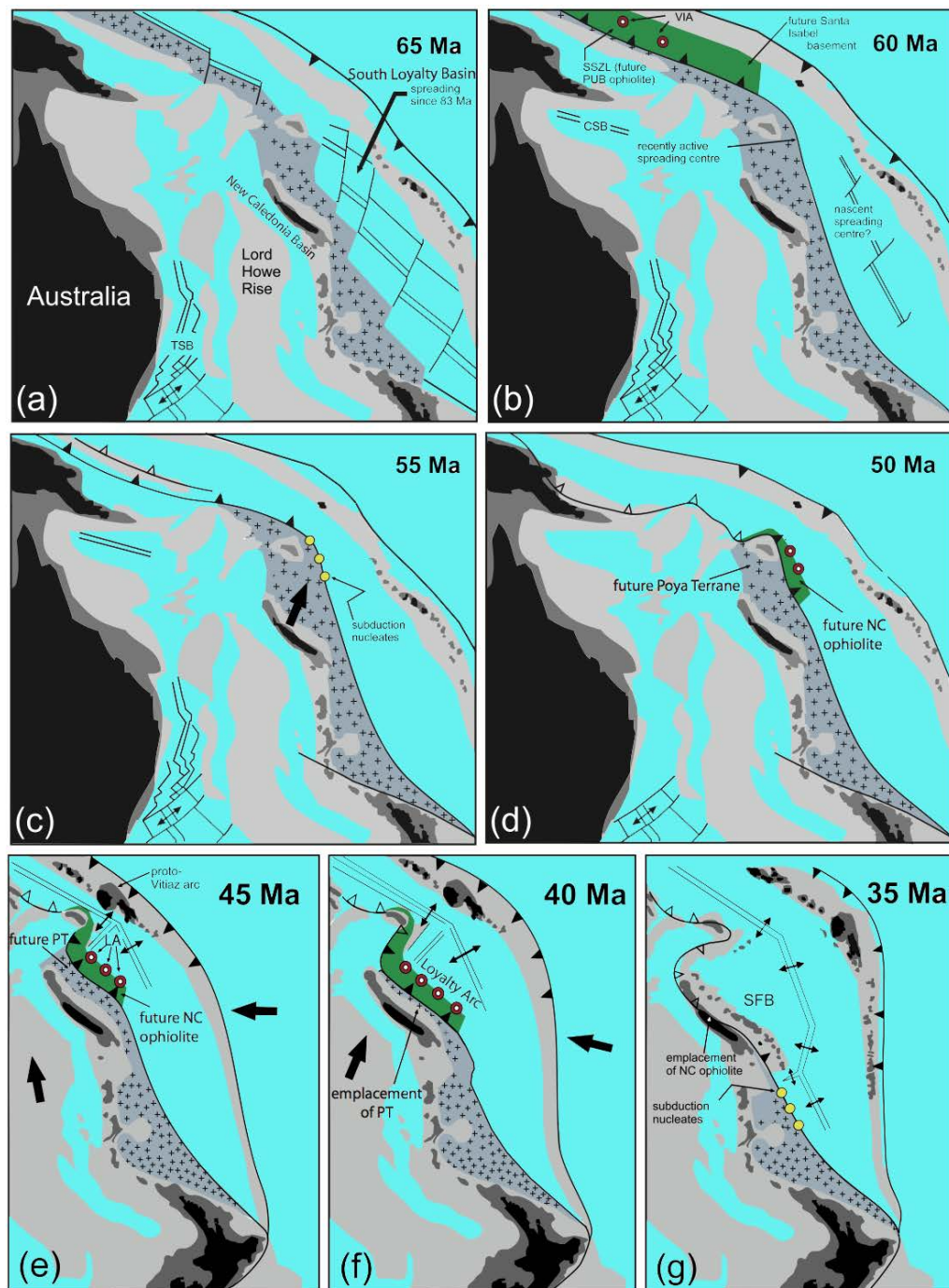


Figure 1.3 – Geodynamic evolution model for New Caledonia from 65 Ma to 35 Ma. (Modified from Whattam et al., 2008).

During the Eocene period, the continental crust in the New Caledonia area was tectonically active, being in collision with the Loyalty Islands arc, and obduction at this time gradually placed a layer of oceanic crust over the submerged continental crust (Fig. 1.3 d-e-f-g). Therefore, the ultramafic rocks in New Caledonia are thought to be oceanic lithosphere of the Loyalty Basin that was obducted at the end of the Late Eocene when the Loyalty arc collided with the Norfolk continental ridge (Collot and Missègue, 1986; Aitchison et al., 1995; Cluzel et al., 2001). New Caledonia itself emerged during an Oligocene lithosphere extension

phase, uplifting with this cover of lithospheric ultramafic rocks (Paris, 1981; Aitchison et al., 1995; Cluzel et al., 2001; Crawford et al., 2003; Schellart et al., 2006).

### 1.2.2 Peridotite nappe

Thanks to the obduction process, the ultramafic rocks extensively outcrop all over the New Caledonia nowadays and cover about 25% of the main island (Fig. 1.4). Being a mother rock for nickel, the peridotite nappe (Avias, 1967) is a fundamental element in the landscape, geology and economy of New Caledonia.

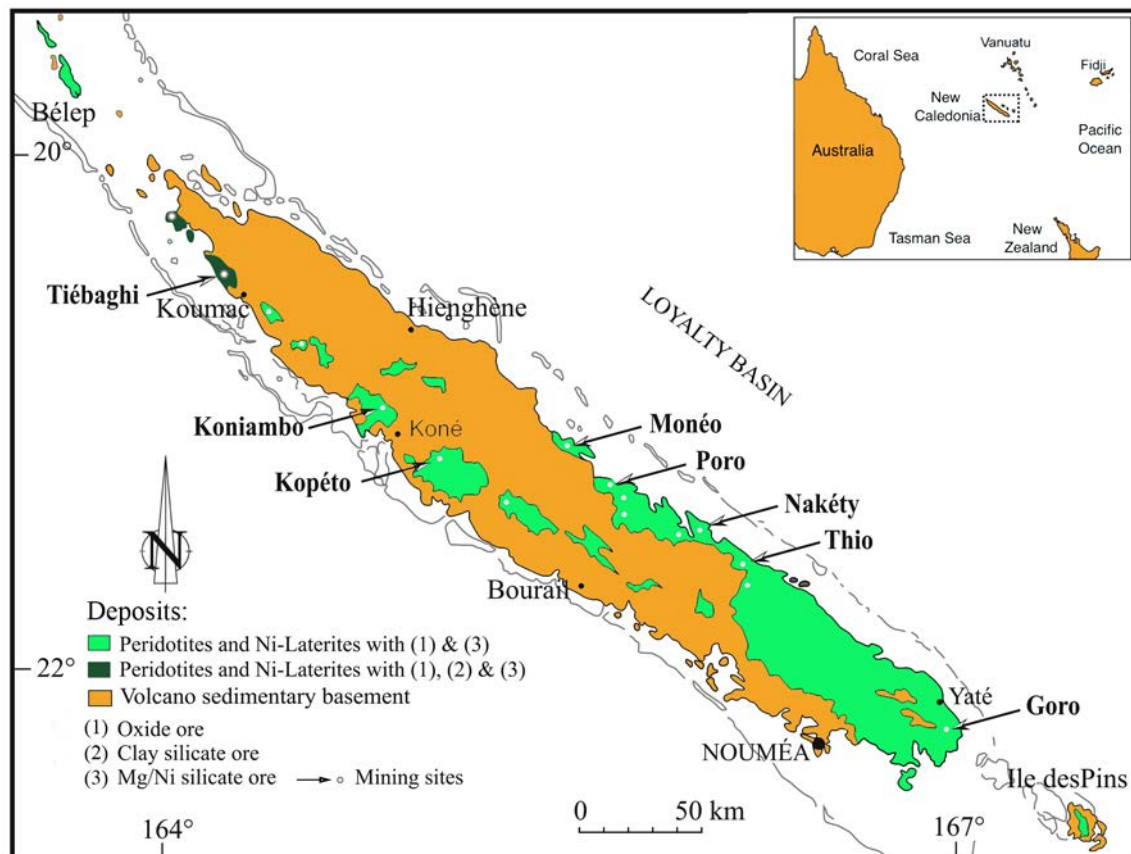


Figure 1.4 – Simplified geological map of New Caledonia. Types of Ni ores and investigated mining sites. (Modified from Fritsch et al., 2016).

The largest continuous massif (the Massif du Sud) occurs in the south of the island. In the Massif du Sud, the thickness of the nappe is at least 1.5 km and may reach 3.5 km (Guillon, 1975). Some smaller isolated klippen along the west coast of the Grande Terre could represent the remains of a once single unit detached from the front of the nappe and are connected to submarine outcrops that extend approximately 300 km north of the island (Collot and Missègue, 1986). Most of the peridotitic volume is extremely fractured (Leguere, 1976; Cluzel and Vigier, 2008) and has a variable but moderate degree of serpentinization (Orloff, 1968).

Due to these two major tectonic events, namely a late Jurassic to Early Cretaceous tectonic collage (Paris, 1981; Meffre, 1995; Aitchison et al., 1998) and a Late Eocene subduction/collision that resulted in the emplacement at the Latest Eocene (38-34 Ma) of a large ophiolitic nappe (Fig. 1.3 g) (Avias, 1967; Paris, 1981; Aitchison et al., 1995; Cluzel et al., 1994, 2001), the island is currently composed of a series of various terranes that can be divided as follows:

- A. composite terranes assembled during a period of convergence from Late Carboniferous to Early Cretaceous (the Late Cretaceous cycle, 300 - 100 Ma).
- B. units emplaced after the Late Cretaceous and before the Miocene (the New Caledonian cycle, 100 - 24 Ma) in which are distinguished:
  - a sedimentary cover deposited in a Late Cretaceous to Paleocene rift or extensive environment, followed in the Eocene by a change to a convergent depositional environment.
  - ophiolitic units obducted at the end of the Late Eocene.
- C. marine and continental post-obduction units (the Miocene to present cycle).

## 1.3 NICKEL LATERITE FORMATION

### 1.3.1 Typical laterite profile in New Caledonia

The nickel ores in New Caledonia were formed during the Neogene (Chevillotte et al., 2006) by tropical weathering of the large ultramafic allochthon - Peridotite nappe (Avias, 1967). These peridotites are mostly represented by harzburgites and minor dunites (Fig. 1.5), except in the northernmost klippe where lherzolites dominate (Ulrich, 2010). The nickel during its formation is principally derived from forsteritic olivine ( $>Fo_{75}$ ), which is highly unstable at earth surface conditions and commonly contains 0.16-0.40% Ni.



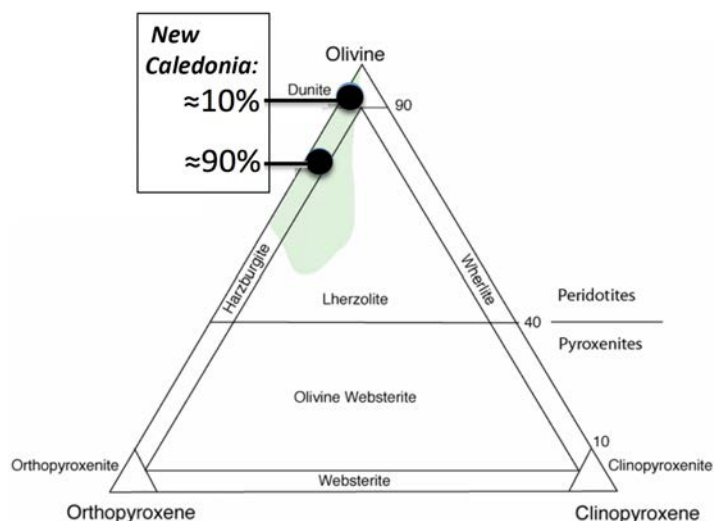


Figure 1.5 – *Classification diagram for ultramafic rocks. Location of the two main poles of compositions corresponding to the ultramafic rocks of New Caledonia.*

Under the exposure to aerial conditions, the peridotites have been a subject to intense weathering which has led to the development of thick Ni-rich lateritic soil horizons up to about 30 m thick (Trescases, 1973, 1975; Latham, 1986) and relict lateritic landsurfaces (Chevillotte et al., 2006). According to calculations of Thorne et al. (2012) Ni laterites develop where rainfall exceeds 1000 mm/y and mean monthly temperatures range between 22 – 31°C (summer) and 15 – 27°C (winter). Tectonics, weathering and erosion have shaped the morphology of the ultramafic massifs of New Caledonia, which are either explored or mined for their saprolitic and lateritic deposits. Leaching of the peridotites by downward infiltrating meteoric waters has resulted in a redistribution of elements, leading to removal of the most soluble ones (Mg, Si) and concentration of the least soluble (Fe, Ni, Mn, Co, Al, Cr) (Brand et al., 1998). As a consequence of such a redistribution four main horizons are formed (Trescases, 1975; Nahon and Tardy, 1992; Anand and Paine, 2002) (Fig. 1.6). At the base, the peridotite is partially weathered leading to the formation of a coarse saprolite; in this layer, Ni is often associated with residual serpentine, amorphous Fe and Mn-oxyhydroxides (asbolane), neoformed smectite (in poorly-drained slightly reducing conditions) and the neoformed green mixture of silicates named "garnierite" (Trescases, 1975). "Garnierite" was initially the name of a single mineral species - a green enigmatic rock, discovered in New Caledonia by a French geologist Jules Garnier on the banks of the Dumbéa river. Nonetheless, later it was proved to be a mixture of different fine - grained Ni-Mg phyllosilicates, mainly the kerolite-pimelite solid solution series, also called talc-like, as well as sepiolite and Ni-serpentine, also called serpentine-like (e.g. Faust, 1966; Brindley and Hang, 1973; Springer, 1974; Brindley, 1978). This Ni ore is the most valuable for mining industry as locally can grade over 20 wt% of Ni (Pelletier, 2003; Cathelineau et al., 2015).

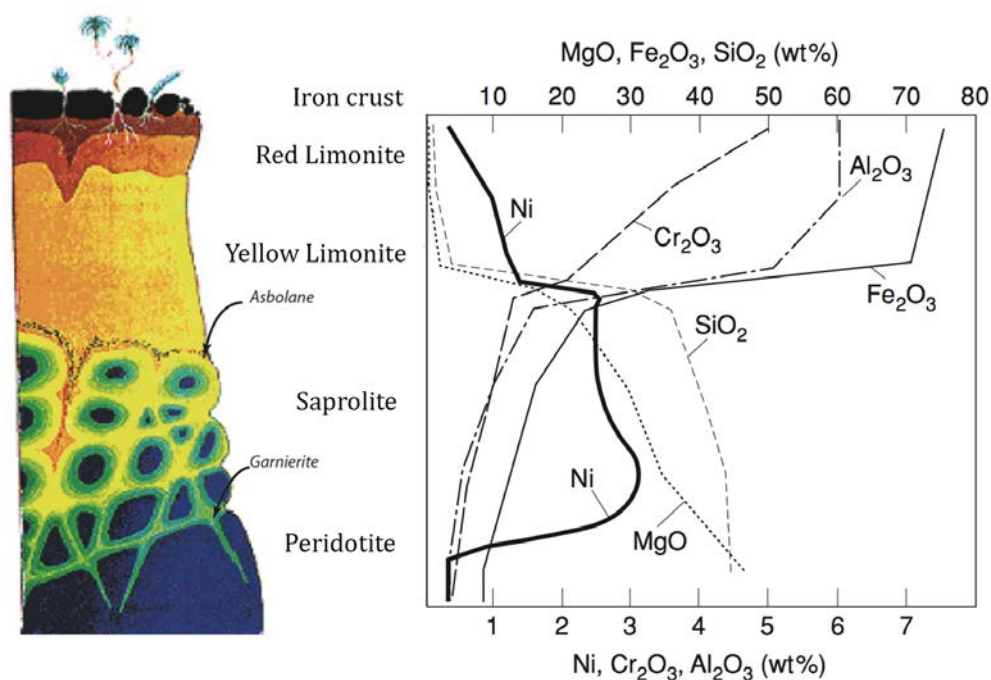


Figure 1.6 – Typical lateritic weathering mantle over ultramafic rocks of New Caledonia correlated with Ni ore distribution in a lateritic regolith. (Modified from Troly et al., 1979; Guilbert and Park, 1986; Trescases, 1975; Pelletier, 2003).

Above, silicate minerals are completely dissolved in the fine yellow limonite overlain by the reddish zone, both being mainly composed of Fe-oxyhydroxides. At the top, the soft nodular ferruginous horizon and the ferricrete cap the profile composed of goethite and hematite. Transition between the saprolite and limonite horizons is marked by a sharp increase in MgO and SiO<sub>2</sub> content and, consequently, by drastic change in mineralogy. Lower Ni concentrations are present at the top of the limonite zone, throughout which they are increasing and peaking in the saprolite zone (Fig. 1.6). Various classification schemes exist for Ni laterites, based on features such as alteration of the host rock, climate, drainage, geomorphological history etc. (e.g. Butt, 1975; Alcock, 1988). However, the most common scheme is based on the dominant Ni-bearing mineralogy and according to this three categories of Ni-ores have been distinguished worldwide (Brand et al., 1998): *oxide ores*, (Fe and Mn oxides, with mean grades 1.0 - 1.6 wt% Ni), *clay silicate* (smectites, e.g., nontronite, 1.0 - 1.5 wt% Ni) and *hydrous silicate* (altered serpentine, “garnierite”, 1.5 - 2.5 wt% Ni).

### 1.3.2 Direct laterite formation

The initial stages of formation for most deposits was lateritization under dominantly humid savanna climates, with high, seasonally fluctuating, water-tables and low erosion rates (Fig. 1.7 A). In free draining environments Mg and Si are strongly leached, with a total mass loss of up to 70%. In contrast, Ni, released by the hydrolysis of olivine or serpentinized olivine,

is largely retained, hosted by goethite as low grade oxide deposits. Higher grades, to over 1.5 wt% Ni are observed in the lower saprolite due to absolute enrichment where Ni form secondary hydrous Mg silicates, or exchange for Mg in serpentine.

### 1.3.3 Multi-stage formation

The richest deposits (>3 wt% Ni) formed where the regoliths were uplifted and Ni leached downwards due to redissolution of previously formed minerals in laterite and saprolite to concentrate in neoformed silicates deeper in a profile. Therefore, tectonic uplift has played an important role in the formation of some deposits in areas of originally low relief by rejuvenating the topography and lowering previously high water-tables. In New Caledonia, the stepped land surfaces indicate that lateritic weathering initially occurred on a landscape of low to moderate relief in the Lower Oligocene and continued as these surfaces were uplifted and partially dissected (Chevillotte et al., 2006; Sevin et al., 2012). The latter process has formed the high grade ores of New Caledonia (Fig. 1.7 B). Where there has been no uplift, but a change to more arid climates (e.g., in much of Australia), further development of Ni laterites is largely terminated and profiles are characterized by precipitation of secondary carbonates and/or silica (Fig. 1.7 C).

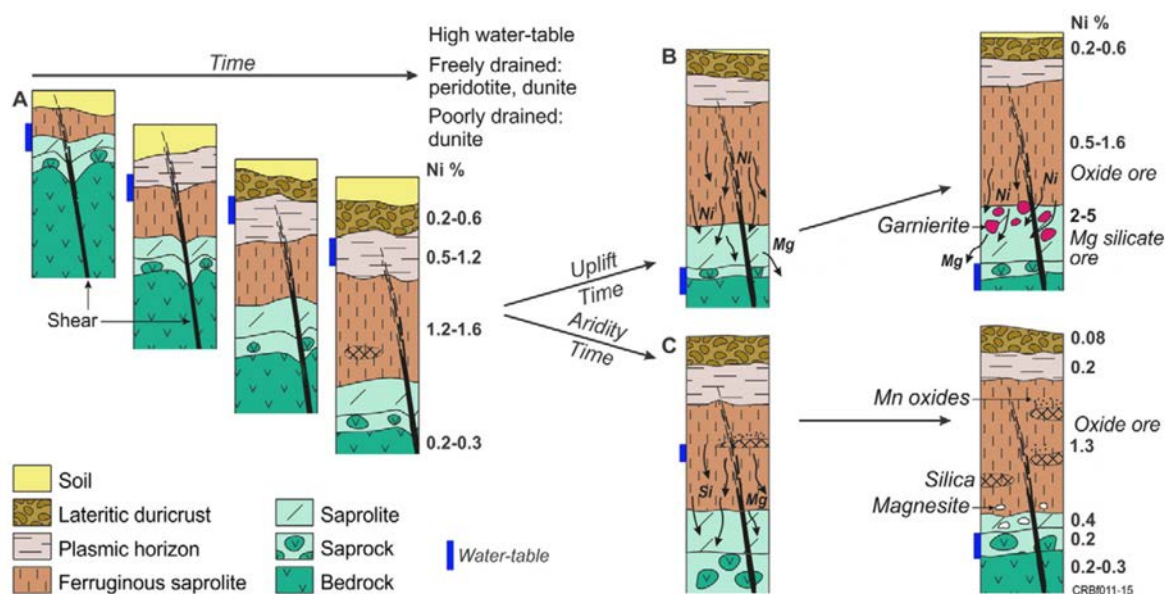


Figure 1.7 – Formation and evolution of oxide and hydrous Mg silicate deposits. (A) Progressive development of a well-differentiated lateritic regolith under a seasonally humid savanna climate in an area with low relief and tectonic stability. (B) With uplift and under a similar climate, leaching and reaction/exchange of Ni yield hydrous Mg silicates. (C) The profile is modified during a change to an arid climate, with precipitation of magnesite and silica (Modified from Freyssinet et al. (2005); Butt and Cluzel (2013)).

## 1.4 DEPOSIT MODEL

### 1.4.1 Per-descensum formation

For the New Caledonian Ni laterite deposits, as well as for other laterites worldwide, a model of downward fluid circulation is classically applied to explain the distribution of elements and geometry of the lateritic profiles (e.g. Avias, 1969; Trescases, 1975). This model is based on general observations of the vertical weathered profiles showing an increase in Ni concentrations from the top to the bottom of the lateritic regoliths and developed ferruginous residual zone where Si, Mg, and Ni are leached (Fig. 1.6). The process that is generally proposed to interpret the distribution of nickel comprises (i) progressive release of the elements during dissolution of the primary silicates of parent rock and (ii) a per-descensum migration of these elements in a soluble form, followed by trapping of Ni in adsorbed or precipitated form by underlying rock. The most soluble minerals, olivine and pyroxene, should remain in the freshest part of the profile, while the least soluble goethite constitutes its most developed part (Fig. 1.8).

The export of silica and nickel appears to happen on a short distance. Leached nickel is reincorporated into goethite and garnierite veins, and silica is reincorporated into both - garnierite and silica veins within the saprolitic level. The magnesium mobility is more problematic. Indeed, given the high intensity of its leaching the erratic occurrences of garnierite are not sufficient to explain the fate of the whole leached magnesium. In New Caledonia it is found in a form of veins at the basis of the peridotite nappe as well as in the form of nodules in a soil (Quesnel et al., 2015). It is still not understood whether this magnesite is a by-product of supergene alteration or its formation is governed by other processes.



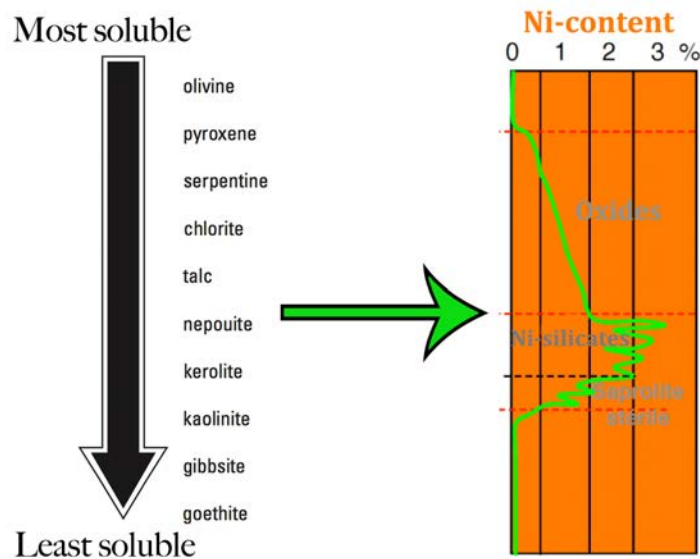


Figure 1.8 – Mineral stability for idealized mineral assemblage found in the progressive weathering of nickel laterite deposits and Ni per-descensum concentration model currently proposed by most mining geologists (e.g Pelletier, 2003). (Modified from Dublet, 2013).

Although recognized by most of the mining geologists, the per-descensum model raises many unresolved questions. For instance, recent mineralogical and structural observations of New Caledonian fields revealed a lot of different types of heterogeneities in Ni ore distributions suggesting that the conditions of fluid circulations in lateritic profiles were more complex than simple downward percolation of meteoric water. The main evidences of this in the literature are the following:

- low-temperature hydrothermal conditions during the formation of the silica veins, frequently associated with garnierites (Quesnel et al., 2016; Fritsch et al., 2016).
- hydraulic brecciation due to the upward medium temperature fluid convection in some of the garnierite fractures (Cathelineau et al., 2016a)
- concentric zonation of Ni-bearing silicates, also called the "target-like ore" exhibited in the saprolite zone (Cathelineau et al., 2016b).
- syntectonic formation of garnierite veins which means that tectonic events occurred during the formation of Ni-rich supergene material (Cluzel and Vigier, 2008; Villanova-de-Benavent et al., 2014).

Moreover, geological observations showing that Ni-rich areas are basically not spatially associated to the main lateritic body (Avias, 1969; Trescases, 1975; Golightly, 1981, 2010; Quesnel et al., 2017) suggest that formation of the Ni laterite ore deposits has to be regarded at least as 2D process, taking into account lateral Ni mobility.

### 1.4.2 Relations of the Deposits to Structures

Geological structures, as well as fractures and faults, can play a key role in the development of Ni laterite deposits. Indeed, the degree of permeability of the parent material together with hydraulic heads are being defining factors in directing the cations and anions released due to hydrolysis of initial phase-olivine, or the secondary precipitating minerals. The process of weathering itself proceeds more rapidly in fractured zones. Fluid follows fractures and complexities of the cracked protolith along a path of least resistance causing enrichment along fissures, settling of boulders and rim enrichment of the protolith fragments (Norton, 1973; De Vletter, 1955, 1978). Moreover, it causes highly irregular boundaries between the weathering layers. The tectonic trends also constitute preferential drainage-axes and are the seat of the most important absolute accumulations, such as garnierites (e.g Trescases, 1975; Cluzel and Vigier, 2008).

Up-to-date mineralogical observations of Koniambo massif revealed two main types of local mineralizing distributions of Ni silicate ore that occur in the saprolite level and formed under the tight structural control. The first (type 1) is represented by mineralized fractures with kerolite(talc-like) infillings of cm to decm width and typically correspond to those described elsewhere in New Caledonia (Fig. 1.9). This infillings occur in the sets of discontinuities. The second (type 2) is shown by concentric zonation of Ni-bearing silicates, green (pimelite) and white (Mg-kerolite) coatings in "target-like" joints that occur always close to the type 1 (Cathelineau et al., 2016b) (Fig. 1.9).

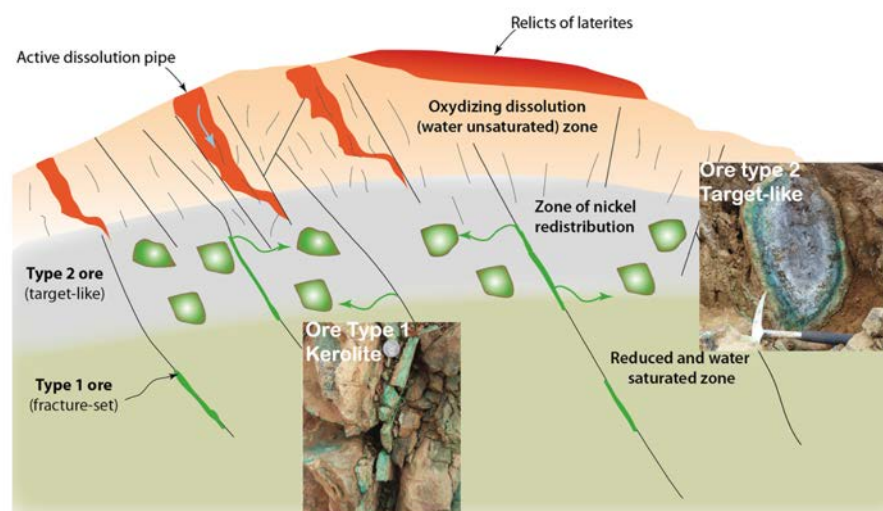


Figure 1.9 – *Field occurrence of ores type 1 and 2 in Koniambo and their redistribution in a profile (Modified from Cathelineau et al., 2016b).*

Last but not least, the heterogeneities of mineralizing distributions could appear in a

profile due to the lateral transfer of metals caused by the topographic differences. In this case the elements are moving downgradient in the landscape until being trapped and reconcentrated (Fig. 1.10). The latter is especially marked by differently rich in Ni saprolitic zones belonging to high and low topographic elevations (Quesnel et al., 2017). Based on the modelling of drill core data in Koniambo massif of New Caledonia it was found that at the top of each massif of peridotites the laterites are well developed with relatively low Ni content in underlying saprolite. In contrast, almost no laterite is found along the steep slopes or in the valleys but higher Ni content is present in saprolites associated with these parts. Quesnel et al. (2017) proposed that nickel-bearing material could have been laterally transferred from topographic highs to downstream slope areas, either by successive mechanical transport of reworked laterite material or by chemical species transport.

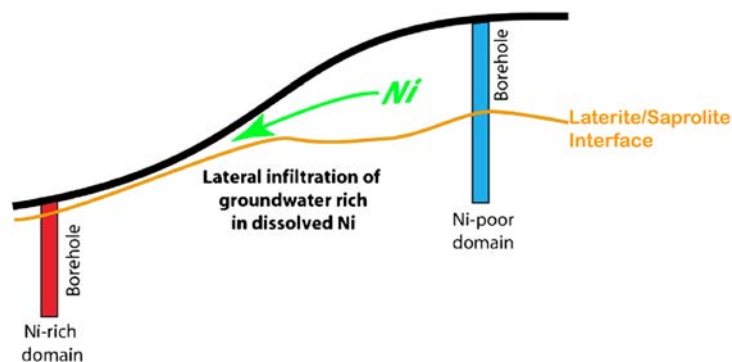


Figure 1.10 – *Schematic interpretation of lateral Ni transfer from topographic highs to the zones of its subsequent reconcentration (Modified from Quesnel et al., 2017).*

Thus, to conclude, lateritization and Ni mineralisation should not be considered as resulting from a strictly vertical progression of the alteration front, but must involve more complex processes. In this way the analysis of the structural and hydrodynamic influence on Ni mineralizing distributions appear to be essential for better understanding the laterite formation and better resource management.

## 1.5 DESCRIPTION AND OBJECTIVES OF THE THESIS

As we have seen, metalliferous laterite deposits are mineralogically complex, discontinuous, and often have heterogeneously spread Ni enrichments due to availability of preferential pathways and geomorphological influence. Some deposits are subsequently mechanically weathered, redeposited, reconcentrated, and possibly covered by new sediment (Lelong et al., 1976; Golightly, 1981). The lack of Ni-grade distribution maps in New Caledonia and poor understanding of factors controlling laterite formation leads to the current extraction issues and production of low-grade ore deposits. Similar extracted ores show huge variety in Ni grade -

up to one order of magnitude (Eramet company, discussion), making this way unpredictable the amount of Ni production. Moreover, most of the Ni ores that will be discovered in the near future will certainly contain valuable elements in very low grades, typically 1 % or less and, thus, require improvements in resource management. This issue becomes particularly important in consequence of current crisis state and decline in production prices.

Present study aims to contribute to a better understanding of parameters governing the behaviour of Ni mineralization during the formation of lateritic profiles. Innovative aspects of this work consist in testing new concepts of ore genesis to explain metal enrichment in saprolites, laterites, and within fractured bedrock. Revealing the conditions for Ni mineralization is essential for better management of the resources and requires the use of modern modelling techniques. Application of reactive transport models to ultramafic environments was firstly performed in 2017 (Domènech et al., 2017) but is very restricted being mostly focused on understanding of the role of adsorption in a formation of oxide deposits. Furthermore, the richest deposits represented by local mineralizing distributions require more complex models coupled with relevant hydrodynamics. Therefore, the concept of the present work is based on the development of i) a powerful 1D model with particular emphasis on Ni geochemical behavior during ophiolite weathering, its comparison with in situ observations, and detailed understanding of trace elements mobility, and ii) 2D coupled Hydro-Chemical model that would additionally provide new insight into the structural and hydrodynamic control of the formation (topographic features, including redistribution on the slopes and within the fractures) and will help to put forward new genetic concepts that will help improve the exploration and our understanding of ore volumes in New Caledonia.



# REACTIVE GEOCHEMICAL TRANSPORT

## MODEL OF THE FORMATION OF NICKEL LATERITE PROFILE

2

### CONTENTS

|     |  |    |
|-----|--|----|
| 2.1 | INTRODUCTION . . . . .   | 22 |
| 2.2 | ARTICLE 1. REVEALING THE CONDITIONS OF NI MINERALIZATION IN LAT-<br>ERITE PROFILE OF NEW CALEDONIA: INSIGHTS FROM REACTIVE GEOCHEM-<br>ICAL TRANSPORT MODELLING. . . . . | 23 |
| 2.3 | CONDITIONS FOR PRECIPITATION OF TALC-LIKE AND SEPIOLITE-LIKE MIN-<br>ERALS . . . . .   | 59 |

## 2.1 INTRODUCTION

For a proper understanding of laterite formation we must focus on the chemical reactions between the parent rocks and the infiltrated rain water. These reactions are above all controlled by the mineral composition of the rocks, their physical properties that favour the access of water and amount of annual rain precipitation. The second relevant factor for the formation of laterites are the properties of the reacting water (dissolved constituents, temperature, acidity pH, redox potential Eh) which are themselves controlled by the climate, vegetation and the morphology of the landscape.

The New Caledonian climate is subtropical, characterised by a hot and wet cyclonic season from December to April and a temperate, drier season from May to November. Trade-wind direction and topography induce large variations in the rainfall, over 4000 mm/y in the eastern windward side and less than 1000 mm/y in the western coastal flats. In such a conditions intense weathering of ultramafic rocks may lead to nickel enrichment. Laterisation of primary rock (olivine), containing relatively small amount of Ni ( 0.4 wt.% NiO), is altered to Ni-enriched secondary phases, represented principally by oxide and silicate deposits. It happens due to the dissolution of mineral components of the protolith and subsequent leaching of soluble elements (Mg, Si and Ni) that eventually redistributed in depth and over time depending on their mobility. Understanding the chemical factors that govern the formation of laterite and Ni enrichment is essential and requires development of a reactive transport model that takes into account all major retention processes in a profile.

Current chapter is based on the research article entitled "Revealing the conditions of Ni mineralization in laterite profile of New Caledonia: insights from reactive geochemical transport modelling", published in Chemical Geology. Here we propose a 1D numerical modelling of the development of a nickel laterite profile. Such a regolith formation from ultramafic bedrock was not yet modelled and gives new profound insights into the Ni vertical mobility, its retention processes in a soil profile and relative enrichment, that are still poorly studied. Particular emphasis in this research paper was made on the detailed understanding of Ni redistribution as a function of time and depth triggered by Ni-bearing silicate precipitation (i.e. garnierite) and by sorption or recrystallization process with goethite. Our long-term simulations (10 Ma) clearly demonstrate that the Ni enrichment and thickening of iron-rich zone are governed by the vertical progression of the pH front. Nickel in limonite zone is mostly substituted for iron and may not be explained by adsorption process, which is additionally influenced by competition with other elements along with Ni for sorption sites. To account for this, the modelling of Ni co-precipitation with goethite was applied. Such a model

appears to be of importance in attempt of explanation Ni mineralization processes, revealing the main keys to understanding the trace elements mobility in ultramafic environment.

The work outline for 1D model is represented by: i) long term (10 Ma) simulation of nickel laterite formation and evolution, ii) analysis of mobility of the elements and understanding its controlling factors, iii) comparison of modelled and in situ Ni enrichment profile and analysis of nickel distribution in between different retention processes, iv) modelling and in depth understanding of these retention processes.

## 2.2 ARTICLE 1. REVEALING THE CONDITIONS OF NI MINERALIZATION IN LATERITE PROFILE OF NEW CALEDONIA: INSIGHTS FROM REACTIVE GEOCHEMICAL TRANSPORT MODELLING.



# Revealing the conditions of Ni mineralization in the laterite profiles of New Caledonia: insights from reactive geochemical transport modelling

Andrey Myagkiy<sup>a</sup>, Laurent Truche<sup>a,b</sup>, Michel Cathelineau<sup>a</sup>, Fabrice Golfier<sup>a</sup>

<sup>a</sup>*GeoRessources Lab., UMR 7359 of CNRS, CREGU, University of Lorraine, F-54518 Vandoeuvre-Lès-Nancy Cedex, France.*

<sup>b</sup>*ISTerre, UMR 5275 of CNRS, University of Grenoble Alpes, F-38041 Grenoble Cedex 9, France.*

---

## Abstract

New Caledonia is one of the world's largest nickel laterite deposits that form from intense chemical and mechanical weathering of a peridotite bedrock. As a result of such a weathering process a subsequent downward migration of Si, Mg and Ni takes place, which eventually leads to redistribution of the elements in depth and over time depending on their mobility. Being released from ultramafic parent rock to groundwater, the mobility of nickel is to a great extent controlled by sorption, substitution and dissolution/precipitation processes. Therefore, the final profile of nickel enrichment is the result of the superposition of these possible fates of nickel. The way how Ni is redistributed in between them represents and defines its mineralization in laterite. Knowledge of these processes along with factors, controlling them appears to be a key to detailed understanding of laterite formation. In this study a numerical model, which solves the reaction-transport differential equations, is used to simulate the formation of laterite profile from ultramafic bedrock with particular emphasis on modelled Ni enrichment curve, its comparison with in situ observations, and detailed understanding of trace elements mobility. Since nickel deposits in New Caledonia is characterized by oxide and hydrous Mg silicate ores, three different concurrent fates of Ni deposition in a profile were taken into account in the modelling: i) Ni in a goethite crystal lattice, ii) Ni sorbed on weak and strong goethite sorption sites, and iii) Ni precipitated with silicates (garnierite). Simulations were performed using PHREEQC associated with llnl.dat thermodynamic database that has been edited in order to account garnierite minerals used in the

calculations. The work outline is represented by: i) long term (10 Ma) simulation of nickel laterite formation and evolution, ii) analysis of mobility of the elements and understanding its controlling factors, iii) comparison of modelled and in situ Ni enrichment profile and analysis of nickel distribution in between different retention processes, iv) modelling and in depth understanding of these retention processes.

The modelling reveals that the vertical progression of the pH front controls thickening of iron-rich zone, explains the vertical mobility of the elements and governs the Ni enrichment. Adsorption itself plays an important role in lateritization process retarding Ni mobility, but i) becomes significant in a narrow range of pH (slightly alkaline) due to competition of Mg and Ni for sorption sites and ii) does not explain such a high nickel content in limonite nowadays, suggesting that Ni is held in goethite mostly by stronger ties i.e. substituted for Fe in the crystal lattice of iron oxyde. 1-D modelling appears to be a powerful tool in understanding the general behavior of trace elements upon the formation of laterite and at the same time reveals that locally Ni mineralizations should be explained by more complex processes, such as lateral transfers, convective flows and preferential pathways.

*Keywords:* Laterite, Transport Modelling, Weathering, Kinetics, Water-rock interactions

---

## **1. Introduction**

Nickel laterite ores account for over 60% of global Ni supply (Butt and Cluzel, 2013), thus, making it an important exploration target in anticipation of the future demand of Ni. One of the biggest nickeliferous laterite reserves in the world is located in New Caledonia, 1300 km east of Australia in the southwest Pacific Ocean. Representing around 30% of the global resources in nickel, these laterites are actively worked by various mining companies (SLN-ERAMET, KNS, SMSP etc.). They occur at the top of the obducted ultramafic massif with an average thickness of 30-40m, resulting from the weathering of the Peridotite Nappe. The initial nickel content of the parent rock, that consists of olivine and various form of serpentine (antigorite, chrysotile, lizardite, polygonal serpentine), can contain up to 0.4wt% of Ni (Ulrich, 2010; Herzberg et al., 2013; Golightly, 1981). The weathering of the olivine-rich ultramafic rocks and their serpentinized equivalents by meteoric water induces the selective

leaching of Fe, Mg, Si and Ni and leads to the formation of a lateritic profile together with an exceptional Ni enrichment (Trescases, 1975; Golightly, 2010). The limonite level, formed at the top of the profile (Fig.1), is mainly composed of iron oxi-hydroxides and followed by the saprolitic level where hydrous Mg silicate deposits form, especially in the mid to lower saprolite. Ni concentration increases constantly throughout the limonite horizon, but the highest Ni grade (locally 2wt% up to 5 wt%) is found in the saprolite horizon which represents about one third of the total Ni laterite resources (Fig.1). In this horizon, Ni is concentrated in nickeloan varieties of serpentine, talc-like, chlorite and sepiolite, some of which are poorly defined and known informally as “garnierite” (Butt and Cluzel, 2013). Transition between the saprolite and limonite horizons is marked by a sharp increase in MgO and SiO<sub>2</sub> content and, consequently, by drastic change in mineralogy (Fig.1). The so-called garnierite is mostly located along fractures (Trescases, 1975). Under the saprolite level, a poorly altered peridotite is situated. The basis of the peridotite nappe hosts numerous pure magnesite veins, sometimes associated with amorphous silica (Quesnel et al., 2015).

The enrichment of nickel in the weathering profile is governed by many interplaying factors that include mineralogical composition of parent rock, climate, chemistry and rates of chemical weathering, tectonics, and drainage (Lelong et al., 1976; Golightly, 1981, 2010; Gleeson et al., 2003; Freyssinet et al., 2005; Butt and Cluzel, 2013). After being leached from rock-forming minerals nickel is thought to be redeposited below, mostly associated with i) Ni-rich ferruginous oxide ore where it is sorbed and/or substituted for Fe in the crystal lattice (Cornell, 1991; Fischer et al., 2007; Singh et al., 2002; Carvalho-e-Silva et al., 2003; Dublet et al., 2012), ii) a wide variety of neo-formed silicate minerals such as talc-like and sepiolite-like minerals (Cathelineau et al., 2015; Villanova-de-Benavent et al., 2014; Wells et al., 2009), and iii) partly weathered primary lizardite, in which Mg to different extent has been exchanged by Ni (Golightly, 1981, 2010). Three different mechanisms have been suggested in the literature in order to explain the association between nickel and goethite: i) isomorphous substitution of Ni for Fe into the goethite structure, ii) association of Ni with poorly crystalline phase, and iii) adsorption of Ni to goethite surface. Singh et al. (2002) and Carvalho-e-Silva et al. (2003) found and confirmed using EXAFS that Ni<sup>2+</sup> is associated

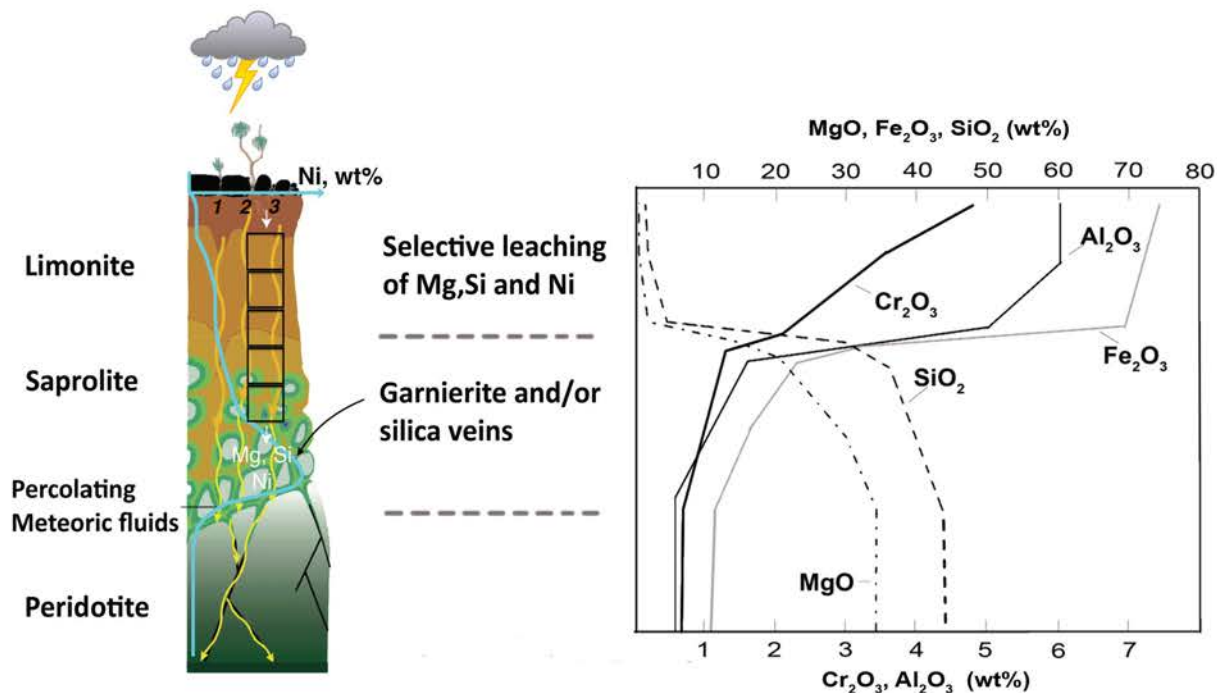


Figure 1: A schematic log of the New Caledonian Peridotite Nappe correlated with approximate elemental composition of different zones. Turquoise line represents nickel distribution in a profile. Modified after (Ulrich et al., 2011; Troly et al., 1979; Guilbert and Park, 1986)

with goethite via isomorphous substitution for  $\text{Fe}^{3+}$ . Using sequential leaching studies of Indian laterite samples Swamy et al. (2003) reported that the quantity of chemisorbed Ni was negligible and most of the nickel was bound in the crystal lattice with some associated with amorphous goethite. Actually such an association is quite complex and literature suggests that there is a continuum going from one stage to other (Davis et al., 1987; Stipp et al., 1992). Therefore, an initial fast adsorption step is followed by a slow step of incorporation of the adsorbed species into the crystal structure with formation of solid solution. Schultz et al. (1987) experimentally documented the irreversible adsorption of metals on ferrihydrite surfaces. Adsorption/desorption of  $10^{-5}$  M  $\text{Ni}^{2+}$  on  $10^{-3}$  M ferrihydrite revealed that after the overnight exposure only about 25 % of the  $\text{Ni}^{2+}$  could be desorbed and the remainder stayed bound in the ferrihydrite structure. Similar hysteresis were found by McKenzie (1980), Brümmer et al. (1988), Barrow et al. (1989), and Gerth et al. (1993). Further

recrystallization of the ferrihydrite leads to a release of the nickel over time. Direct evidence was established for a negative correlation between the bulk Ni content and the crystallinity of goethite as a function of depth in the New Caledonian Ni laterites (Dublet et al., 2012, 2015).

There are a number of scientific articles dealing with modelling of regolith formation from bedrock. For example Soler and Lasaga (1996, 1998) have been working on an advection-dispersion-reaction model of bauxite formation, Fletcher et al. (2006) and Lebedeva et al. (2007) on granite bedrock (albite + FeO-bearing phase + quartz) transformation to saprolite (goethite + kaolinite + quartz), Navarre-Sitchler et al. (2011) on a reactive transport model for weathering rind formation on basalt etc. Nevertheless, the mobility and transport of trace elements in ultramafic bedrock was not yet modelled with the only exception of a recent study by Domènech et al. (2017). Their work provides valuable insights into the formation of the different laterite horizons in the profile from partially serpentinized peridotite. However, the analysis seems to miss important elements that suggest Ni should be included into the goethite structure and cannot be explained by adsorption alone. In addition, the formation of garnierite is not considered and Ni enrichment is shown only in oxide part of deposits. Thus, the processes of Ni retention in a profile and their controlling parameters are still poorly understood.

In the present work, we used a reactive transport modelling in order to study the development of the secondary nickel ores upon vertical progression of the alteration front. We analyse the effect of key parameters governing i) sorption processes on a goethite surface, ii) precipitation/dissolution of secondary minerals, and iii) kinetic dissolution of serpentinized olivine due to meteoric water flow (Fig.2). Moreover, the effect of pimelite/kerolite (Ni-bearing phases) being present as a solid solution and incorporation of Ni into the goethite structure were also studied. The role of sorption processes on goethite in Ni redistribution in space during the mineralization, as well as the detailed understanding of their mechanisms have particular emphasis in this paper. Direct comparison of Ni distribution obtained after the modelling with its typical distribution in the profiles provides us in depth understanding of the weathering process in laterite deposits, reveals the validity of the model and gives

new insights into the other processes that might have also governed the mobility of elements and formation of these increasingly important Ni deposits.

## 2. Materials and methods

### 2.1. Modelling the hydrodynamic system

A reactive multicomponent 1-D transport model of supergene enrichment of lateritic Ni deposits has been simulated by assuming the weathering of a one-dimensional vertically oriented column of serpentinized olivine due to steady state meteoric water flow. The code used for the simulations is PHREEQC (V 3.1.4) (Parkhurst and Appelo, 2013). The 1-D column is defined by a series of 40 cells of 0.5 m. in length. The velocity of water in each cell is determined by the length of the cell, porosity and amount of annual rain precipitation. Solute concentrations at some point on a flowline may change by i) advection of concentration gradients, ii) reactions with the solid material, and iii) dispersion and diffusion. The Advection-Reaction-Dispersion equation that describes these changes along the flowline and implemented on Phreeqc is the following:

$$\left(\frac{\partial c}{\partial t}\right)_x = -v\left(\frac{\partial c}{\partial t}\right)_t - \left(\frac{\partial q}{\partial t}\right)_x + D_L\left(\frac{\partial^2 c}{\partial x^2}\right)_t \quad (1)$$

where  $c$  is the solute concentration ( $mol.l^{-1}$ ),  $v$  is pore water flow velocity ( $m.s^{-1}$ ),  $D_L$  is hydrodynamic dispersion coefficient ( $m^2.s^{-1}$ ) and  $q$  is the concentration in the solid ( $mol.l^{-1}$  of pore water). In our calculations we neglect dispersion and set  $D_L$  to 0. According to in situ observations, indeed, transport of the chemical components is controlled by advection and high reaction rates. Neglecting dispersion will cause sharper reaction front and higher concentration peaks. In other words, spreading of the concentration front should be slightly underestimated.

Flux boundary conditions (Cauchy) were defined for the first and last cell. A slightly acidic tropical rainwater with pH=5.6 due to its equilibrium with atmospheric CO<sub>2</sub> represents an incoming solution and is injected in the first cell (Fig.3). Regarding separately the values of the experimental rates of kinetic dissolution of the parent rock constituents

(olivine, serpentine, enstatite), presented in the literature (*e.g.* Brantley and Chen (1995); Pokrovsky and Schott (2000); Wilson (2004); Thom et al. (2013)), one may note that olivine has a highest rate of the dissolution process among them. The rates of enstatite and serpentine are extremely sluggish compared to those of olivine, being one to a few orders of magnitude lower depending on pH. This makes olivine the main initial mineral in a system that provides nickel and other elements (Mg, Si and Fe). In this way, the numerical modelling was performed assuming olivine in each cell of the 1-D column at initial state (Fig.2).

The New Caledonia is situated in seasonally humid wet savannas, thus, characterized by summer rainfall of 900-1800 mm and a 2-5 months winter dry season (Butt and Cluzel, 2013). Nevertheless, these values are related to the current climatic circumstances and most likely were not the same during all 10 Ma of laterite formation. According to calculations of Thorne et al. (2012) Ni laterites develop where rainfall exceeds 1000 mm/y and mean monthly temperatures range between 22-31°C (summer) and 15-27°C (winter). For our simulations the value of 2000 mm/y was chosen as acceptable.

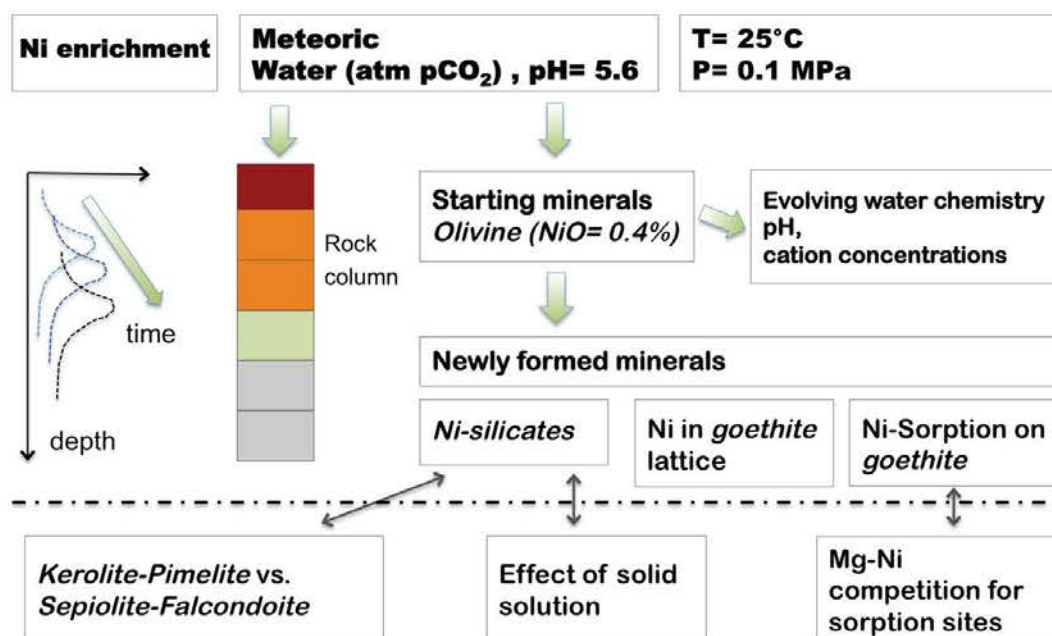


Figure 2: Interaction between a rock column and meteoric water: main variables taken into account.

Porosity of the ultramafic bedrock was chosen to be about 2% but is highly dependent

on the fractures density (Join et al., 2005; Jeanpert and Dewandel, 2013). Due to code limitations, the porosity remains constant throughout the calculations. There are some other codes with improved hydrodynamic part (PhreeqcRM, Crunchflow, etc) that handle porosity changes but from a 1-D modeling point of view such an assumption has a minor influence on the results of simulation. Indeed, when magnesium and silica are leached from limonite zone a total mass loss of up to 70-80% appears there. At the same time, the density ahead of the pH front, where silicates form, will still be much closer to the initial value than in the goethite zone. Since 1-D column does not allow any kind of lateral fluid movements, the fluid flow rate is constant along the column. In real profiles, the goethite zone density is so low that it collapses under the weight of the profile to a near constant value (Golightly, 1981).

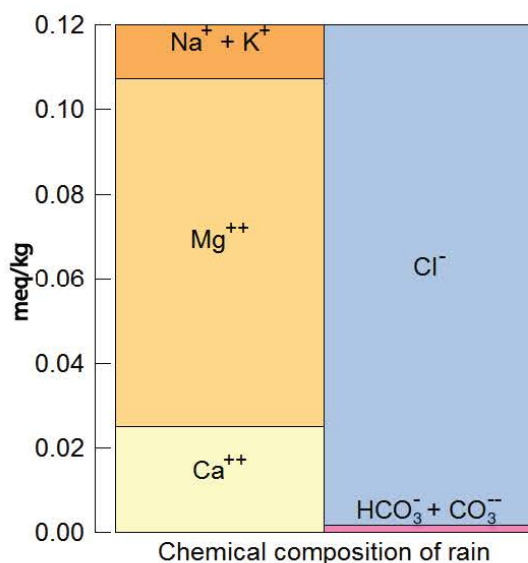


Figure 3: Bar chart of chemical composition of incoming solution (rainwater) at equilibrium with atmospheric  $\text{CO}_2$  and subsequent pH of 5.6. In accordance with Trescases (1975).

The total computing time for 1-D transport calculations is defined as 250,000 pore volumes of filling solution that are moved through the column ( $10^7$  shifts of solution per 40 column cells). The real geological time in years could be estimated from residence time of solution in a cell multiplied by number of solution shifts. Since the residence time per cell was defined as 100,000 seconds, it will correspond to a summary computing time of about



10 Ma. We take this value as a connection of our results to real geological time but it should be noted that in reality the residence time will greatly change (decrease) due to porosity changes, formation of fractures and lateral dissipations of fluid. Therefore, this value of 10 Ma is an upper limit and certainly overestimated. Further planned investigations will require implementation of this code into a 2D/3D fully coupled hydrological model to resolve this drawback.

## 2.2. Modelling the geochemical system

Olivine composition in the model was selected according to Trescases (1975) as following:  $\text{Mg}_{1.82}\text{Fe}_{0.17}\text{Ni}_{0.01}\text{Al}_{0.006}\text{SiO}_4$ . Olivine dissolution is assumed to be kinetically controlled whereas the precipitation of secondary weathering products is considered to occur according to local equilibrium. Pokrovsky and Schott (2000) provided in their work the following steady state specific dissolution rate for olivine at 25°C in  $\text{CO}_2$ -free solutions:

$$\log(r) = -0.5pH - 6.64 \quad (2)$$

Which is consistent with an Arrhenius equation of the form of:

$$r = Aa_{H^+}^n \exp(-E_a/RT) \quad (3)$$

where  $r$  signifies the specific dissolution rate of olivine in ( $\text{mol.m}^{-2}.\text{s}^{-1}$ ),  $a_{H^+}$  is the activity of protons ( $\text{mol.l}^{-1}$ ),  $A$  refers to a pre-exponential factor,  $E_a$  designates an activation energy,  $R$  represents the gas constant, and  $T$  denotes absolute temperature.

Generally, the effect of atmospheric  $\text{CO}_2$  on olivine dissolution rate is very weak in acid to neutral solutions but may be important in alkaline conditions. Results of Wogelius and Walther (1991) show a decrease of the dissolution rate at elevated pH and low  $\text{CO}_2$  pressure while experiments conducted under similar conditions by Pokrovsky and Schott (2000) and Golubev et al. (2005) did not account such a decrease in comparison with their  $\text{CO}_2$ -free experiments. Current modelling was performed according to the equation (2) and without taking into account the effect of presence of  $\text{CO}_2$ .

The overall olivine reaction rate in the model is as follows:

$$R_d = r \left( \frac{A_0}{V} \right) \left( \frac{m}{m_0} \right)^n \quad (4)$$

where  $R_d$  signifies the overall reaction rate ( $\text{mol.l}^{-1}.\text{s}^{-1}$ ),  $r$  is the specific dissolution rate ( $\text{mol.m}^{-2}.\text{s}^{-1}$ ) extracted from equation (2),  $A_0$  refers to the initial surface area of the solid ( $\text{m}^2$ ),  $V$  designates the volume of solution ( $l$ ),  $m_0$  represents the initial moles of solid, and  $m$  is the moles of solid at given time.

The factor  $(m/m_0)^n$  accounts for changes in surface area during dissolution of olivine. For a monodisperse population of uniformly dissolving spheres or cubes,  $n = 2/3$ , since  $m$  is proportional to the volume, or  $r^3$  (here  $r$  is the radius of the sphere or the side of the cube), while the surface area is proportional to  $r^2$ .

The rate expression is embedded in the PHREEQC third order Runge-Kutta-Fehlberg algorithm (Parkhurst and Appelo, 2013). Equilibrium phase composition is calculated before a kinetic calculation is initiated and after a kinetic reaction increment. Calculations were done at 25°C with the code PHREEQC associated with the llnl.dat thermodynamic database (Johnson et al., 2000), that has been edited in order to account for garnierite minerals. The reactions, involved in the precipitation or dissolution of Mg and Ni end-member phyllosilicates are given in Table 1.

Basically, Mg-Ni-phyllosilicates are parts of solid-solution series extending from Mg to Ni end-members (*e.g.* Springer (1974, 1976); Reddy et al. (2009)) and effect of them being present as an ideal solid solutions instead of separate minerals will be discussed. The process of substitution of Ni for Mg in the lattice of serpentine is not considered here due to the lack of thermodynamic data needed to perform such kind of modeling. Trescases (1975) demonstrated that many ground waters from the base of the nickel laterite profiles in New Caledonia are saturated or supersaturated with respect to talc-like mineral but rarely saturated in serpentine. For the moment serpentine has been seldom reported to form under earth-surface conditions and, thus, suppressed from equilibrium phases that were allowed for precipitation. Instead, in nature the precipitation rates favor the formation of metastable

Table 1: Dissolution reactions for Mg and Ni end-members of garnierite and Saponite-Mg, with the corresponding equilibrium constants at 25°C and 1 bar.

| Mineral            | Reaction  | Log K                   |
|--------------------|---|-------------------------|
| <i>Kerolite</i>    | $Mg_3Si_4O_{10}(OH)_2: H_2O + 6H^+ = 3Mg^{2+} + 4SiO_2 + 5H_2O$   | 25.79 (Stoessell, 1988) |
| <i>Pimelite</i>    | $Ni_3Si_4O_{10}(OH)_2: H_2O + 6H^+ = 3Ni^{2+} + 4SiO_2 + 5H_2O$   | 11.46 (Nriagu, 1975)    |
| <i>Sepiolite</i>   | $Mg_4Si_6O_{15}(OH)_2: 6H_2O + 8H^+ = 4Mg^{2+} + 6SiO_2 + 11H_2O$   | 30.44 (Stoessell, 1988) |
| <i>Falcondoite</i> | $Ni_4Si_6O_{15}(OH)_2: 6H_2O + 8H^+ = 4Ni^{2+} + 6SiO_2 + 11H_2O$   | 12.31 (Nriagu, 1975)    |
| <i>Saponite-Mg</i> | $Mg_{3.16}Al_{0.33}Si_{3.67}O_{10}(OH)_2 + 7.32H^+ =$<br>$3.16Mg^{2+} + 0.33Al^{3+} + 3.67SiO_2 + 4.66H_2O$ | 26.25 (llnl.dat)        |

sepiolite and kerolite in Al-poor environments (Stoessell, 1988). Thus, for transport calculations at 25°C the list of secondary weathering products is following: Ferrihydrite, Gibbsite, Saponite-Mg, Kerolite, Pimelite, Sepiolite, Falcondoite, Quartz. Ferrihydrite is known to be an initial precursor phase in the formation of goethite but is difficult to be identified using standard characterisation techniques (such as PXRD) due to its poorly crystalline nature. According to Cornell et al. (1992) the introduction of nickel to the system increases the stability of the ferrihydrite phase, inhibiting its transformation to goethite and also suggesting that ferrihydrite could be still present in nickeliferous laterites. Goethite and hematite form later on from ferrihydrite and the ratio and cristallinity of these products are strongly influenced by pH. Schwertmann and Murad (1983) showed that at 24°C maximum hematite was formed in between pH 7 and 8, while maximum goethite at pH below 4 and above 12. This way, relying on a diagram of pH change with depth, one can suppose what will be the final products in each part of profile.

The surface complexation model of Dzombak and Morel (1990), that takes into account binding of metals and protons on both strong and weak sites of ferrihydrite, which develops a charge depending on the ions sorbed, has been used in order to simulate adsorption process.

The adsorption constants required to parameterize the model for Ni adsorption at the surface of ferrihydrite were obtained by fitting experimental data (Dzombak and Morel, 1990) and are given in Table 2.

Two sites are defined for a diffuse-double-layer: i) Hfo\_s, which is strong binding site, and ii) Hfo\_w, which is weak binding site. Dzombak and Morel (1990) used 0.2 mol weak sites/mol ferrihydrite and 0.005 mol (2.5% of weak sites) strong sites/mol ferrihydrite with a surface area  $5.33 \times 10^4$  ( $m^2.mol^{-1}$ ) and a weight of 89 g Hfo/mol Fe. To be consistent with their model, the relative number of strong and weak sites is kept constant as the total number of sites varies. In reactive 1-D transport modeling presented in this paper oxi-hydroxide surfaces change in proportion as the ferrihydrite dissolves or precipitates.

Table 2: Thermodynamic data for a diffuse-double-layer surface “Hfo”(Hfo stands for hydrous ferric oxide, i.e. ferrihydrite), derived from Dzombak and Morel (1990).

| Reaction                                 | Log k |
|--|-------|
| $Hfo\_sOH + H^+ = Hfo\_sOH_2^+$          | 7.18  |
| $Hfo\_sOH = Hfo\_sOH^- + H^+$            | -8.82 |
| $Hfo\_sOH + Ni^{2+} = Hfo\_sONi^+ + H^+$ | 0.37  |
| $Hfo\_wOH + H^+ = Hfo\_wOH_2^+$          | 7.18  |
| $Hfo\_wOH = Hfo\_wOH^- + H^+$            | -8.82 |
| $Hfo\_wOH + Ni^{2+} = Hfo\_wONi^+ + H^+$ | -2.5  |

It is worth noting that the llnl.dat database contains thermodynamic data for sorption of many trace metals. Once surface Ni complexes, Hfo\_s and Hfo\_w, are introduced in the model, the effect of other cations, such as  $Mg^{2+}$ ,  $Fe^{2+}$ ,  $Ca^{2+}$  can be accounted for. Cations competition for sorption at the surface of ferrihydrite will, thus, influence the mobility of leaching metals. In order to analyse this competition a transport modelling through one-cell with flux-open boundaries was performed. The input of one-cell model is identical to the

main one with 40 cells. This model has been used in order to reduce calculation time and gain insight into the aforementioned competition of metals for sorption sites and precipitation of Ni-goethite solid solution with 2wt% of Ni. It should be noted that in a results and discussion section we always use the name goethite in spite of the fact simulations are done with ferrihydrite constants (same chemical formula and different solubility constant value). This latter choice is applied to avoid any kind of confusions since ferrihydrite is being more geochemical rather than geological term.

### 3. Results and discussion

#### 3.1. 1-D Reactive transport model

Figure 4 shows the evolution of the paragenetic sequence and the development of the secondary nickel ores as a function of time. The results represent mass fractions of secondary weathering products formed after 50,000 PV, 150,000 PV and 250,000 pore volumes (PV) of filling solution that are moved through the column and corresponds to 2 Ma, 6 Ma and 10 Ma, respectively. The reactive transport model reproduces both the formation of the laterite profile in time with thickening of iron-rich zone and change of the Ni content with depth. Here, nickel supplied in the system by olivine dissolution was supposed to be redistributed in between solution, adsorption on goethite and dissolution/precipitation of Ni-bearing minerals. In the following chapter of detailed understanding of Ni behaviour during weathering is displayed. As can be seen from Figure 4, the obtained chemical profile clearly distinguishes the ferruginous/aluminous residual part where Si, Mg, and Ni are leached, from the zone where silicates start to precipitate. The effect of silicate weathering on the water chemistry is primarily the addition of cations ( $\text{Ni}^{2+}$ ,  $\text{Mg}^{2+}$ ,  $\text{Fe}^{2+}$ ,  $\text{Fe}^{3+}$ ;  $\text{Al}^{3+}$ ) and silica. pH variation is balanced on one hand by silicate weathering reactions which consume  $\text{H}^+$  and on the other hand by leaching of the elements out of the cell and renewing with low pH meteoric water which tend to decrease the pH value. Migration of the pH front, subdividing slightly acidic at the surface to alkaline pH at depth, appears to have the main influence in controlling the precipitation/dissolution of neo-formed silicate minerals,

and, thereby, regulating the transport of elements in the profile. The limonite zone is represented by goethite and minor precipitations of gibbsite. Beneath, after the pH front, the secondary weathering products are represented by falcondoite (Ni bearing phase), and massive precipitations of sepiolite and Saponite-Mg. Considering the results after 2 Ma, one can observe that part of olivine mass is not yet dissolved, providing pH up to 11 at the bottom of the column, and that pimelite (Ni talc-like) precipitation (indicated by a narrow black line on Fig.4) occurs at depth, after the pH front. Pimelite precipitation is no more observed after 4 Ma. Indeed, after 4 Ma, olivine disappears and the maximum pH value decreases from 11 to 9.5 after the pH front.

It worth noting that in New Caledonia the silicates, precipitated in fractures or in a form of concentric zoning of Ni-bearing silicates (Cathelineau et al., 2016), are mostly represented by talc-like minerals. This is in contrast to sepiolite-like phases (falcondoite, sepiolite), obtained in current numerical modelling which is more common for Falcondo Ni-laterite deposits observed in Dominican Republic (Villanova-de-Benavent et al., 2014). In order to find out why sepiolite-like precipitated instead of talc-like minerals let us turn to the literature. According to Stoessell (1988) the difference in solubility between kerolite and sepiolite is small enough that precipitation kinetics is probably decisive in their formation. The metastability of kerolite relative to sepiolite, determined in the study of Stoessell (1988), was suggested by Jones (1986). He reported kerolite as a precipitate at Stewart springs (California, USA) from waters with pH above 12, but with aqueous silica concentrations below (25°C and 1 bar) quartz saturation. Jones (1986) suggested that with increasing pH and Mg content in water and decreasing silica content, kerolite should precipitate at the expense of sepiolite. Same conclusion might be reached for pimelite (Ni talc-like) and falcondoite (Ni sepiolite) precipitation since they are the Ni counterparts of kerolite and sepiolite, respectively.

It is consistent with the numerical results (Fig.4) where, as it was mentioned above, pimelite (narrow black line, 2 Ma column) precipitated in the deeper part of profile where high pH of about 11 was maintained by dissolution of still presenting olivine. In this way it could be concluded that for precipitation of talc-like minerals at 25°C in Al-poor environ-

ments it is necessary and sufficient to have an ample amount of olivine in a system.

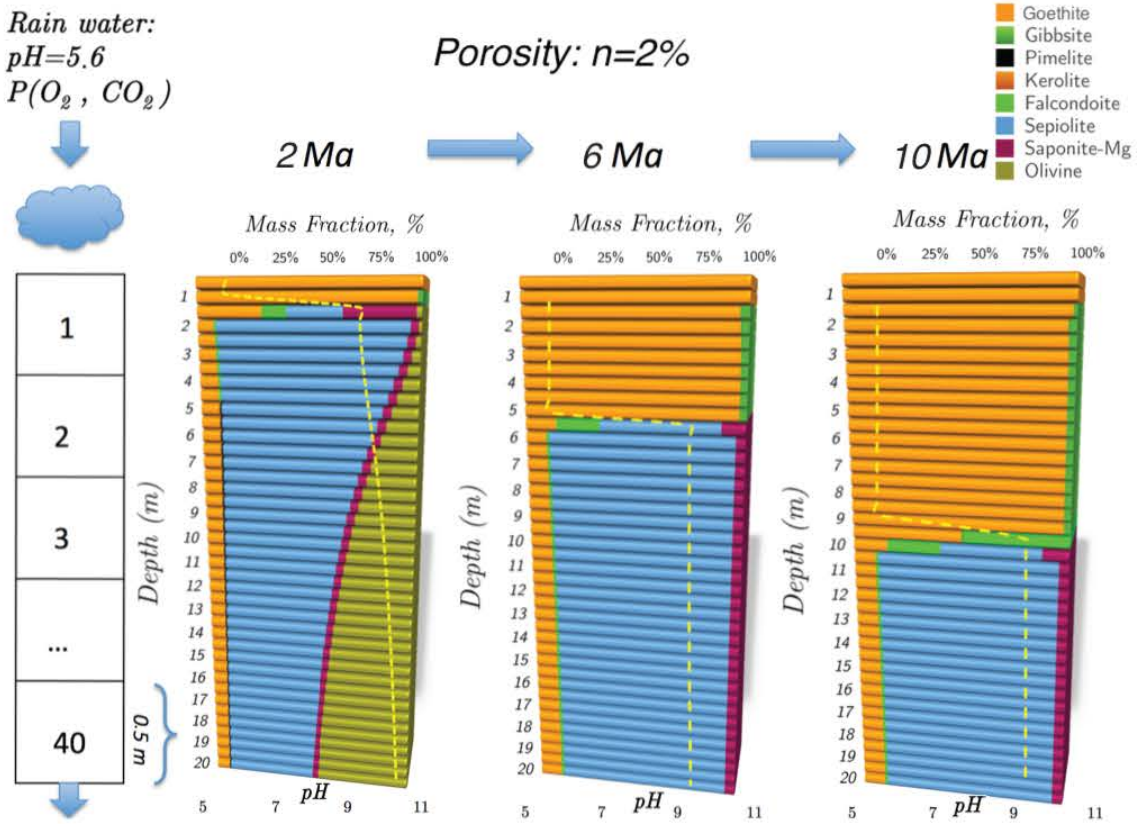


Figure 4: Mass fraction of secondary weathering products after 50,000 PV (2 Ma), 150,000 PV (6 Ma) and 250,000 PV (10 Ma). Yellow dotted line represents current pH front in the column.

It should be noted that in real profiles olivine would persist for longer time due to the different character of the porosity distribution. In fact, the extreme instability of olivine results in its replacement by silicate phases in situ with the cations in the solutions diffusing outwards to joints, where the water is flowing downwards. Because of this the olivine in the bulk material does not disappear before 6 million years as in the model. Nevertheless, an accurate representation of the process will not be achieved until 2D modelling is attempted.

Returning to the results of the model the entire dissolution of olivine in the column after 6 Ma and 10 Ma (Fig.4) led to a change in pore water pH with values of 5.6 close to the surface to about 9.5 at the bottom. Present day water analyses at Koniambo (northwest of New Caledonia) indicated similar pH condition: from 5.5 near the surface to about 10

at depth, either in the laterite or in the serpentized peridotite (Jeanpert and Dewandel, 2013). Concerning the mass fraction of Ni bearing sepiolite (falcondoite), its accumulation and downward movement with pH front migration can be observed. The increase of Ni content with time and depth is shown in Figure 5.

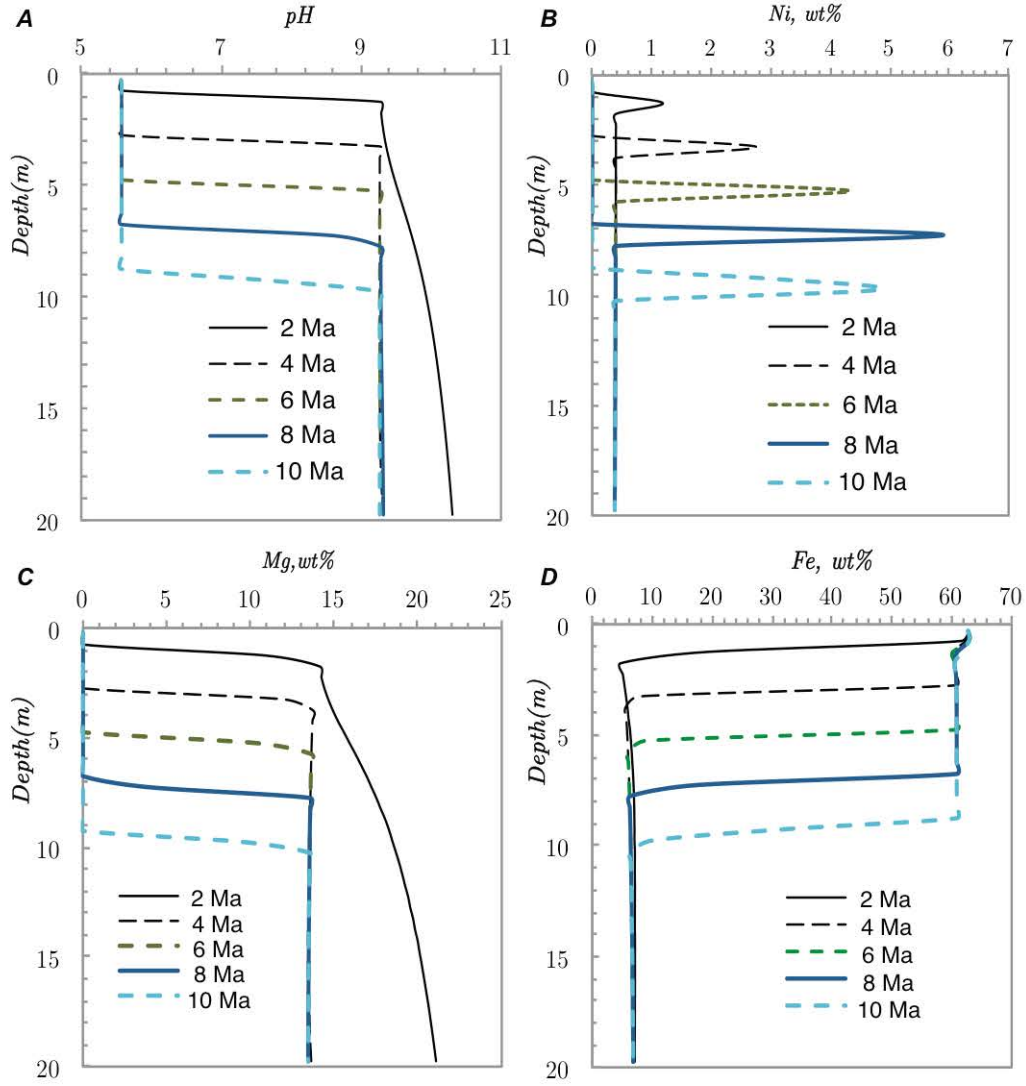


Figure 5: Migration of pH front along the profile with corresponding Ni, Mg and Fe concentrations in the secondary weathering products.

It should be noted that the Ni concentration in wt% here is related to initial mass of olivine in a cell, serving as reference in order to be able comparing it through time. Normalizing to the current mass of minerals presented in a cell adds a complexity in following



comparison of Ni enrichment since this mass is changing due to the leaching. Despite the fact that in the Figure 5 at 250,000 PV (10 Ma) maximum concentration of nickel (4.8 wt.% ) seems to be lower than in previous step (6 wt.% after 200,000 PV, or 8 Ma), it appears that the thickness of the Ni rich zone is also higher after 250,000 PV than after lower PV circulation. Therefore, the precipitation of Ni in the two closest cells after 250,000 PV (10 Ma) (Fig. 4) with Ni content of 3.06 wt.% and 4.80 wt.% at 9.25 m and 9.75 m of depth respectively, yields an overall equivalent Ni content of 7.89 wt.%. This value is much higher comparing to typical New Caledonian profile presented in Figure 1 which exhibits up to 2-3 wt.% of Ni distributed throughout limonite and saprolite zone. The cause of it might be related to precipitation of silicates at local equilibrium in our model, implying that simultaneous precipitation occurs once favorable conditions are reached in a cell and resulting in a narrow zone of Ni precipitation. Also, in nature, nickel, released due to peridotite dissolution, may be partly lost by lateral movement in solution.

The overall concentration of nickel of 7.89 wt.% at the last step of simulation (10 Ma) represents 97.2 % of the initial nickel content in the column and distributed as follow: i) 4.27 wt.% of Ni sorbed on ferrihydrite surface, ii) 95.7 wt.% precipitated with Ni-silicate (falcondoite) and iii)  $1.69 \times 10^{-4}$  % in solution along the whole column. From Figure 5 one can observe the movement of transition zone from the limonite horizon to the saprolite, which is marked by a sharp increase in MgO content from 0 to up to 20 wt.%. Iron content meanwhile varies from values of about 65 wt.% before the reaction front down to 5 wt.% after it. Whilst the iron has been oxidized, the nickel remains bivalent and is somewhat mobile, more so than iron, less so than magnesium. This chemical distribution of elements is consistent with Figure 1 and clearly distinguishes the ferruginous residual part where Si, Mg, and Ni are leached and Mg discontinuity zone appears.

Nevertheless, in Figure 1 Ni concentration is increasing throughout limonite zone up to 2 wt.% at the contact with saprolite, while in numerical modelling this zone comes out to be free of Ni. According to the modelling results, adsorbed nickel appears to be governed by pH front. Being initially retarded compared to fluid movement, adsorbed Ni has been eventually liberated into pore water at pH as low as 5.6 due to reaction front downward advancement

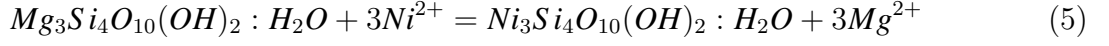
upon silicates dissolution. Dependence of nickel sorption on pH along with competitive retardation is discussed in the following chapter, devoted to a detailed understanding of the weathering process. Yet, it could be concluded that adsorption can not explain such a high nickel content in limonite nowadays since the actual pH of soil waters can be in some instances as low as 4.5 due to dissolved organic acids, thus, suggesting that nickel is held here by stronger ties. The latter might be explained by isomorphous substitution of Ni for Fe in goethite and either significant process in soils related to specific binding of elements to the variable charge surfaces of organic matter. Adsorption on organic matter is similar to that on ferrihydrite since surface charge likewise depends on pH and solution composition, but the difference is that the sorption edge for organic matter is shifted to lower pH. It implies that at low pH from about 4 to 7 adsorption on organic matter will be dominating, but at higher pH the major role will be passed to adsorption on oxyhydroxides. Present study does not consider the issue of DOC due to its low concentration in well-drained and scarce in terms of soil terrains of New Caledonia.

### *3.2. Detailed understanding of the weathering process*

#### *3.2.1. Effect of pimelite/kerolite being present as solid solution*

The numerical simulations presented above consider the Mg-Ni-phyllosilicates to be pure end-members although in reality they are being members of solid-solution series extending from Mg and Ni end-members (*e.g.* Springer (1974, 1976); Reddy et al. (2009); Villanova-de-Benavent et al. (2014); Cathelineau et al. (2015)). Usually solid solutions show deviations from ideal behavior and the activity coefficients, that account for non-ideality, become a function of the excess free energy of mixing. The free energy of mixing might be obtained from different non-ideal thermodynamic properties such as variations in fractionation factor, miscibility gaps etc. (Glynn, 2000). Despite the fact that many researchers describe Mg-Ni-phyllosilicate members of solid solutions, the possibilities of modelling such a system remain poor due to the lack of thermodynamic data, thus, limiting simulations by assumption of ideality. In this way, for example, Galí et al. (2012) have calculated Lippmann diagrams for the garnierite solid solutions. This subchapter aims at understanding the effect of *e.g.*

pimelite and kerolite being present as a solid solution instead of separate mineral phases. Linear combination of reactions for kerolite and pimelite, presented in Table 1 results in Equation (5):



At first, let us consider a situation where a solution is in equilibrium with kerolite and pimelite as separate minerals. The mass action expression for Equation (5) looks as follows:

$$K = \frac{[Ni_3Si_4O_{10}(OH)_2 : H_2O]}{[Mg_3Si_4O_{10}(OH)_2 : H_2O]} \times \frac{[Mg^{2+}]^3}{[Ni^{2+}]^3} = \frac{K_{Kerolite}}{K_{Pimelite}} = 10^{14.33} \quad (6)$$

Then, in Equation (6) the activities of two pure solid phases will be equal to one. Therefore, the ratio  $\frac{[Mg^{2+}]^3}{[Ni^{2+}]^3}$  in solution is fixed to  $10^{14.33}$  and  $\frac{[Mg^{2+}]}{[Ni^{2+}]} = 59795$ . The concentration of  $[Ni^{2+}]$  is much smaller than of  $[Mg^{2+}]$  because the solubility of pimelite is much smaller than of kerolite.

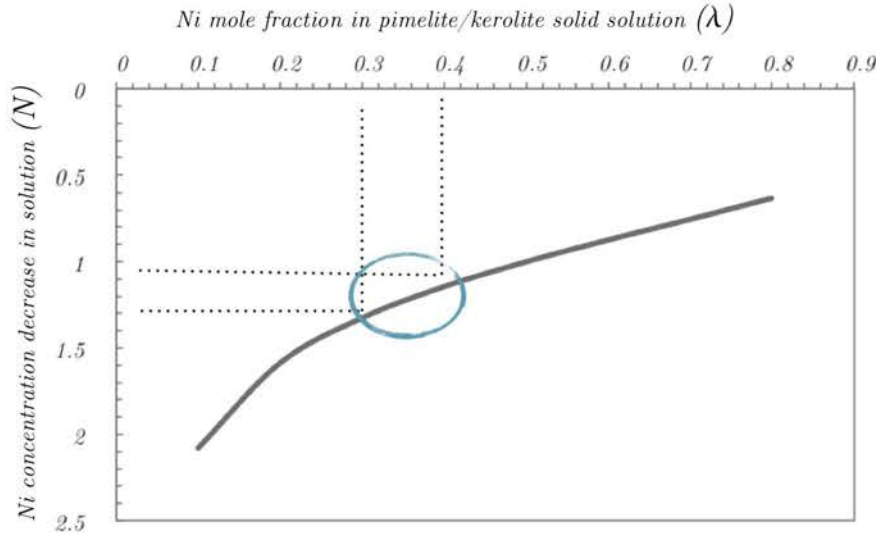


Figure 6: Effect of Ni substitution in pimelite/kerolite solid solution ( $\lambda$ ) on the relative Ni concentration decrease in solution ( $N$ ).

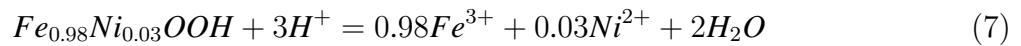
In the second situation  $[Ni^{2+}]$  is incorporated in the kerolite structure as an ideal solid solution, which may be written as  $Ni_\lambda Mg_{3-\lambda} Si_4 O_{10} (OH)_2 : H_2 O$ , where  $\lambda$  represents the

nickel mole fraction. In this way, activities of kerolite and pimelite in Equation (6) will no longer be equal to one as for separate minerals, but will depend on  $\lambda$ . Therefore, if Mg concentration remains the same as before, then the Ni concentration must now be lower. It can clearly be seen in Figure 6, that shows the effect of Ni substitution in pimelite/kerolite solid solution on the relative Ni concentration decrease in solution. Therefore, the common values of Ni mole fraction in New Caledonian pimelite/kerolite solid solutions, *i.e* around  $\lambda = 0.3-0.4$ , will lead to a decrease of the Ni concentration by about 20% from the case with pure phases on assumption that Mg concentration remains the same (Fig.6).

Thus, to conclude it should be said that the formation of solid solution lowers the aqueous concentration of the minor component, in our case nickel, but does not have a drastic effect on the global Ni mass balance. The latter means that despite the use of separate mineral phases our results of simulations may be considered as reliable.

### 3.2.2. *Ni in solid solution with goethite*

It has already been mentioned above that sorption alone cannot explain increase of Ni content throughout the limonite zone (Fig.1). In our 1-D model all Ni, adsorbed on goethite, was released in solution and shifted at depth once the pH decrease below six after the front. Obviously, this latter phenomenon is not observed in the field, where Ni still persists in the limonite zone. According to Dublet et al. (2012), nickel content up to 2wt.% is common for New Caledonian laterites, where  $Ni^{2+}$  is associated with goethite via isomorphous substitution for  $Fe^{3+}$ . In order to account for this gap, here, we perform a sensitivity test that considers additionally to our previous transport model (Fig.4) a precipitation of Ni-bearing goethite. In this way, reaction for precipitation of Ni-bearing goethite has been added in the thermodynamic database as follows:



The influence of such a small amount of Ni in structure of goethite on its equilibrium constant has been neglected. Indeed, this constant, according to Equation (7), will be defined as:

$$\text{Log}K = 0.98 \times \log [Fe^{3+}] + 0.03 \times \log [Ni^{2+}] + 3pH \quad (8)$$

Considering that the Ni concentrations in the model are as low as  $10^{-9}$  to  $10^{-6}$  moles per liter, and taking into account Equation (8) one can see that the effect of Ni presence on the equilibrium constant will be minor.

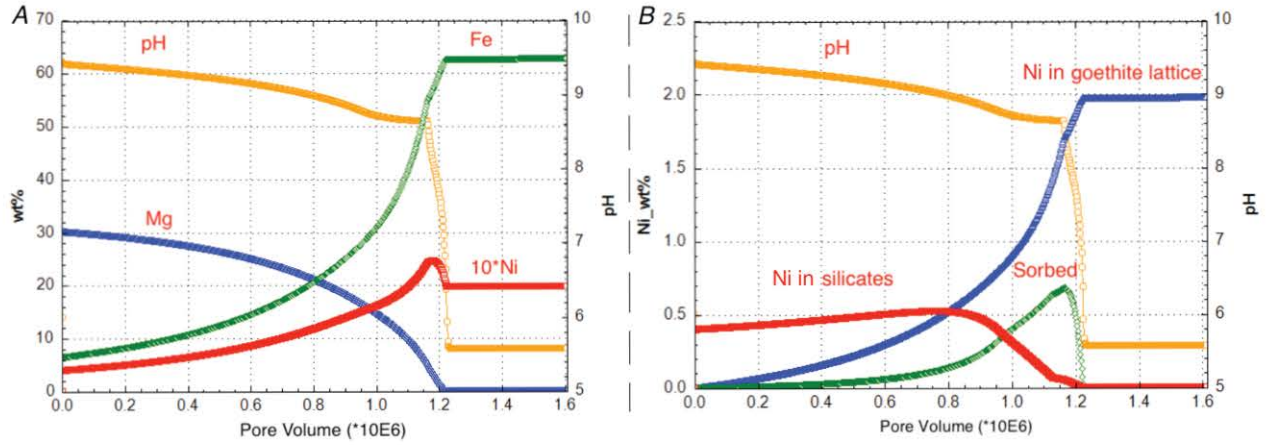


Figure 7: **A** represents the mobility of the elements in a 1-D reactive transport modelling through one cell; supergene enrichment of Ni and its retention by three different mechanisms: i) Sorption on goethite surface, ii) Retention in goethite structure, and iii) Precipitation with Ni-silicates. **B** shows the split (redistribution) of Ni between different retention mechanisms upon the formation of laterite.

Figure 7(A) shows the chemical distribution of the elements in minerals versus pore volume (one million of PV represents one million years). Current reactive transport modelling has been performed through one cell with flux-open boundaries instead of 40 cells column. Incoming solution, olivine content and dissolution rate here are identical to those used in 1-D transport model previously presented and such a test case was done in order to get detailed understanding of the weathering processes in each cell. X-axis in Figure 7 represents pore volumes, which is a number that shows how many times filling solution moved through the cell. Therefore, this axis represents time of evolution of the bedrock until the formation of oxide-rich zone. This way the principal shape Ni enrichment curve in Figure 7(A) can be easily compared to Figure 1. Indeed, we can highlight three zones for Ni enrichment: i) a zone of plateau where Ni co-precipitated with goethite, followed at pH higher than six

by ii) a peak and iii) a decrease up to the value of Ni concentration in parent rock. Of course, since we investigate a cell stand alone, it has not any income of the elements from the upper cells as it was in a column modelling, but the principal shape of Ni enrichment curve will remain the same with some differences in values. This shape, shown in Figure 7(A), is very close to that presented in Figure 1. Similarly as it is observed in the field, the zone of residual laterites (Fig.7(A)) is mostly composed of iron oxy-hydroxides, and Ni, being more mobile, reaches its maximum concentrations at the base of this region. This area is marked by a sharp increase in pH and subsequently MgO content (Fig.7(A)). The latter means that pH appears to be the most important chemical parameter that drives the enrichment of nickel in the weathering profile. Nevertheless, some differences can be spotted in between Figure 7(A) and Figure 1 chemical distributions. First and foremost, as one can see, oxide Ni deposits show a regular decrease of bulk nickel content towards the surface (Fig.1) (*e.g.* Trescases (1973); Wells et al. (2009); Dublet et al. (2012)), while Figure 7(A) with the modelling results represents a stable plateau with value of 2 wt.% of Ni. Dublet et al. (2012) have explained it by ageing of goethite in situ through successive dissolution and precipitation cycles during lateritization. Due to a strong mismatch with  $\text{Fe}^{3+}$  both in terms of ionic radii and valence, nickel, substituted for Fe in goethite, is likely to be expelled during each dissolution/precipitation cycle which leads to purification and increase of crystallinity of goethite. In addition, such a decrease in Ni content might be related to the fact that some part of Ni in nature is also bonded in Mn-oxides (up to 10 %). As far as these Mn-oxides are more soluble than iron oxy-hydroxides, they have been leached from upper limonite zone and, therefore, a consequent drop in Ni grade appears.

Another difference lies in a form of a peak and distribution of Ni concentrations around it. Here, there is a number of possible processes that might have influenced the peak shape making it smoother and wider, namely: diffusion, dispersion, convective flows, kinetics of precipitation of silicates, etc. It is important to note that the shape of nickel enrichment curve represents itself a superposition of different processes of Ni retention that are all evolving in time due to chemical conditions change. In our simulations three different concurrent fates of Ni deposition in a profile were taken into account: i) Ni in a goethite crystal lat-

tice, ii) Ni sorbed on weak and strong goethite sorption sites, and iii) Ni precipitated with silicates (garnierite). Therefore, the superposition that represents the Ni enrichment curve (red line) in Figure 7(A) stands for the sum of these three processes. The contribution of each process in the total Ni enrichment is shown in Figure 7(B).

One can see that nickel mineralization begins with the formation of Ni-silicates at high pH, at the moment when ultramafic bedrock just starts to dissolve. At the same time the precipitation of Ni-goethite occurs, with subsequent adsorption of Ni on its surface. Due to the leaching of the elements out of the cell in course of olivine dissolution and refilling it by slightly acidic meteoric water at each time step, the pH in a modelled cell tends to decrease. Thus, according to the Figure 7(B), at pH value above 9, Ni retention triggered by silicates precipitation prevails over the other processes. Then, the retention of nickel in goethite lattice becomes increasingly important with the maximum achieved at pH 6 and lower. In between these two important mechanisms, there is another one, related to adsorption of Ni on goethite. This process has its specific place during the weathering (Fig.7(B)); it appears where pH is high enough to have sufficient charge of oxide surface to enhance sorption for binding of nickel. At the same time, at the values of pH of 8.5 or higher, it seems to be inhibited by some other process and subsequently replaced by precipitation of Ni-silicate (Fig.7(B)). Therefore, adsorption is being rather a “transitional ore” since being released from silicates the adsorbed nickel further passes to the lattice of goethite or precipitates with it. As it has been noticed previously, the pH front in the nature most likely represents smoother curve due to diffusion, dispersion, convective flows etc., and the window of existence of such a “transitional ore” on the surface of oxides might be geometrically larger. The following subchapter is fully devoted to understanding of adsorption process of nickel alone in batch calculations, as well as in competitive environment of transport modelling.

### *3.2.3. Competition of elements for sorption sites*

According to the results of the 1-D numerical transport modelling, presented in chapter (3.1), adsorption of nickel strongly depends on pH (Fig.5 and 7(B)) and does not appear in limonite zone due to full dissolution of silicates and decrease of pH to the value of rainwater

(*i.e.* 5.6). Indeed, the surfaces of oxides carry a charge that enhances sorption of metals and depends on pH and composition of the solution. Figure 8 represents a batch calculation of nickel distribution among the aqueous phase and strong/weak sorption sites of 0.09 g of goethite, while Figure 9 shows the shape of the sorption edge of  $\text{Ni}^{2+}$  as a function of pH. These calculations are based on the Gouy-Chapman model from Dzombak and Morel (1990) and show the results of distribution for low ( $10^{-8}$  M) and high ( $10^{-4}$  M) nickel concentrations. Concentrations of Ni, representative in our modelling, generally lie in this interval, being lower than  $10^{-6}$  M.

As one can see from both Figures 8 and 9, nickel is more strongly sorbed at high pH values than at low pH values. The shape of the sorption edge is shown in Figure 9 and actually depends on the Ni concentration. At low concentrations (e.g.  $10^{-8}$  M) the pH domain where Ni is sorbed to the surface of goethite increases from pH 8 to 10.5 while at higher concentrations it reduces, general shape of the Ni sorption edge smooths, and the acid branch shifts to the higher pH.

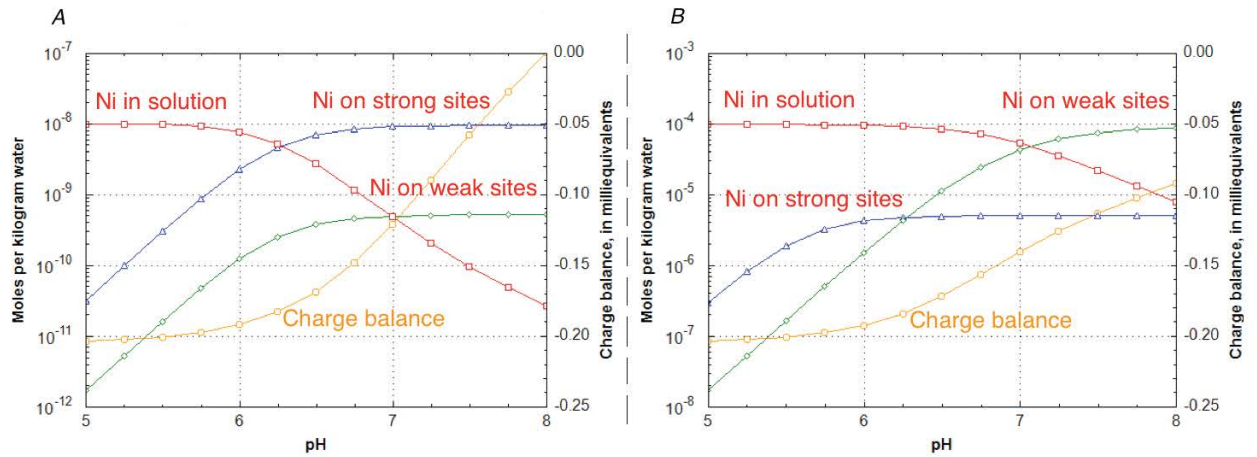


Figure 8: Distribution of Ni among the aqueous phase and strong/weak surface sites of goethite (ferrihydrite) as a function of pH. Picture on the left (**A**) corresponds to low Ni concentration ( $10^{-8}$  M), while **B** represents high Ni concentration ( $10^{-4}$  M). Additional Y-axis represents charge balance of the solution. Solution was prepared with 0.1M NaCl, which permits to use HCl or NaOH as reactant to keep pH increasing, and 90 mg pre-equilibrated ferrihydrite.

This is related to the fact that adsorption of high Ni concentrations also occurs on



weak sites, what can be seen from the Figure 8. Indeed, the distribution of Ni among the solution and sorption sites of goethite does also depend on the Ni concentration. At low concentrations of nickel (Fig.8(A)) the strong binding sites outcompete the weak binding sites over the entire pH range. Therefore, at high pH, most of the nickel resides at the strong binding sites. In case of larger nickel concentrations (Fig.8(B)), the strong binding sites prevail only at low pH.

Surface complexation theory appears to be a useful tool, helping to obtain a conceptual understanding of metal sorption behavior on mineral surfaces. While previous model (Fig.8 and 9) was oversimplified representing closed system, fixed goethite amount, and showing a sorption just for Ni, assumed to be the only metal in solution, the following one deals with competition of metals for sorption sites in a real case. The phenomenon is highlighted in Figure 10, where reactive transport modelling has been performed through one cell with flux-open boundaries as in previous subchapter (3.2.2).

Once the goethite has been formed in the system, adsorption starts to regulate the mobility of metals and retarding their movement. As can be seen in Figure 10, Mg at some point starts occupying weak sites of goethite, attaining maximum at pH of about 9.2 where, as it was shown in Figure 9, nickel, being alone in the system, would have attained its maximum sorption.

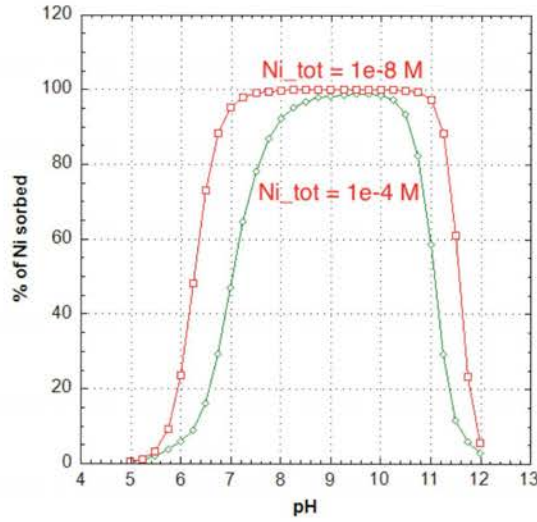


Figure 9: The sorption edge of ( $10^{-8}$  M) and ( $10^{-4}$  M)  $\text{Ni}^{2+}$  at the surface of 0.09 g of goethite (ferrihydrite) as a function of pH in 0.1M NaCl solution.

With the subsequent decrease of pH magnesium releases again into pore water, giving way to Ni adsorption, which has a maximum at pH of 8.5. It appears that at higher values of pH the Ni adsorption is inhibited by Mg binding, which competes with Ni for the sorption sites. At lower ones nickel is released to pore water due to the decrease of surface charge. In this way at pH equal 6 all Ni has left goethite sorption sites, which explains why no Ni sorption occur in the 1-D column (Fig. 5 and 7) before pH front (pH 5.6).

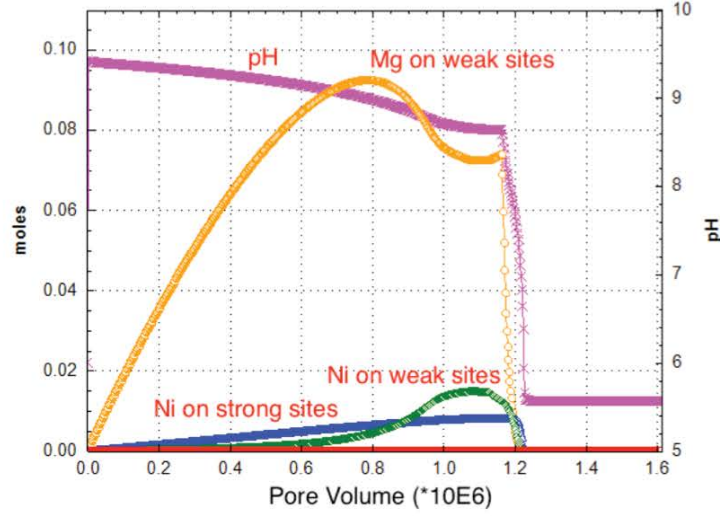


Figure 10: Competition of Mg and Ni for sorption sites of goethite, based on the 1-D transport through 1 cell as in a subchapter 3.2.2.

Thus, to conclude, adsorption of nickel on oxy-hydroxide surfaces (goethite) should not be regarded for Ni alone due to the big influence of other cations releasing during the ultramafic bedrock alteration, in particular Mg. This competition of cations for the sorption sites is to large extent controlled by pH. Adsorption of Ni becomes important in a restricted range of pH around 8, quickly releasing at lower than neutral pH values to pore water and being minor due to competition with Mg at higher ones.

#### 4. Conclusions

The formation of Ni laterite profile from ultramafic parent rock, at 25°C, has been simulated by means of Phreeqc one-dimensional reaction-transport code. The main conclusions are listed below:

- The downward progression of the pH front controls thickening of iron-rich zone, explains the mobility of the elements and governs the Ni enrichment.
- Precipitation of talc-like silicates at the expense of sepiolite-like at 25°C is favored by high pH due to dissolution of still persisting olivine.

- The use of separate silicate phases instead of their solid solutions in the simulations may be considered as reliable since it does not have a drastic effect on the global Ni mass balance.
- Modeling of Ni co-precipitation with goethite explains the presence of Ni in upper limonite zone, where adsorption cannot retain Ni anymore due to acidic pH. The decrease of bulk NiO content towards the surface might be explained by ageing of goethite in situ through successive dissolution and precipitation cycles during lateritization and also by dissolution of Mn oxides.
- Adsorption is being rather a “transitional ore” since after its release from silicates the adsorbed nickel further passes to the lattice of goethite or precipitates with it. The process is fully controlled by pH front and its shape.
- Nickel is more strongly adsorbed at high pH values than at low pH values up to some limit, when alone in the system.
- Adsorption of Ni becomes significant in a narrow range of pH due to the competition of Mg and Ni for sorption sites of goethite surface. Thus, it is of importance to take into account the competition between cations for sorption sites during the ultramafic bedrock alteration

Presented in this paper reactive transport modelling of secondary nickel ore development is rather homogeneous (constant temperature, 1D flow) and aims at understanding the main chemical and hydrological influence on it. Further successive dissolution and precipitation cycles of the minerals during lateritization are very closely tied to inherited ores, tectonics, formation of preferential pathways, lateral movement, change of relief, higher temperatures, that might explain ore distribution heterogeneities observed on many Ni-laterite sites. Therefore, 2D/3D reactive transport simulations will be conducted to assess these aspects based on a coupling approach between geochemistry, hydrodynamics and heat and mass transfer.

## 5. Acknowledgments

This work has been supported by the French National Research Agency through the national program “Investissements d’avenir” with the reference ANR-10-LABX-21-01 / LABEX RESSOURCES21.

## References

- Barrow, N. J., Gerth, J., and Brümmer, G. W. (1989). Reaction kinetics of the adsorption and desorption of nickel, zinc and cadmium by goethite. 2. Modeling the extent and rate of reaction. *J. Soil Sci.*, 40:437–450.
- Brantley, S. L. and Chen, Y. (1995). Chemical weathering rates of pyroxenes and amphiboles. *Reviews in Mineralogy*, 31:119–172.
- Brümmer, G. W., Gerth, J., and Tiller, K. G. (1988). Reaction kinetics of the adsorption and desorption of nickel, zinc and cadmium by goethite. I. Adsorption and diffusion of metals. *J. Soil Sci.*, 39:37–51.
- Butt, C. R. M. and Cluzel, D. (2013). Nickel laterite ore deposits: Weathered serpentinites. *Elements*, 9:123–128. <http://dx.doi.org/10.2113/gselements.9.2.123>.
- Carvalho-e-Silva, M. L. M., Ramos, A. Y., Nogueira Tolentino, H. C., Enzweiler, J., Netto, S. M., and Martins Alves, M. C. (2003). Incorporation of Ni into natural goethite: An investigation by X-ray absorption spectroscopy. *Am Mineral*, 88:876–882. DOI: 10.2138/am-2003-5-617.
- Cathelineau, M., Caumon, M. C., Massei, F., Brie, D., and Harlaux, M. (2015). Raman spectra of Ni-Mg kerolite: effect of Ni-Mg substitution on O-H stretching vibrations. *J. Raman Spectrosc*, 46 (10):933–940.
- Cathelineau, M., Quesnel, B., Gautier, P., Boulvais, P., Couteau, C., and Drouillet, M. (2016). Nickel dispersion and enrichment at the bottom of the regolith: formation of

- pimelite target-like ores in rock block joints (Koniambo Ni deposit, New Caledonia). *Mineralium Deposita*, 51 (2):271–282.
- Cornell, R. M. (1991). Simultaneous incorporation of Mn, Ni and Co in the goethite (  $\alpha$ -FeOOH) structure. *Clay Miner*, 26:427–430.
- Cornell, R. M., Giovanoli, R., and Schneider, W. (1992). The effect of nickel on the conversion of amorphous iron(III) hydroxide into more crystalline iron oxides in alkaline media. *Journal of Chemical Technology and Biotechnology*, 53:73–79.
- Davis, J. A., Fuller, C. C., and Cook, A. D. (1987). A model for trace metal sorption processes at the calcite surface: Adsorption of Cd and subsequent solid solution formation. *Geochim. Cosmochim. Acta*, 51:1477–1490.
- Domènech, C., Galí, S., Villanova-de Benavent, C., Soler, J. M., and Proenza, J. A. (2017). Reactive transport model of the formation of oxide-type ni-laterite profiles (punta gorda, moa bay, cuba). *Mineralium Deposita*, pages 1–18.
- Dublet, G., Juillot, F., Morin, G., Fritsch, E., Fandeur, D., and Brown, J. G. (2015). Goethite aging explains Ni depletion in upper units of ultramafic lateritic ores from New Caledonia. *Geochim Cosmochim Ac*, 160:1–15.
- Dublet, G., Juillot, F., Morin, G., Fritsch, E., Fandeur, D., Ona-Nguema, G., and Brown, J. G. (2012). Ni speciation in a New Caledonian lateritic regolith: A quantitative X-ray absorption spectroscopy investigation. *Geochim Cosmochim Ac*, 95:119–133.
- Dzombak, D. A. and Morel, F. M. M. (1990). *Surface Complexation Modeling:Hydrous Ferric Oxide*. New York, John Wiley and Sons.
- Fischer, L., Brümmer, G. W., and J, B. N. (2007). Observations and modelling of the reactions of 10 metals with goethite: adsorption and diffusion processes. *Eur J Soil Sci*, 58:1304–1315. doi: 10.1111/j.1365– 2389.2007.00924.x.

- Fletcher, R. C., Buss, H. L., and Brantley, S. L. (2006). A spheroidal weathering model coupling porewater chemistry to soil thicknesses during steady-state denudation. *Earth Planet Sci Lett*, 244:444–457.
- Freyssinet, P., Butt, C. R. M., Morris, R. C., and Piantone, P. (2005). Ore-forming processes related to lateritic weathering. *Economic Geology*, 100th Anniversary Volume:681–722.
- Galí, S., Soler, J. M., Proenza, J. A., Lewis, J. F., Cama, J., and Tauler, E. (2012). Ni-enrichment and stability of Al-free garnierite solid solutions: a thermodynamic approach. *Clays Clay Miner*, 60:121–135.
- Gerth, J., Brümmer, G. W., and Tiller, K. G. (1993). Retention of Ni, Zn and Cd by Si-associated goethite. *Z. Pflanzenern. Bodenk.*, 156:123–129.
- Gleeson, S. A., Butt, C., and Elias, M. (2003). Nickel laterites: A review. *SEG Newsletter*, 54:9–16.
- Glynn, P. D. (2000). Solid-solution solubilities and thermodynamics: sulfates, carbonates and halides. *Rev. Mineral.*, 40:481–511.
- Golightly, J. P. (1981). Nickeliferous laterite deposits. *Economic Geology*, 75th anniversary volume:710–735.
- Golightly, J. P. (2010). Progress in understanding the evolution of nickel laterites. *Society of Economic Geologists Special Publication*, 15:451–485.
- Golubev, S. V., Pokrovsky, O. S., and Schott, J. (2005). Experimental determination of the effect of dissolved CO<sub>2</sub> on the dissolution kinetics of Mg and Ca silicates at 25 °C. *Chem. Geol*, 217:227–238.
- Guilbert, J. M. and Park, C. F. (1986). *The geology of ore deposits. 4th ed.* New York : W.H. Freeman.

- Herzberg, C., Asimow, P. D., Ionov, D. A., Vidito, C., Jackson, M. G., and Geist, D. (2013). Nickel and helium evidence for melt above the core-mantle boundary. *Nature*, 493:393–397.
- Jeanpert, J. and Dewandel, B. (2013). Analyse préliminaire des données hydrogéologiques du massif du Koniambo. *Public Report BRGM/RP-61765-FR*, page 102p.
- Johnson, J., Anderson, G., and Parkhurst, D. (2000). Database from thermo.com.v8.r6.230 prepared at lawrence livermore national laboratory. (Revision: 1.11).
- Join, J.-L., Robineau, B., Ambrosi, J.-P., Costis, C., and Colin, F. (2005). Système hydrogéologique d’un massif minier ultrabasique de nouvelle-calédonie. *Comptes Rendus Geoscience*, 337(16):1500–1508.
- Jones, B. F. (1986). Clay mineral diagenesis in lacustrine sediments. *Studies in Diagenesis. U.S. Geol. Surv. Bull.*, 1578:291–300.
- Lebedeva, M. I., Fletcher, R. C., Balashov, V. N., and L, B. S. (2007). A reactive diffusion model describing transformation of bedrock to saprolite. *Chem Geol*, 244:624–645.
- Lelong, F., Tardy, Y., Grandin, G., Trescases, J. J., and Boulange, B. (1976). Pedogenesis, chemical weathering and processes of formation of some supergene ore deposits, in Wolf K.H., ed., supergene and surficial ore deposits. Texture and fabrics. *Handbook of strata-bound and stratiform ore deposits: Amsterdam, Elsevier*, v. 3:93–133.
- McKenzie, R. (1980). The adsorption of lead and other heavy metals on oxides of Mn and Fe. *Aust. J. Soil Res.*, 18:61–73.
- Navarre-Sitchler, A., Steefel, C. I., Sak, P. B., and Brantley, S. L. (2011). A reactive-transport model for weathering rind formation on basalt. *Geochim Cosmochim Acta*, 75:7644–7667 doi:10.1016/j.gca.2011.09.033.
- Nriagu, J. O. (1975). Thermochemical approximation for clay minerals. *American Mineralogist*, 60:834–839.



- Parkhurst, D. L. and Appelo, C. A. J. (2013). Description of input and examples for PHREEQC version 3-A computer program for speciation, batch-reaction, one-dimensional transport, and inverse geochemical calculations. *U.S. Geological Survey Techniques and Methods*, book 6, chap. A43, 497 p., available only at <http://pubs.usgs.gov/tm/06/a43/>.
- Pokrovsky, O. S. and Schott, J. (2000). Kinetics and mechanism of forsterite dissolution at 25°C and pH from 1 to 12. *Geochim. Cosmochim. Acta*, 64:3313–3325.
- Quesnel, B., Boulvais, P., Gautier, P., Cathelineau, M., C dric, M. J., Dierick, M., Agrinier, P., and Drouillet, M. (2015). Formation of silica and magnesite veins in the Massif of Peridotite of Koniambo: Geometric and stable isotopes data. *13th SGA Biennial Meeting 2015. Proceedings*, 3:1189–1192.
- Reddy, B. J., Frost, R. L., and Dickfos, M. J. (2009). Characterisation of Ni silicate-bearing minerals by UV- vis-NIR spectroscopy. Effect of Ni substitution in hydrous Ni-Mg silicates. *Spectrochimica Acta Part A: Molecular and Biomolecular Spectroscopy*, 71(5):1762–1768.
- Schultz, M. F., Benjamin, M. M., and Ferguson, J. F. (1987). Adsorption and desorption of metals on ferrihydrite: Reversibility of reaction and sorption properties of the regenerated solid. *Env. Sci. Technol*, pages 663–669.
- Schwertmann, U. and Murad, E. (1983). Effect of pH on the formation of goethite and hematite from ferrihydrite. *Clays and Clay Minerals*, 31(4):277–284.
- Singh, B., Sherman, D. M., and Gilkes, R. J. (2002). Incorporation of Cr, Mn and Ni into goethite (  $\alpha$ -FeOOH): Mechanism from extended X-ray absorption fine structure spectroscopy. *Clay Miner.*, 37:639–649.
- Soler, J. M. and Lasaga, A. C. (1996). A mass transfer model of bauxite formation. *Geochim Cosmochimi Ac*, 60:4913–4931.

- Soler, J. M. and Lasaga, A. C. (1998). An advection-dispersion-reaction model of bauxite formation. *J Hydrol*, 209:311–330.
- Springer, G. (1974). Compositional and structural variations in garnierites. *The Canadian Mineralogist*, 12:381–388.
- Springer, G. (1976). Falcondoite, nickel analogue of sepiolite. *The Canadian Mineralogist*, 14:407–409.
- Stipp, S. L. S., Hochella, M. F., Parks, G. A., and Leckie, J. O. (1992). Cd uptake by calcite, solid-state diffusion, and the formation of solid-solution: Interface processes observed with near-surface sensitive techniques (XPS, LEED and AES). *Geochim. Cosmochim. Acta*, 56:1941–1954.
- Stoessell, R. K. (1988). 25°C and 1 atm dissolution experiments of sepiolite and kerolite. *Geochimica et Cosmochimica Acta*, 52:365–374.
- Swamy, Y., Kar, B. B., and Mohanty, J. K. (2003). Physico-chemical characterization and sulphatization roasting of low-grade nickeliferous laterites. *Hydrometallurgy*, 69:89–98.
- Thom, J. G. M., Dipple, G. M., Power, I. M., and Harrison, A. L. (2013). Chrysotile dissolution rates: Implications for carbon sequestration. *Applied Geochemistry*, 35:244–254.
- Thorne, R. L., Roberts, S., and Herrington, R. (2012). Climate change and the formation of nickel laterite deposits. *Geology*, 40:331–334.
- Trescases, J. J. (1973). Weathering and geochemical behaviour of the elements of ultramafic rocks in New Caledonia. *Bureau Mineral Res Geol Geophys Dep Mineral Energy Canberra Bull*, 141:149–161.
- Trescases, J. J. (1975). *L’évolution géochimique supergène des roches ultrabasiques en zone tropicale: Formation des gisements nickélifères de Nouvelle-Calédonie: Mémoires ORSTOM (Office de la Recherche Scientifique et Technique Outre-Mer)*. PhD thesis.

- Troly, G., Esterle, M., Pelletier, B., and Reibel, W. (1979). Nickel deposits in New Caledonia: some factors influencing their formation. *International Laterite Symposium, New Orleans*,, pages 85–119.
- Ulrich, M. (2010). *Péridotites et serpentinites du complexe ophiolitique de la Nouvelle-Calédonie*. PhD thesis, Université de la Nouvelle-Calédonie et Université de Grenoble.
- Ulrich, M., Muñoz, M., Guillot, S., Chauvel, C., Cluzel, D., and Picard, C. (2011). Weathering effects on the mineralogical and geochemical composition of the New Caledonia ophiolite. *Goldschmidt Conference*.
- Villanova-de-Benavent, C., Proenza, J. A., Galí, S., García-Casco, A., Tauler, E., Lewis, J. F., and Longo, F. (2014). Garnierites and garnierites: Textures, mineralogy and geochemistry of garnierites in the Falcondo Ni-laterite deposit, Dominican Republic. *Ore Geology Reviews*, 58:91–109.
- Wells, M. A., Ramanaidou, E. R., Verrall, M., and Tessarolo, C. (2009). Mineralogy and crystal chemistry of garnierites in the Goro lateritic nickel deposit, New Caledonia. *Eur. J. Mineral.*, 21:467–483.
- Wilson, M. (2004). Weathering of the primary rock-forming minerals: Processes, products and rates. *Clay Minerals*, 39:233–266.
- Wogelius, R. A. and Walther, J. V. (1991). Olivine dissolution at 25°C - effects of pH, CO<sub>2</sub>, and organic-acids. *Geochim. Cosmochim. Acta*, 55:943–954.

## 2.3 CONDITIONS FOR PRECIPITATION OF TALC-LIKE AND SEPIOLITE-LIKE MINERALS

Highlighted partly in the 1D reactive transport modelling results the issue of talc-like and sepiolite-like minerals formation is further extended in this subsection. The major problem lies in the fact that the typical Ni-laterite profiles of New Caledonia are characterized by the development of talc-like Ni-bearing silicates (kerolite, pimelite) and do not reproduce any (with rare exception) traces of sepiolite material in minerals precipitation sequence (Cathelineau et al., 2015, 2016b). The latter is in contrast to sepiolite-like phases (falcondoite, sepiolite) extensively formed in similar ultramafic environment within the Falcondo weathering profile (Cuba) (Villanova-de-Benavent et al., 2014). The explanation of such a phenomenon may be achieved from the investigation of relative stability domains of Mg/Ni silicates. Figure 2.1 demonstrates the activity diagram with stability fields of secondary magnesium silicates (Table 1, Chapter 2). The reaction pathway represents a gradual dissolution of primary rock (olivine). Kerolite/Pimelite, Sepiolite/Falcondoite and Quartz are allowed for precipitation at achievement of local equilibrium. As can be seen from Figure 2.1 the meteoric fluid (chemical composition from Myagkiy et al. (2017)) upon the contact with olivine quickly arrives to the zone of kerolite stability with transitory formation of sepiolite and quartz. The pH in this case is changing from 5.6 at the first reaction step up to 9.7 after subsequent dissolution of  $10^{-1}$  moles of olivine. As long as sufficient amount of primary dissolving mineral persists within the profile the talc-like phase appear to be the only secondary weathering silicate product. Subsequent consumption of olivine would lead to decrease of pH and a reverse of the reaction pathway through the stability zone of sepiolite followed eventually by quartz precipitation. Therefore, an important conclusion that can be made at this step is the following: at temperature of 25°C talc-like phase should be followed by precipitation of sepiolite and then eventually by quartz upon the pH decrease due to the continuous dissolution of olivine. It should be noted that the reaction pathway in case of serpentine dissolution has exactly the same behaviour as in case of olivine which excludes the influence of degree of serpentinization on mineral succession.

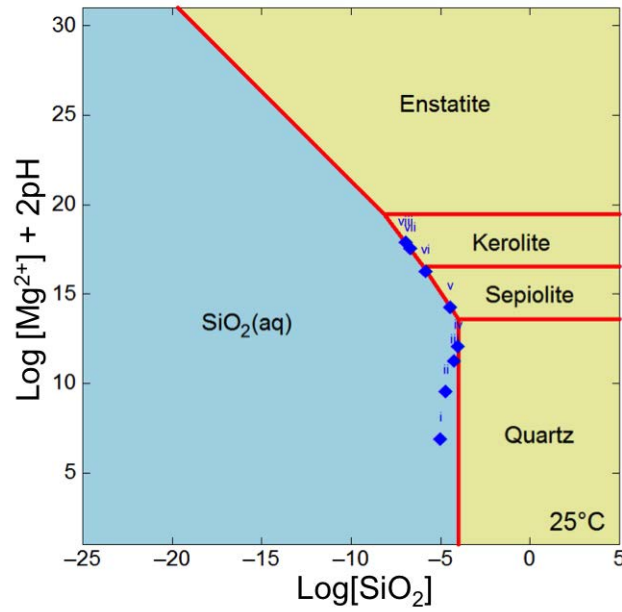


Figure 2.1 – Activity diagram for secondary nickel and magnesium silicates, showing their zones of stability at 25°C. Reaction path represents gradual dissolution of  $10^{-1}$  mol of olivine in 8 steps. Constructed in the Geochemist's Workbench® 11

Paragenesis defined in a diagram (Fig. 2.1) totally reproduces in situ observations of the silicate ore in Falcondo weathering profile which is characterized by the precipitation sequence as follows: kerolite-pimelite, and sepiolite-falcondoite, quartz being the final product (Villanova-de-Benavent et al., 2014). Thus, it can be inferred that these Ni deposits show a classic example of secondary ore development at earth-surface conditions (around 25°C). The latter may put an additional constrain on conditions of type 1 ore formation in New Caledonia which represents the veins with several mineral fillings including serpentine and then talc-like minerals directly followed by quartz (Cathelineau et al., 2016b). The lack of sepiolite in this sequence can be explained by the direct comparison of the activity diagrams at different temperatures. Indeed, as one can see from Figure 2.2 constructed for both Ni and Mg end-members of studied phases, the sepiolite becomes more soluble with the increase of the temperature. Its stability zone continuously shrinks in a size and fully disappears at around 55 – 60°C. At this point falcondoite and sepiolite should be replaced by Ni and Mg talc-like respectively.

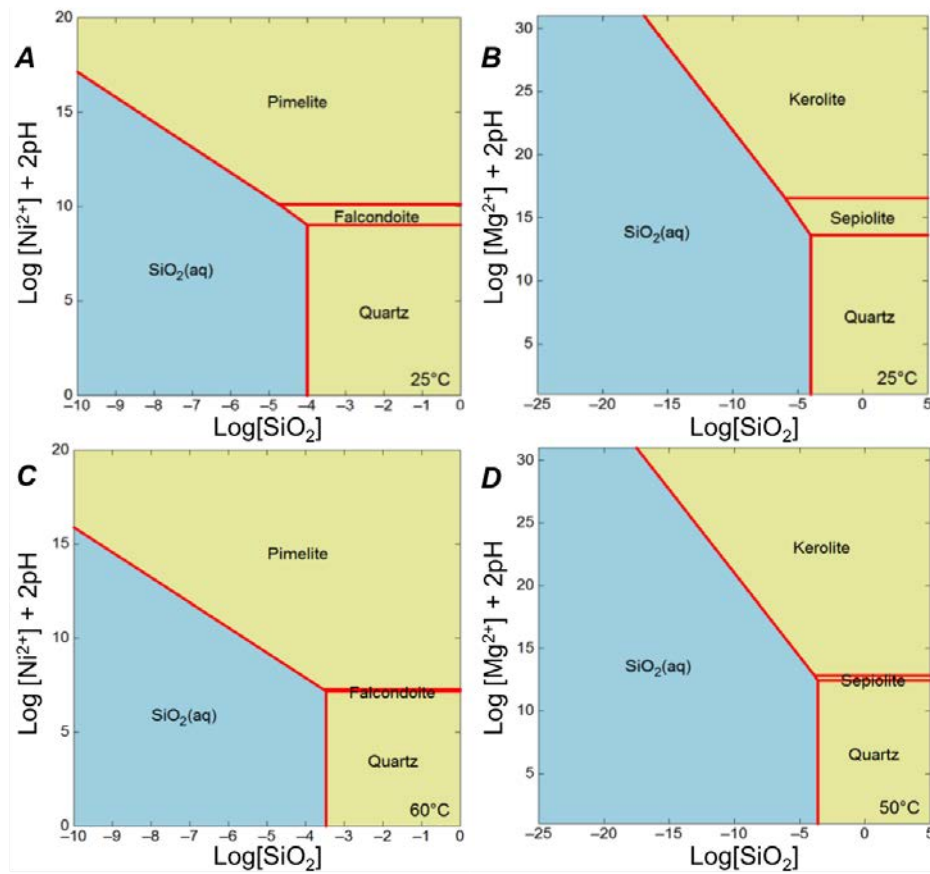


Figure 2.2 – Solvi for secondary nickel and magnesium silicates, showing their zones of stability at 25°C (A-B) and higher temperatures (50 – 60°C) (C-D). Constructed in the Geochemist's Workbench® 11

An analytical expression for the temperature dependence of log K for falcondoite was estimated from sepiolite log K behavior, while those of kerolite and pimelite are estimated from talc. To sum up, i) the talc-like phases alone can be present in a part of profile with still persisting and dissolving olivine (or serpentine), ii) after the complete weathering of olivine to secondary mineral phases, talc-like phase should be followed by precipitation of sepiolite and then eventually by quartz if the temperatures ranges around 25°C, and iii) directly by quartz if temperature exceeds 55 – 60°C.



# REACTIVE TRANSPORT MODELLING APPLIED TO NI ORE DEPOSITS IN NEW CALEDONIA: ROLE OF HYDRODYNAMIC FACTORS AND GEOLOGICAL STRUCTURES ON NI MINERALIZATION.

## CONTENTS

|       |   |    |
|-------|---|----|
| 3.1   | INTRODUCTION . . . . .  | 64 |
| 3.2   | MATERIALS AND METHODS . . . . .   | 66 |
| 3.2.1 | Conceptual model of Saprolitic nickel-ore formation in New Caledonia . . . . .            | 66 |
| 3.2.2 | Physical assumptions and equations governing hydrodynamic system . . . . .                | 68 |
| 3.2.3 | Geochemical system . . . . .  | 70 |
| 3.3   | NUMERICAL MODEL AND VALIDATION . . . . .  | 72 |
| 3.4   | RESULTS AND DISCUSSION . . . . .  | 74 |
| 3.4.1 | 2D reactive transport model of saprolitic deposits formation . . . . .                    | 74 |
| 3.4.2 | Impact of fractures on redistribution of ore deposits . . . . .                           | 77 |
| 3.4.3 | Weathering of peridotite corestone within the set of fractures. Target-like ore . . . . . | 81 |
| 3.5   | CONCLUSIONS . . . . .   | 83 |

THIS chapter is devoted to understanding the influence of hydrodynamics on formation of local mineralizing distributions and laterite development. In our simulations, we coupled the porous media flow in 2D geometry along with mass solute transport and geochemical processes that include precipitation/dissolution of oxide and silicate ores, kinetic dissolution of a primary rock forming mineral as well as sorption model that have an impact on a mobility of Ni. The influence of fractures on hydrodynamics and subsequent redistribution of Ni mineralizations in a profile were investigated. New models including migration of pH dissolution front in 2D within uplifted environments, remobilization and successive redeposition of Ni-silicate ore downslope as well as impacted by fracture, and concentric, so-called "target-like", ore formation were proposed.



### 3.1 INTRODUCTION

Formation of Ni laterite deposits from ultramafic bedrock is a complex geological process involving the interplay of tectonics, climate, hydrodynamics and geochemical reactions (Trescases, 1975; Golightly, 1981, 2010; Butt and Cluzel, 2013). Indeed, the full complexity of chemical and physical phenomena are acting together over the millions of years to shape this composite systems and drive the exceptional Ni enrichment observed locally along the soil profiles nowadays. The hydrolysis and redox reactions are responsible for the destruction of the primary rock-forming minerals and the formation of the secondary minerals of the regolith. After being released the elements (Mg, Ni and Si) are leached from the surface and later may be: i) held within the mineral crystal lattice, ii) bound within a layer of the changing potential field at the interface and iii) mobile in solution, either solvated by the water molecules or "complexed" (Thornber, 1992). Depending on the physico-chemical conditions, the superposition of these possible fates of nickel will define the Ni mineralization.

With its intermediate behavior, being more mobile than iron and less than magnesium, Ni is often found to be concentrated at the base of the lateritic profile and in the saprolite horizon, where it attains economic concentrations (over 1 wt.%). In New Caledonia a typical lateritic profile begins at the top with laterite zone (Fig. 3.1), which is mainly composed of iron oxy-hydroxides (hematite, goethite). This horizon is further replaced by the saprolitic zone that represents an intermediate state of the parent-rock alteration, and hosts the most concentrated Ni ores.

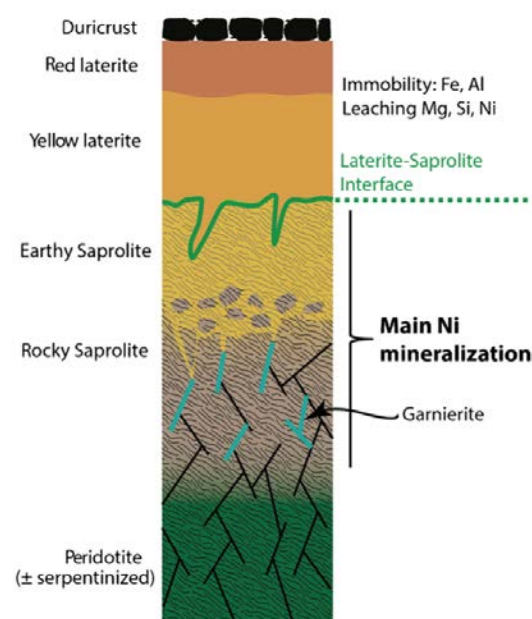


Figure 3.1 – *Typical laterite profile of New Caledonia with different zones developed on ultramafic rocks due to the weathering processes. (Modified from Pelletier, 2003; Ulrich, 2010)*

The current principal genetic model for Ni ores in New Caledonia is based on a classical per-descensum fluid transfer process where most elements (Mg, Ni and Si) are leached from

the surface (Trescases, 1975; Troly et al., 1979; Pelletier, 1996). Transport of Ni is then regarded as a chemically controlled gradual redeposition along the vertical flowline under the propagation of acidic meteoric agent. Nevertheless, a thorough structural and mineralogical investigation over the last decades revealed a complex influence of structures, geomorphological development, and topography on ore distribution (Leguere, 1976; Chevillotte et al., 2006; Cluzel and Vigier, 2008; Villanova-de-Benavent et al., 2014; Quesnel et al., 2017). Some authors propose that neogenic tectonic activity was facilitating supergene alteration by promoting meteoric water circulation and contributed to a local redistribution of nickel in the saprolitic level (Cluzel and Vigier, 2008). The last advances in geometrical modelling of the lateritic cover at Koniambo (west side of New Caledonia) correlated with the metal content in drill cores suggests a huge influence of relief on laterite thickness (Quesnel et al., 2017).

In addition, the presence of local heterogeneity in Ni enrichments, such as concentric zonation of Ni silicates, so-called "target-like ore", first described by Cathelineau et al. (2016b), along with the presence of garnieritic veins, and geological observations demonstrating that the most Ni-rich areas are not usually associated in space to the thickest lateritic body leads to conclusion that formation of the Ni laterite ore deposit has to be regarded as at least 2D process and current per-descensum model, thus, should be revised.

To date only two research papers have been published on reactive transport modelling of the development of a nickeliferous laterites from peridotite. First attempt of making such a model for ultramafic environment was done by Domènech et al. (2017) and Myagkiy et al. (2017) highlighting the main chemical retardation processes for Ni and reproducing in situ observations of Ni-enrichment in vertical lateritic profiles. Providing a detailed understanding of trace elements mobility and weathering process along with powerful chemical basis these models, nonetheless, have a weak point in their 1D hydrodynamic part. Therefore, the idea of coupling state of the art geochemical model with relevant hydrodynamics became an objective of this work. Yet a few coupled geochemical and fluid flow models have been developed to study hydrodynamic impact on locations of deposits in a some mineral-rich terrains in the world. Some of examples concern the formation of gold (Zhang et al., 2008), uranium (Aghbelagh and Yang, 2017) and Pb/Zn deposits (Hobbs et al., 2000), and not covering ultramafic environments. The models are generally studying simple hydrodynamics and restricted by one chemical domain.

Here we test a new concept of ore genesis to explain metal enrichment in saprolites and laterites by taking into account preferential pathways, lateral movement, and topographic influence during the supergene alteration processes. The main objective of this paper is to understand the driving forces of this control and provide an explanation of local mineral-

izing distributions. Therefore, 2D reactive transport simulations were conducted to assess these aspects based on a coupling approach between geochemistry, hydrodynamics and mass transfer. We present investigations of local hydrodynamics control on ore development with particular emphases on: i) the conceptual model of laterite formation based on migration of pH dissolution front within the ultramafic uplifted environment, ii) nickel remobilization of nickel and subsequent redistribution in a profile, iii) impact of fracture on local mineralizing distributions.

## 3.2 MATERIALS AND METHODS

### 3.2.1 Conceptual model of Saprolitic nickel-ore formation in New Caledonia

Formation of mineral deposits often results from interaction between several key processes including structural (faults, fractures, topographic changes), hydrological (fluid flow), thermal (geothermal transport) and geochemical (mineral dissolution and precipitation) impact. Lateritic Ni ore deposits in New Caledonia are not an exception. Here, the stepped-land surfaces suggest that the weathering of laterites originally started on a landscape of low to moderate relief (Lower Oligocene) and further continued as these surfaces were uplifted (e.g. Chevillotte et al., 2006; Sevin et al., 2012). A unidimensional concept of evolution of Ni deposits with their subsequent uplift and redeposition was proposed in a work of Butt and Cluzel (2013). The model implies remobilization of Ni from the oxide zone of uplifted formation due to redissolution of Ni-bearing goethite and its subsequent accumulation in hydrous Mg-Ni silicates deeper in the saprolite (Fig. 3.2a). Nevertheless, none of the present-day Ni ore genesis concepts analyse the hydrodynamic control of Ni-remobilization that constitute an important part of mineralization model.

Here we propose a renewed examination of the per-descensus migration model based on a hydrodynamic study at a deposit scale with the purpose to demonstrate the structural controls associated with the location of nickel-bearing deposits. In coherence with Butt and Cluzel (2013) we assume the development of lateritic and saprolitic horizons began on a flat relief with subsequent downward leaching of the components. Then, in some stage of formation regolith underwent the tectonic uplift that has led to rejuvenation of the topography, formation of new sets of fractures and, thus, change of hydraulic gradients. This latter process modified the behaviour of fluid flow and consequently the direction of chemical solution drainage. As a result, the weathering of this complex system led to the formation of different locally observed Ni enrichments.

The mechanism accounting for the formation the Ni-enriched hotspots was proposed to

be the following. The migration of meteoric fluid along the slope triggered the lateral transfer of mineral constituents, namely Ni, Si and Mg, from upper horizon. These successive dissolution/precipitation cycles driven by movement of pH front eventually led to redeposition of Ni-bearing minerals in the direction of the flow and an increase of Ni grade in the saprolite, especially in downstream of ridges and in low relief zone. In addition, the presence of preferential pathways within the bedrock resulted in partial migration of the fluid into these highly permeable sites. Subsequent oversaturation of the solution with respect to Ni-bearing pimelite within the fractures contributed to the formation of high-grade Ni silicate ore. Another type of local Ni mineralization, also closely associated with fractures network, was formed in joints within the peridotite blocks occurring within the first hundred meters below the surface. This so-called target-like ore represents a concentric zonation of a pimelite and Mg-kerolite with the extension ranges from a few decimetres to one meter. The formation of this ore is closely tied to the fluid penetration and subsequent chemical alteration of the individual blocks within the regular fractures network.

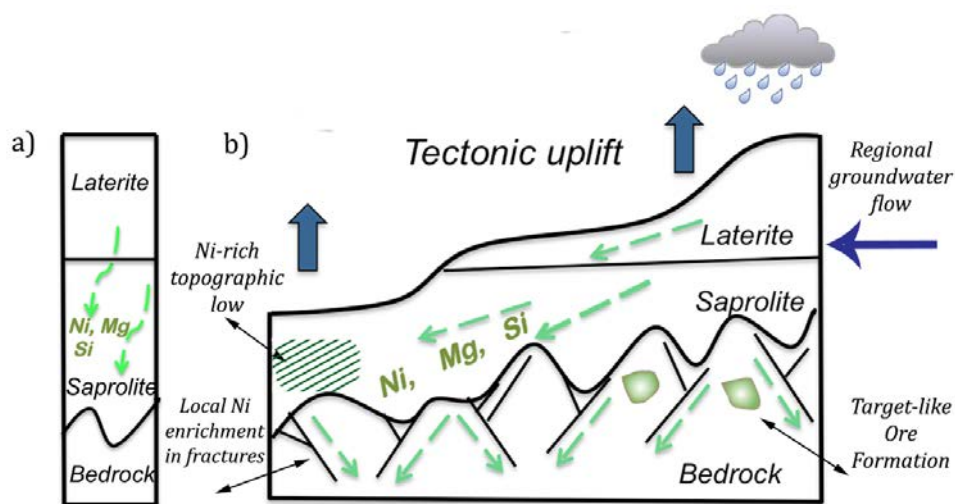


Figure 3.2 – **A)** *Present-day unidimensional concept of redistribution of Ni deposits in uplifted profile according to Butt and Cluzel (2013), and B)* *Proposed conceptual 2D model with formation of different Ni mineralization hotspots after tectonic uplift of regolith*

Presented mineralization model highlights the critical control of geological structures on Ni ore development. In the following, we will pay specific attention to understanding the above discussed local Ni-enriched hotspots, namely: i) topographically controlled increase of Ni grade in the zone of low relief, ii) precipitation of Ni-bearing pimelite within the fractures, and iii) formation of concentric Ni-silicate ore under the control of fractures network. This

numerical investigation will be performed through a three separate multi-component reactive transport models accompanied by the appropriate hydrodynamic system. The models include the analyses of i) the lateral propagation of the dissolution front under the influence of a topographic gradient, ii) the impact of fractures on the fluid hydrodynamics along the profile and the subsequent remobilization of nickel, and iii) the effect of fracture network on weathering and successive dissolution/precipitation cycles within the corestone. The obtained results provide detailed understanding of metal enrichment in saprolites and laterites and further support presented concept of Ni ore genesis.

### 3.2.2 Physical assumptions and equations governing hydrodynamic system

Due to the complicated nature of an ore-forming process, it is very tough to simultaneously simulate the entire mineralizing system and, thus, the model includes several assumptions listed below. First of all, we neglect any mechanical or tectonic deformations that may occur during a mineralization event. Since the time scale of syn-mineralization mechanical deformation is way shorter than that of deposit formation we assume that the syn-mineralization mechanical deformation divides the mineralizing system into two episodes and, thus, simulate pre- and post-deformational one in separate models. Assuming a typical intracontinental geothermal gradient of  $30^{\circ}\text{C}/\text{km}$  (Fridleifsson et al., 2008) and the formation of deposits generally within the first hundred meters below the surface we neglect the temperature changes as its influence on thermodynamic constants will be minor.

As long as the conceptual model is focused on redistribution of Ni minerals within the profile that happened on a time scale after the tectonic uplift of weathered laterite the system should have already underwent the main mass losses up to 80 % due to the downward leaching of Ni, Si and Mg. Together with short modeling time of up to 500 years it leads to negligible possible changes in porosity and permeability within the profile and, thus, not taken into account in simulations. We consider the water table to be close to the ground surface and limit our analysis to the fully saturated region. Finally, we assume the fluid phase as an ideal mixing of highly diluted solutes so that liquid density and viscosity variations can be ignored.

A coupled model considers the concentrations of several species and is able to simulate both, solute transport processes, namely advection and dispersion, and chemical reactions, such as dissolution, precipitation, complexation and adsorption. Equations that govern the hydrodynamic system are represented by the conservative solute-transport equation that describes the time rate of change of solute concentration for a single solute, continuity equation and Darcy flow equation:

In liquid phase:

$$\frac{\partial(\phi \mathbf{c}_l)}{\partial t} + \nabla \cdot (\mathbf{u} \mathbf{c}_l) = \nabla \cdot (\phi \mathbf{D}_l \nabla \mathbf{c}) + R_l^*. \quad (3.1)$$

In solid phase:

$$\frac{\partial((1 - \phi) \mathbf{c}_s)}{\partial t} = R_s^*. \quad (3.2)$$

Continuity equation:

$$\nabla \cdot \mathbf{u} = 0 \quad (3.3)$$

where  $\mathbf{c}_l$  and  $\mathbf{c}_s$  are concentrations per volume of fluid and solid respectively ( $mol.m^{-3}$ ),  $\mathbf{u}$  is the Darcy velocity ( $m.s^{-1}$ ),  $\mathbf{D}_l$  is the local diffusion/dispersion tensor ( $m^2.s^{-1}$ ),  $\phi$  is the porosity ( $m^3.m^{-3}$ ).

Darcy flow is defined as following:

$$\mathbf{u} = -\frac{\mathbf{k}}{\mu} \cdot (\nabla \mathbf{p} - \rho \mathbf{g}) \quad (3.4)$$

where  $\mathbf{k}$  stands for the intrinsic permeability tensor of the medium,  $\mu$  denotes the dynamic viscosity,  $p$  refers to the liquid pressure and  $\mathbf{g}$  is the acceleration of gravity.

Note that the reaction terms  $R^*$  in the Equation 3.1 and 3.2 take into account changes due to both surface complexation mechanism, equilibrium reactions and kinetic dissolution of primary rock (see details in section 3.2.3)

The studied hydrodynamic system reproduces typical laterite profile after the formation was uplifted. Four zones with different hydrodynamic parameters are explicitly defined in the simulation, namely: laterite, saprolite, bedrock and fracture (Fig. 3.2). In New Caledonia, permeability values in the saprolite and laterite layers are high. The present-day permeability values for the coarse saprolite of New Caledonia have been estimated at around  $10^{-13} m^2$  (Join et al., 2005). Effective permeability of the ultramafic bedrock was chosen to be about  $10^{-15} m^2$  but is highly dependent on the fractures density (Join et al., 2005; Jeanpert and Dewandel, 2013). Centimeter-thick fractures presented within the bedrock of New Caledonian profiles were assumed to have a permeability of  $10^{-5} m^2$  in accordance with the cubic law, implying that transmissivity is proportional to cube of the aperture. Further, the local dispersion tensor is assumed to be constant an homogeneous. It will be fixed to  $4 * 10^{-7} (m^2.s)$ . The main physical parameters used in the model are listed in Tab. 3.1.

Table 3.1 – *Physical parameters applied in simulations*

|                                   |          |                                  |
|-----------------------------------|----------|----------------------------------|
| Dynamic viscosity                 | $\mu$    | $10^{-3}$                        |
| Temperature                       | T        | 25°C                             |
| Density                           | $\rho$   | $10^3 \text{ kg.m}^{-3}$         |
| Porosity: Saprolite, Laterite     | $\phi_1$ | 0.4                              |
| Porosity: Bedrock                 | $\phi_2$ | 0.1                              |
| Porosity: Fracture                | $\phi_3$ | 1                                |
| Permeability: Saprolite, Laterite | $K_1$    | $10^{-13} \text{ m}^2$           |
| Permeability: Bedrock             | $K_2$    | $10^{-15} \text{ m}^2$           |
| Permeability: Fracture            | $K_3$    | $10^{-5} \text{ m}^2$            |
| Constant injection rate           | $Q_0$    | $6.3 * 10^{-8} \text{ m.s}^{-1}$ |
| Hydraulic head: upslope           | $H_1$    | 70 m                             |
| Hydraulic head: downslope         | $H_2$    | 20 m                             |
| Length                            | $L$      | 140 m                            |
| Pressure: fracture                | $P$      | $3 * 10^5 \text{ Pa}$            |

Incoming solution reproducing the atmospheric precipitation is introduced at the geometrical top of each modeling case as a constant recharge rate boundary. It has a chemical composition of a slightly acidic tropical rainwater with pH=5.6 due to its equilibrium with atmospheric CO<sub>2</sub>. For our simulations the value of 2000 mm/y of rainfall was chosen as acceptable in accordance with Butt and Cluzel (2013). The boundary conditions, imposed on the left and right part of simulated domain are hydraulic heads with the corresponding values of topographic dimensions. The bottom of bedrock is flux insulated, unless the fracture is introduced. In the latter case, a pressure condition is imposed at the end of the crack. Natural outflow of the fractured system is assumed to occur a few hundred meters below the ground surface.

### 3.2.3 Geochemical system

The geochemical system reproduces typical laterite profile after the formation was uplifted (Fig. 3.2). First simulated profile is represented by three different chemical horizons with relative mineralogical composition of laterite, saprolite and bedrock. The composition is taken in accordance with the results of 1D model (Myagkiy et al., 2017) after 10 Ma of laterite development and minerals are homogeneously spread within each horizon. Distribution of the minerals in the chemical domains is the following: a) lateritic zone is infilled with goethite, b) saprolitic horizon, representing an intermediate step in ultramafic rock alteration, is composed of Ni-rich silicates presented by sepiolite-like and talk-like phases, goethite and partially preserved kinetically dissolving olivine, and c) the bedrock is fully composed of fresh peridotite (olivine). Irregular boundaries between the saprolite and bedrock layers are schematically represented in accordance with in situ observations within the quarries of New Caledonia and caused by the initial sets of fractures in the early stages of ophiolite weathering (Fig. 3.2). Molar fractions of minerals presented in each chemical domain are listed in Tab. 3.2.

Table 3.2 – *Mineral composition of modelled horizons*

| Zone      | Mineral  | Molar fraction |
|-----------|----------|----------------|
| Laterite  | Goethite | 1              |
| Saprolite | Olivine  | 0.184          |
|           | Kerolite | 0.389          |
|           | Pimelite | 0.146          |
|           | Goethite | 0.281          |
| Bedrock   | Olivine  | 1              |

Complementary simulations introduce the presence of fractures in a bedrock. The fractures are modelled as 2D objects of 3.5 cm width which, thus, lead to some limitation on their presented number in a model regarding the computational cost. First we simulate the impact of one fracture of 18 meters within the peridotite on redistribution of Ni ore deposits in saprolite zone. At second, we introduce 4 fractures in a peridotite system that is reproducing the corestones alteration in a regular fractures network within the bedrock horizon.

These latter simulations have also additional chemical domain that is being computed within the fracture. In initial state all the fractures are assumed to be void. The precipitation/dissolution processes are activated in every presented in a model domain, namely laterite, saprolite, bedrock and fracture and considered to occur according to local equilibrium. Olivine composition in the model was selected according to Trescases (1975) as following:  $\text{Mg}_{1.82}\text{Fe}_{0.17}\text{Ni}_{0.01}\text{Al}_{0.006}\text{SiO}_4$  and assumed to be kinetically controlled during the simulation. Specific dissolution rate for olivine was simulated in accordance with research paper of Pokrovsky and Schott (2000). The surface complexation model of Dzombak and Morel (1990), that takes into account binding of metals and protons on both strong and weak sites of goethite, which is present in both laterite and saprolite horizons was kept active as it was proved to have an impact on Ni and Mg mobility (Myagkiy et al., 2017). Chemical calculations were performed at 25°C within the code PHREEQC associated with the *llnl.dat* thermodynamic database (Johnson et al., 2000), that has been edited in order to account for garnierite minerals. The reactions involved in simulations along with minerals allowed for precipitation/dissolution are listed in Tab. 3.3

| Mineral     | Reaction  | Log K                     |
|-------------|---|---------------------------|
| Kerolite    | $\text{Mg}_3\text{Si}_4\text{O}_{10}(\text{OH})_2: \text{H}_2\text{O} + 6\text{H}^+ = 3\text{Mg}^{2+} + 4\text{SiO}_{2(\text{aq})} + 5\text{H}_2\text{O}$   | 25.79 (Stoessell, 1988)   |
| Pimelite    | $\text{Ni}_3\text{Si}_4\text{O}_{10}(\text{OH})_2: \text{H}_2\text{O} + 6\text{H}^+ = 3\text{Ni}^{2+} + 4\text{SiO}_{2(\text{aq})} + 5\text{H}_2\text{O}$   | 11.46 (Nriagu, 1975)      |
| Sepiolite   | $\text{Mg}_4\text{Si}_6\text{O}_{15}(\text{OH})_2: 6\text{H}_2\text{O} + 8\text{H}^+ = 4\text{Mg}^{2+} + 6\text{SiO}_{2(\text{aq})} + 11\text{H}_2\text{O}$ | 30.44 (Stoessell, 1988)   |
| Falcondoite | $\text{Ni}_4\text{Si}_6\text{O}_{15}(\text{OH})_2: 6\text{H}_2\text{O} + 8\text{H}^+ = 4\text{Ni}^{2+} + 6\text{SiO}_{2(\text{aq})} + 11\text{H}_2\text{O}$ | 12.31 (Nriagu, 1975)      |
| GoethiteNi  | $\text{Fe}_{0.98}\text{Ni}_{0.03}\text{OOH} + 3\text{H}^+ = 0.98\text{Fe}^{3+} + 0.03\text{Ni}^{2+} + 2\text{H}_2\text{O}$                                  | 0.53 ( <i>llnl.dat</i> )  |
| Quartz      | $\text{SiO}_2 = \text{SiO}_{2(\text{aq})}$  | -3.99 ( <i>llnl.dat</i> ) |

Table 3.3 – *Dissolution reactions for precipitating minerals with the corresponding equilibrium constants at 25°C .*



### 3.3 NUMERICAL MODEL AND VALIDATION

The coupling between fluid flow and geochemistry was performed using iCP (interface COMSOL-PHREEQC), platform for solving THC (Thermo-Hydro-Chemical) problems (Nardi et al., 2014). It unites the capabilities of both - geochemical code PHREEQC (Parkhurst and Appelo, 2013) and the multiphysics software COMSOL Multiphysics® v. 5.1. The parallelization of chemical reactions is achieved by grouping sets of nodes which are then solved on different threads. The reactive transport equations are solved with a sequential noniterative approach (SNIA) that consists of separately solving the chemical equations and the transport equations (e.g Saaltink et al., 2001). The conservative multicomponent transport is, thus, computed in the first step with COMSOL. Reactive chemistry is evaluated by Phreeqc in a second step. In comparison with an existing iterative scheme, the used noniterative approach does not pose global convergence problems. Nevertheless, it requires a strong control of the time step connecting geochemical and hydrodynamic parts of calculation in order to avoid huge operator-splitting errors (e.g Barry et al., 1996; Carrayrou et al., 2004; Jacques et al., 2006).

In this way, the correctness of the implementation was assessed by solving a test case using iCP. This validation part was performed on a rectangular 2D domain with symmetry conditions on both sides in order to obtain 1D perpendicular flowlines (Fig. 3.3). The results of iCP are then has been compared to the same length column of 1D reactive transport model calculated with Phreeqc code, which is here used to solve both transport and geochemical reactions. Observation point was chosen to be at the last cell of 1D flowline and at the lower boundary in Phreeqc and iCP respectively. Chemical boundaries, mineral composition of the domain, as well as the list of reaction were reproduced from the geochemical conceptual model of peridotite weathering from Myagkiy et al. (2017), on a reduced time-scale which was set as  $10^8$  s (3 years). Thereby, the chemical models and transport pathways were identical in both, iCP and Phreeqc simulations.

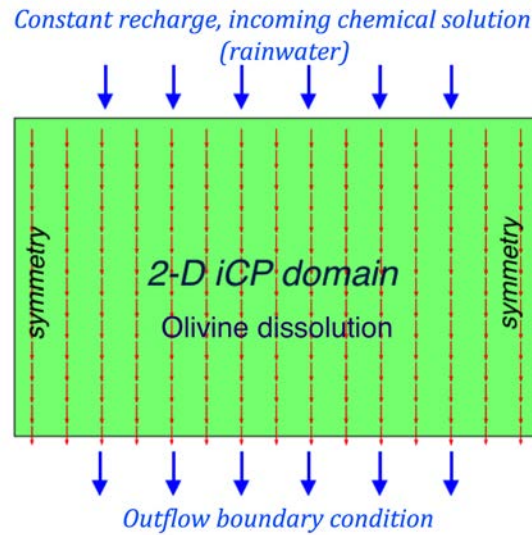


Figure 3.3 – Simplified model used for validation of iCP results.

As the COMSOL Multiphysics is based on the finite element method the concentrations were, therefore, calculated at the nodes. Each node concentration is further passed through the iCP interface to PHREEQC at every communication time step in order to perform the chemical calculations. The validation of the algorithm prior to launching the modeling exercise proved to be of critical importance in coupled simulations with iCP. Indeed, the use of a sequential noniterative approach in combining of Phreeqc and Comsol Multiphysics appeared to be sensitive to the size of communication time steps and required particular attention.

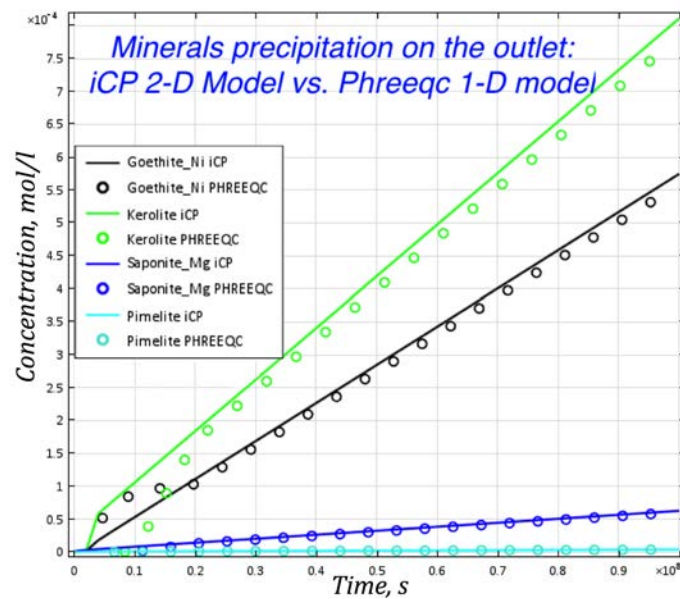


Figure 3.4 – Comparison of the results with iCP and PHREEQC observed at the output of the column for the 1D verification case.

Correct result was eventually achieved with the size of the communication time steps of data exchange between physics (i.e. COMSOL calculations) and chemistry (i.e. Phreeqc calculations), equal to  $10^6$  s. Infiltration of water into the system led to the weathering of initially presented primary rock (olivine) to the secondary minerals: Goethite, Pimelite, Kerolite, Saponite. The evolution of paragenesis at the outlet of the column over the studied time domain of  $10^8$  s is displayed in Fig. 3.4. The results computed with iCP were proved to closely match the solution obtained by using PHREEQC. Further presented simulations were then performed conserving the verified communication step. In the following, the three hotspots of interest for Ni mineralization will be investigated.

### 3.4 RESULTS AND DISCUSSION

#### 3.4.1 2D reactive transport model of saprolitic deposits formation

Most of the deposits in New Caledonia provide classic examples of topographic controls on laterite/saprolite development. The topography of the ultramafic massifs in the southern (Massif Sud) and western part (Koniambo massif) of the main island is the result of the progressive uplift and dismantling of a Tertiary plain (Trescases, 1975; Latham, 1986; Murphy et al., 2005). The uplift may attain a few tens or hundred meters of elevation and terrane often forms V-shaped mountain valleys with slopes of  $> 20^\circ$ . Thickest nickel lateritic zones are preserved on fragments of the uplifted and dismantled peneplain generally localized on topographic highs. In opposite, thin and incomplete laterite profiles were found on low slopes and at their base (Quesnel et al., 2017). In order to reveal the influence of topographic gradients on the formation of laterite and distribution of saprolitic ore deposits let us turn to the results of numerical modelling.

Mineral composition of the simulated domain is chosen in accordance with Table 3.2. Hydraulic heads were imposed on the left and on the right boundary of the domain and correspond to the topographic heights. At first approximation, impact of heterogeneities (fractures) within the bedrock is neglected so that fluid flow in the lower bedrock layer is very slow compared to upper saprolite horizon.

The incoming solution is introduced by slightly acidic tropical rainwater with  $\text{pH}=5.6$  from the top as well as from the right where the regional groundwater flow enters. Chemical outflow of the species out of the domain is imposed on the left profile boundary.

Figure 3.5 shows the evolution of the pH front, the main governing parameter of elements mobility upon the formation of Ni laterite deposits (Domènech et al., 2017; Myagkiy et al., 2017). Compared to the results of 1D reactive transport model which accounts only for

vertical downward propagation of pH dissolution front one can notice that the migration of pH in 2D domain is in contrast tightly shaped by the topographic gradients. Indeed, the results of present study indicate the downslope progression of oxidizing fluid system, that propagates deeper into the formation with time (Fig. 3.5 a, b). Such a topography-driven dissolution front movement is accordingly forcing the leaching and remobilisation of Ni-bearing minerals previously accumulated in the upper part. The exportation of the soluble elements (Ni, Mg and Si) in this way should appear from the right to the left part of the profile in a direction of flow convergence.

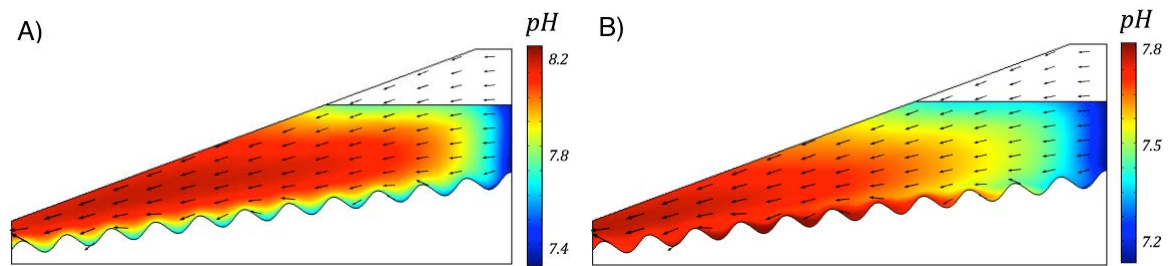


Figure 3.5 – Propagation of pH front in saprolitic layer after A) 50 years and B) 100 years.

The lateral movement of Ni is shown in Fig. 3.6. It can be noticed that the most intense weathering appears upslope of the saprolitic horizon. The latter leads to the progressive dissolution of Ni-bearing minerals, namely pimelite and subsequent release of nickel to the pore water where it is further transported toward a low relief zone to reach favourable conditions for reprecipitation. As the consequence of this process the downward movement of the Ni plume with time, displayed in Fig. 3.6 would result in a constant depletion in nickel concentration within the upper part situated under the lateritic cover. In contrast, transport of Ni with downward moving solution suggests the future formation of most Ni concentrated zones in topographic lows. This downward leaching of the components deeper into the saprolitic formation would also lead to the development of residual laterites faster in the upslope zone.

Such a redistribution of the components by means of lateral migration through successive dissolution-precipitation cycles of secondary minerals highlights a complete difference with classic per-descensum model. Indeed, the vertical development of laterite profile implies formation and further development of Ni-silicate zones directly under the lateritic cover. It would suggest then that the most Ni concentrated locations should form straight under the thickest laterites. Inversely, proposed in this work model of downslope directed lateral migration of the trace elements by successive dissolution/precipitation cycles would define the development of saprolitic zone and Ni enrichment shifted from the main lateritic body toward the topographic low.

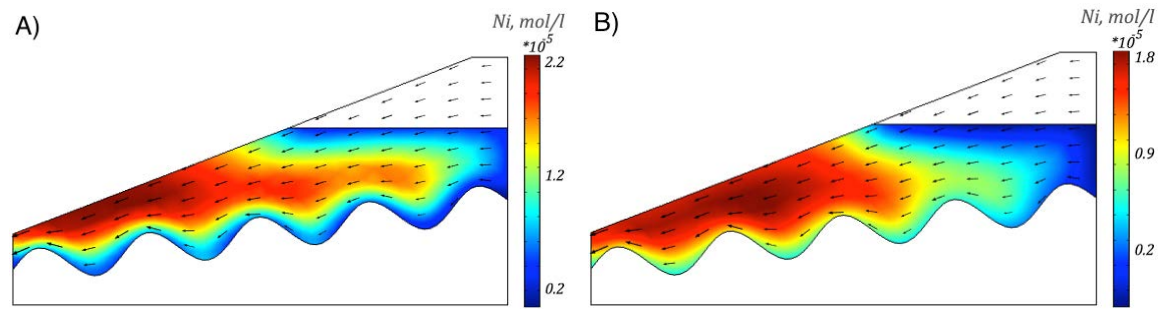


Figure 3.6 –  $Ni$  in solution after A) 50 years and B) 100 years.

Extent of the computational time up to 500 years leads to subsequent increase of Ni-content in a zone of low relief as it was shown in Fig. 3.7 a. Highest Ni concentrations are present mostly along the slope surface, peaking in the lowest topographic part. Moreover, one can observe an additional increase in intensity of olivine weathering within the bedrock horizon in a direction from right to left away from topographic maximum (Fig. 3.7 b). This can be explained by the flow convergence. The fluid maximum speed and circulation in this part has a direct control on the rate of weathering and leads to the most pronounced development of secondary minerals, in particular pimelite toward the topographic low (Fig. 3.7 b).

The lateral redistribution of nickel may at least partially explain the geometry of the laterite nickel deposits. Indeed, the simulation suggests that the fastest formation of laterite occurs on topographic highs with subsequent development of saprolitic zone in a downslope direction. Such an observation is coherent with recent 3D geometrical modeling of lateritic covers along with the analyses of core samples at Koniambo massif (Quesnel et al., 2017). Furthermore, the latter observations additionally proved that the most Ni-rich zones form usually where laterite is thin or absent, while the areas with lowest Ni are located in topographic highs under the thickest lateritic cover. It was additionally proposed by Quesnel et al. (2017) that this process of nickel redistribution may have been probably enhanced by mechanical transport of laterite materials on the slopes.

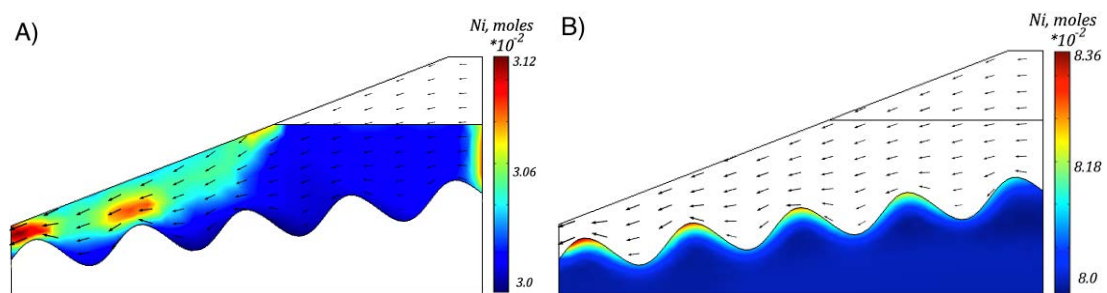


Figure 3.7 – Distribution of total  $Ni$  content (in moles) within the saprolitic zone after 500 years.

The lack of Ni-grade distribution maps for such uplifted profiles complicates the direct

comparison of modeling data with in situ observations. Nonetheless, the results of simulations support the new conceptual model of nickeliferous laterites formation through the consistent lateral transfers of nickel, first proposed by Quesnel et al. (2017) and demonstrate the hydraulic gradient control on the migration of dissolution front within the saprolitic layer. Moreover, it highlights the development of Ni enriched hotspots within the topographic low in both zones: i) saprolite, due to the lateral progression and reconcentration of nickel and ii) bedrock due to the flow convergence and velocity increase enhancing the fluid-rock interactions. The least Ni concentrated regions are then developing in the zones of topographic highs regarding the downslope loss of nickel. It should be noted, that there were no significant changes recorded in the amount of precipitated Ni-bearing phases within the slope range of 20° to 30°, common for New Caledonia. Thus, to conclude the topographic features take an important part of mineralisation model as they govern and shape the dissolution front propagation, control the directions of Ni mineralizing agents and, this way, Ni content redistribution and, therefore, may play an important role in Ni exploration.

### 3.4.2 Impact of fractures on redistribution of ore deposits

The richest Ni silicate ore in New Caledonian Ni deposits, occur in centimeter-thick fractures within the bedrock and saprolite, located several tens of meters to hundred meters below the present-day surface. Compared with saprolite that contains only 2-5 wt% Ni, garnierite veins may grade up to 25-40 wt% Ni. The development of fracture sets enhances the infiltration and mobility of superficial waters and makes room for new material to crystallize. The mineralization of preferential pathways as well as its impact on remobilization of nickel from upper layers will be discussed in this section. For the sake of simplicity and for illustrative purposes, only a single fracture will be considered and impact of fractures network connectivity will be discarded.

The model conserves all the chemical and hydrodynamic boundary conditions from the previous one with the only exception being the fracture present in the bedrock. Permeability of the fracture is set as  $10^{-5} \text{ m}^2$  in accordance with the cubic law, while the hydraulic head imposed at the end of the fracture is in accordance with Table 3.1 and allows outflow of chemical species.

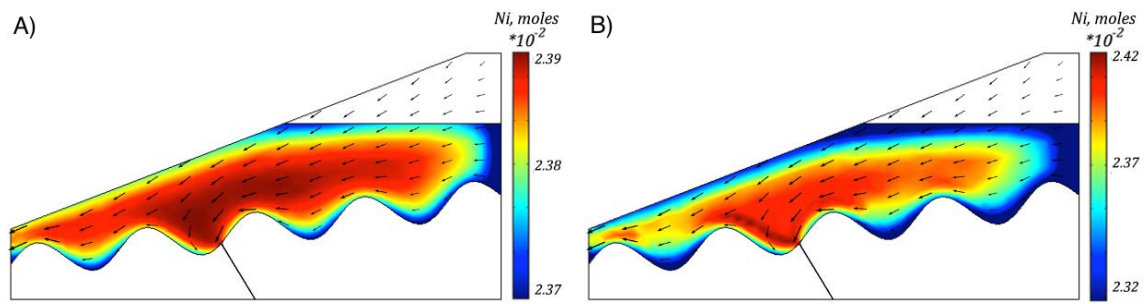


Figure 3.8 – Evolution of total Ni content within the saprolite zone after A) 50 years and B) 100 years

Figure 3.8a displays the redistribution of initially uniformly spread Ni-silicate within the saprolite zone after 50 and 100 years. Flow vectors (arrows) show the influence of fracture presence on local hydrodynamic system in terms of Darcy velocity field. The fracture impact is distinctly marked by divergence of the flow into two primary components. The first one moves the chemically active fluid with dissolved remobilized Ni, Si and Mg toward the preferential pathway. As a result, it leads to an increase of Ni concentration in the vicinity of fracture at the saprolite-bedrock interface (Fig. 3.8b). Eventually as the flow converges in this zone the solutes propagate inwards the fracture through successive dissolution/precipitation cycles. The second component of the flow accordingly moves the solution in the direction of topographic low, downslope where the subsequent increase of Ni-content occurs. Such a formation of Ni mineralization hotspot was discussed in the previous section case. It is only necessary to note that, that the redistribution in between the flow components (and transport) depends on the position of fracture, its length and the location of aquifer discharge defined by the value of hydraulic head at the fracture tip. Thus, lower the discharge than more passive will be the preferential pathway impact on hydrodynamics. Nevertheless, the phenomenon stays the same leading to both formation of deposits i) in low relief zone and ii) within the fractures.

The occurrence of relatively large amounts of nickel silicate in veins makes the investigation of fracture-controlled tectonic drainage an important part of Ni mineralization model. In order to find out how these deposits develop let us turn to geochemical modeling outputs. The presence of the crack in the bedrock would result in the increase of infiltration and mobility of circulating fluids within and in the vicinity of preferential pathway. The latter respectively leads to a significant rise of the weathering rate in this zone and results in a progressive dissolution of primary rock-olivine. Indeed, as one can see from Fig. 3.9 b olivine mostly dissolves along the fracture path with the biggest rate of dissolution at the place where the fluid enters the fracture. Subsequently it results in a formation of secondary weathering product - Ni-bearing pimelite which formation after 100 years of simulated time

is demonstrated in Fig. 3.9 a. Therefore, the increase in the fluid velocity toward the fracture has a direct impact on the dissolution processes and consequent formation of Ni deposits.

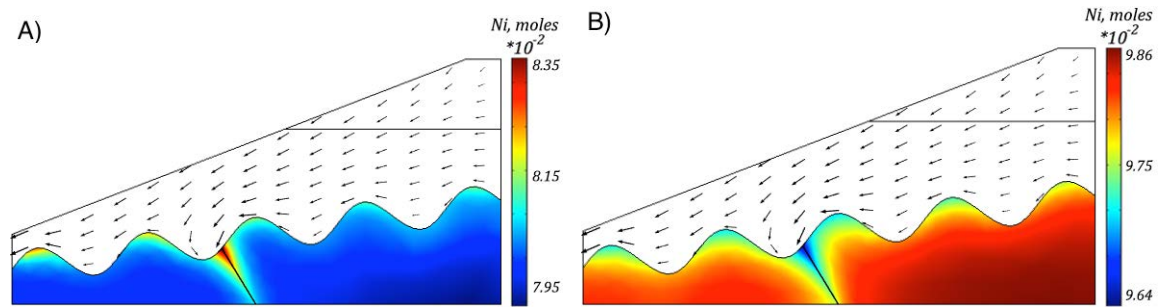


Figure 3.9 – A) *Precipitation of pimelite in the bedrock zone and in the vicinity of fracture.* B) *Dissolution of olivine within the bedrock zone*

Additional cross-section through the fracture may give an insight into the volumes and distribution of Ni ore within this zone. As can be expected the entrance of fluid in the crack leads to the transport of soluble components, in particular Ni, from the upper saprolitic horizon (Fig. 3.8 b) and subsequent oversaturation with respect to pimelite (Fig. 3.10). The effect is enhanced by the dissolution processes that occur on fracture walls presented by olivine material. The impact of fracture presence on a fluid velocity field and weathering rates is discussed above and may lead to the additional enrichment in Ni through the advective/diffusive solute transport from bedrock inward the crack. As a result we can observe precipitation of Ni-bearing pimelite all along the fracture as displayed in Figure 3.10. Still, we note the dramatic decrease in volumes of precipitated material along the fracture's length. Indeed, the biggest precipitation occurs in the very onset of the crack, especially in its first few meters. Then, the amount of precipitated material is gradually and non-linearly reducing while the difference in precipitation between the inlet of the fracture and its tip is further noted to grow with time (Fig. 3.10). Such a phenomenon is caused by the depletion of the dissolved mineralizing components of the fluid at the entrance of the fracture and further enhanced by more intense dissolution of olivine at the upper fracture part (Fig. 3.9).



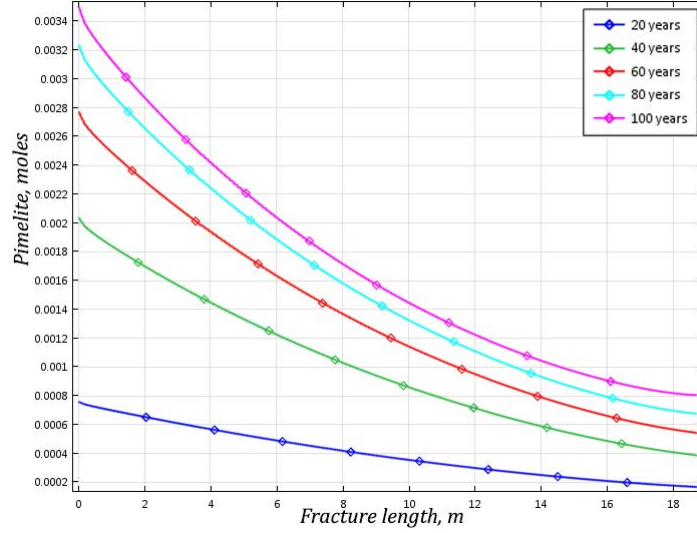


Figure 3.10 – *Precipitation of pimelite within the fracture. Data is presented along the fracture length with time*

Most cracks in New Caledonia are filled with garnierite only, have homogeneous green color, rich in nickel, and most probably have been formed during one single episode of supergene enrichment (Cluzel and Vigier, 2008). Nevertheless, recent study of sets of fractures sealed by Ni-rich silicates and quartz that occur within the fractured bedrock of the New Caledonian regolith revealed a more complex enrichment process through multiple stage formation. It was inferred that most of the veins represented by Ni-Mg kerolite and quartz-hematite materials correspond to stages of cracking and sealing of preexisting fractures probably formed by fluid overpressure (Cathelineau et al., 2016a). Linear extrapolation of modelling results on precipitation within the fracture (Fig. 3.10) would lead to its estimated entire clogging over around 150,000 years during the Ni-stage (i.e. pimelite formation) assuming the density of pimelite as  $2,75 \text{ g/cm}^3$  and, thus, its molar volume ( $V_m = M/\rho$ ) as  $0.18532 \text{ l/mol}$ . Then the fracture is meant to be mechanically reopened again which leads to a new stage of minerals precipitation as discussed in Cathelineau et al. (2016a).

To summarise, the occurrence of supergene nickel ore in fractures is a consequence of both i) nickel-saturated fluid migration through a fractured rock with dissolved mineralizing components from saprolite horizon, and ii) dissolution of bedrock reinforced by the presence of crack that leads to more intense weathering in its vicinity zone. Moreover, the modelling didn't reveal any noticeable chemical dissolutions in goethite-rich lateritic horizon thus making a conclusion that its contribution in remobilized Ni enrichment is minor. This is in opposite to proposed unidimensional concept of Butt and Cluzel (2013) that suggested reactivation of Ni from the oxide zone of uplifted formation due to redissolution of Ni-bearing goethite and its subsequent accumulation in hydrous Mg-Ni silicates deeper in the saprolite

zone. The part of Ni, however, could come from recrystallization of the goethite due to its aging (Dublet et al., 2015).

### 3.4.3 Weathering of peridotite corestone within the set of fractures. Target-like ore

And last but not least, the final model presented in this work is an investigation of the impact of fractures network on weathering processes and mineralizations that occur within the bedrock horizon. More interestingly, this model can easily explain the problem of silicates precipitation process in New Caledonia, namely zonation in silicates. First discriminated by Cathelineau et al. (2016b), similar to a shooting target and that is why called "target-like" (Fig. 3.11 a), this mineralization is characterized by mineralogical concentric zoning that consists of (from edge to the centre): i) a highly oxidized and altered zone, ii) a green pure Ni-rich pimelite zone, iii) a zone (limited to a few centimetres) with a mixture of Ni-poor kerolite and Ni-rich pimelite and iv) a large white Mg-kerolite mineralization zone. Current genetic model of this concentric type of ore proposes the oversaturation of the solution, with respect to silicate due to the water evaporation which occurs when the water table level is low. In this way, increased activities of Ni, Mg, Si in solution may lead to pimelite and kerolite precipitation. In the present work, we propose an alternative formation model of target-like ore based on direct supergene weathering of blocks under fully saturated conditions.

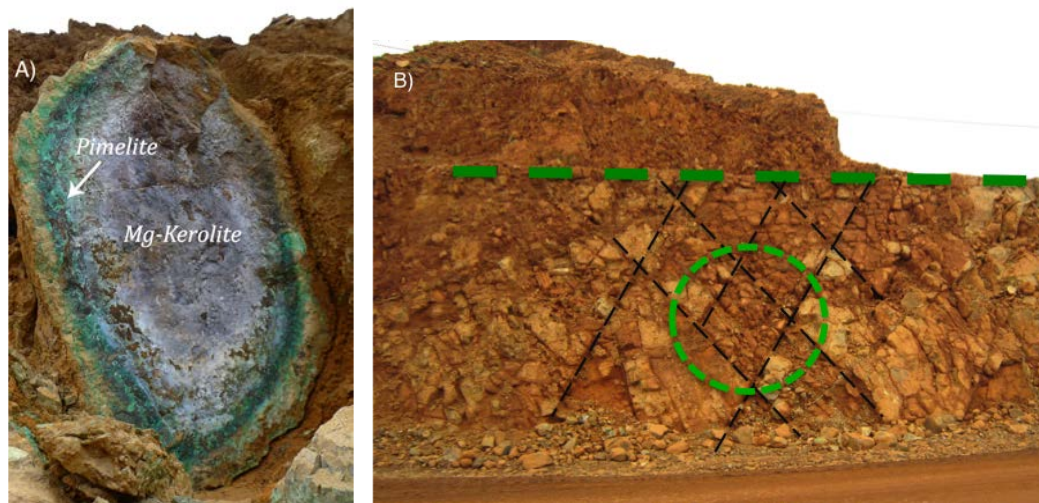


Figure 3.11 – A) Field occurrences of target-like ores and B) Representation of regular fractures network.

Representative element of regular fractures network used to simulate the formation of boulders is displayed in Fig. 3.11 b. The rocky blocks are found within the first hundred meters below the surface and closely associated to the mineralized fractures with pimelite infilling discussed in the previous section. The extension of the blocks ranges from a few decime-

ters to one meter. Initially modelled system represents a fully saturated domain. It contains a pure bedrock presented by olivine and 4 cracks delinating the weathering block. The reactions involved in simulations along with minerals allowed for precipitation/dissolution are listed in Tab. 3.3. The imposed boundary conditions are presented in details in Fig. 3.12 a.

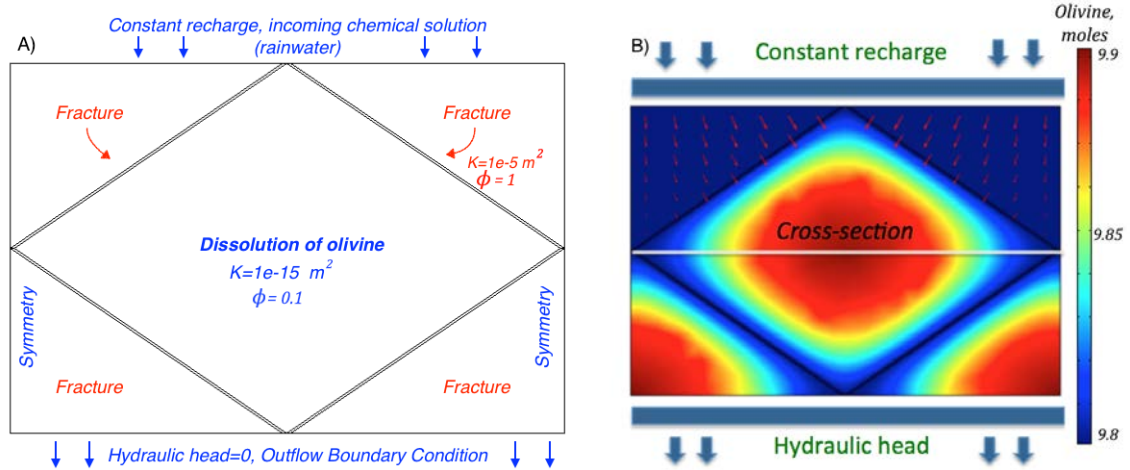


Figure 3.12 – A) Boundary conditions of modelled representative element. B) Weathering of peridotite corestone within the fracture network. Olivine dissolution (in moles) after 30 years.

In Figure 3.12 b, one can observe the result of dissolution of the primary material in a block within the set of fractures and subsequent boulder formation. After 30 years, around 2% of olivine was dissolved resulting in precipitation of goethite, pimelite and kerolite. The impact of cracks system is direct, as it promotes fluid circulation and weathering of the delineated boulder. Mineralization this way occurs toward the centers of the blocks with most intense weathering around the rim. Simulated paragenesis along a boulder cross-section (Fig. 3.13 b) reproduces perfectly the formation of concentric zonation of goethite and Ni-Mg silicates by taking into account i) the respective solubility product of pimelite and kerolite, ii) the geometry of the fracture network, and iii) the solution flow along the fractures.

The precipitation sequence is explained by the pH dependence of the solubility of the minerals. As it is displayed in Figure 3.13 lower pH values of the fluid entering from the edges of the block result in consequent oxidation of the block rim with formation of oxides (goethite) that is followed by precipitation of Ni-Mg silicates, from less soluble Ni-rich pimelite to more soluble Mg-rich kerolite. The sequence is controlled by thermodynamic constants that are listed in Tab. 3.3.

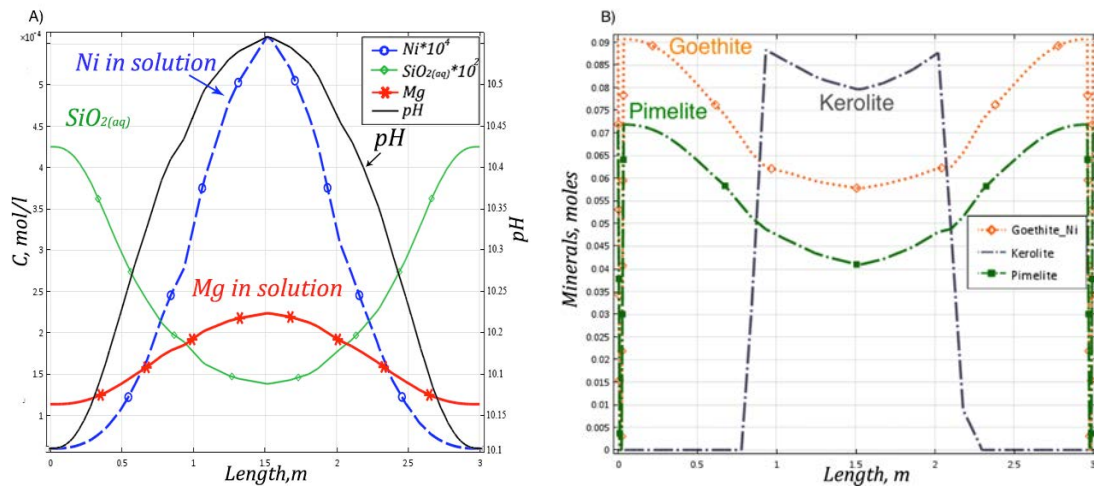


Figure 3.13 – Simulation results after 30 years. A) pH values and chemical composition of the fluid along a boulder cross-section. B) Secondary mineral precipitations along a boulder cross-section.

Concentration of Ni dissolved in solution has a shape which is similar to pH distribution along a boulder cross-section (Fig. 3.13 a). Indeed, being released by dissolution of olivine nickel attains its maximum concentration at the center of the block with minimum values at the edges. The latter is caused by the largest precipitation of Ni-bearing pimelite at the external layer of the boulder (Fig. 3.13 b) that prevails over dissolution of olivine. On the contrary, aqueous silica concentration in solution is dramatically decreasing toward the center of the block. Such an effect is enhanced by simultaneous precipitation of both pimelite and kerolite in the vicinity of block center that leads to the minimum concentration of silica in this area. Finally, Mg concentration which is upon initial inspection should be in accordance with precipitation of kerolite (Fig. 3.13 b) and, thus, should decrease towards the center, demonstrates the reverse behavior. Indeed, one can notice an increase in concentration of magnesium from  $1.12 \cdot 10^{-4} \text{ (mol.l}^{-1}\text{)}$  up to  $2.2 \cdot 10^{-4} \text{ (mol.l}^{-1}\text{)}$  when approaching the center of the block (Fig. 3.13 a). The latter may be explained by relatively low concentration of magnesium contained in incoming solution  $4.1 \cdot 10^{-5} \text{ (mol.l}^{-1}\text{)}$  (Chapter 2, Figure 3) that penetrates from the fractures into the delineated boulder. Subsequent mixing with infiltrating fluid, therefore, results in observed decrease in Mg in the vicinity of block rim.

### 3.5 CONCLUSIONS

Presented mineralization model provides a new concept of ore genesis to explain metal enrichment in saprolites as well as within the fractured bedrock zone, taking into account preferential pathways, lateral movement, and topographic influence during the supergene alteration processes. In contrast to metallogenic models developed for New Caledonian deposits, namely per-descensum formation with vertical downward leaching of mineralizing

components it highlights a critical control of geological structures on Ni ore development. This renewed examination based on a hydrodynamic and geochemical study allowed to provide a numerical explanation of the distinguished in situ main Ni-enriched hotspots observed in the profiles of New Caledonia. First, the simulations suggest that the lateral progression of the pH front in uplifted profiles is tightly shaped by geometry of weathering zones and its propagation deeper in the saprolite leads to a faster development of lateritic horizon upslope with subsequent leaching of soluble components, in particular Ni in a downslope direction. The latter results in increase of the nickel content of the saprolite located in the slope zones and topographic lows which further supports the concept of lateral Ni migration proposed by Quesnel et al. (2017) based on the borehole dataset coupled with 3D geometrical model of nickel laterite ore deposit. Second, the modeling revealed a direct impact of presence of the preferential pathways within the bedrock on redistribution of the flow and, thus, on a transport of mineralizing components with subsequent enrichment within the fractures. The phenomenon was additionally found to be enhanced by the dissolution processes that occur in the vicinity of fracture and lead to the entrance of dissolved elements inward the fracture from bedrock. Third, the modeling of a system that is reproducing the corestones alteration in a regular fractures network within the bedrock horizon revealed the direct impact of cracks system on mineralization processes, as it promotes fluid circulation and increase the intensity of weathering of the delineated boulder. The results of the mineral paragenesis within the rocky block allowed to propose a new model of concentric ore formation in a fully-saturated media.

To sum up, mineralizing processes including remobilization, chemical solution drainage, and ore formation are strongly linked with the hydrodynamics of studied profiles. The present-day distribution of minerals within the regolith of New Caledonia appears thus as the result of complex superimposed chemically and structurally controlled processes acting simultaneously and shaping the Ni ore deposits to its current form. Developed conceptual model is certainly simpler than the real flow system in the profiles, but captures the important overall features of the real system. Thus, the presented model further can be extended to simulation of specific geological structures at the deposit scale and may be of a great help in mineral prospecting and forecasting the distribution of future resources by mining companies

# CONCEPTUAL MODEL OF MULTISTAGE FRACTURE FILLING DUE TO THE FLUID OVERPRESSURE. EVIDENCES OF LOW-TO-MEDIUM-TEMPERATURE HYDROTHERMAL FLUID CIRCULATION DURING THE FORMATION OF THE NI SILICATE VEINS

4

## CONTENTS

|   |    |
|---|----|
| 4.1 ARTICLE 3. MULTISTAGE CRACK SEAL VEIN AND HYDROTHERMAL NI EN-<br>RICHMENT IN SERPENTINIZED ULTRAMAFIC ROCKS (KONIAMBO MASSIF,<br>NEW CALEDONIA) . . . . . | 86 |
|---|----|


THIS chapter propose a new conceptual model of formation of Ni silicate veins with multiple infillings, namely Ni-rich silicates and quartz within saprock of the New Caledonian regolith. Based on the quantitative analyses of the breccia samples found in faults from bedrocks of New Caledonia as well as on the oxygen isotopic composition of microcrystalline quartz which ends the main stage of formation of Ni-Mg kerolite it was inferred that the great part of Ni-silicate fracture infillings were formed during a series of fluid-assisted fracturing and brecciation process triggering the upward medium temperature fluid convection and subsequent fluid mixing with mineral deposition. Thus, most of the veins sealed by Ni-Mg kerolite and quartz-hematite correspond to stages of cracking and sealing of preexisting fractures. In addition the mechanism for the precipitation of the goethite microcrystalline quartz was proposed including divalent iron migration in a reduced environment. The present-day distribution of minerals, thus, in part appears as the result of complex superposition of hydrothermal and supergene processes and can not be interpreted by simple downward migration of a nickel front during the main stage of laterite formation.

4.1 ARTICLE 3. MULTISTAGE CRACK SEAL VEIN AND HYDROTHERMAL NI  
ENRICHMENT IN SERPENTINIZED ULTRAMAFIC ROCKS (KONIAMBO  
MASSIF, NEW CALEDONIA)



ARTICLE

# Multistage crack seal vein and hydrothermal Ni enrichment in serpentinized ultramafic rocks (Koniombo massif, New Caledonia)

Michel Cathelineau<sup>1</sup>  · Andrey Myagkiy<sup>1</sup> · Benoît Quesnel<sup>2</sup> · Marie-Christine Boiron<sup>1</sup> · Pierre Gautier<sup>2</sup> · Philippe Boulvais<sup>2</sup> · Marc Ulrich<sup>3</sup> · Laurent Truche<sup>1</sup> · Fabrice Golfier<sup>1</sup> · Maxime Drouillet<sup>4</sup>

Received: 15 February 2016 / Accepted: 17 October 2016  
© Springer-Verlag Berlin Heidelberg 2016

**Abstract** Sets of fractures and breccia sealed by Ni-rich silicates and quartz occur within saprock of the New Caledonian regolith developed over ultramafic rocks. The crystallization sequence in fractures is as follows: (1) serpentine stage: lizardite > polygonal serpentine > white lizardite; (2) Ni stage: Ni-Mg kerolite followed by red-brown microcrystalline quartz; and (3) supergene stages. The red-brown microcrystalline quartz corresponds to the very last stage of the Ni sequence and is inferred to have precipitated within the 50–95 °C temperature range. It constitutes also the main cement of breccia that has all the typical features of hydraulic fracturing. The whole sequence is therefore interpreted as the result of hydrothermal fluid circulation under medium to low temperature and fluctuating fluid pressure. Although frequently described as the result of a single downward redistribution of Ni and Mg leached in the upper part of the regolith under

ambient temperature, the Ni silicate veins thus appear as the result of recurrent crack and seal process, corresponding to upward medium temperature fluid convection, hydraulic fracturing and subsequent fluid mixing, and mineral deposition.

## Introduction

The genesis of lateritic Ni deposits developed over ultramafic rocks is generally considered as the result of multi-phase development through a weathering process where most elements (Mg, Ni, and Si) are leached from the surface and are redeposited at the base of the regolith profile (Trescases 1975; Golightly 2010; Butt and Cluzel 2013; Freyssinet et al. 2005). Recent works on lateritic Ni deposits worldwide have emphasized the complexity in time and space of the distribution of Ni-

Editorial handling: B. Orberger

✉ Michel Cathelineau  
michel.cathelineau@univ-lorraine.fr

Andrey Myagkiy  
andrey.myagkiy@univ-lorraine.fr

Benoît Quesnel  
benoit.quesnel@univ-rennes1.fr

Marie-Christine Boiron  
marie-christine.boiron@univ-lorraine.fr

Pierre Gautier  
pierre.gautier@univ-rennes1.fr

Philippe Boulvais  
philippe.boulvais@univ-rennes1.fr

Marc Ulrich  
mulrich@unistra.fr

Laurent Truche  
laurent.truche@univ-lorraine.fr

Fabrice Golfier  
fabrice.golfier@univ-lorraine.fr

Maxime Drouillet  
mdrouillet@koniambonickel.nc

<sup>1</sup> Université de Lorraine, CNRS, CREGU, GeoRessources Lab., 54506 Vandoeuvre-lès-Nancy, France

<sup>2</sup> Géosciences Rennes, Université Rennes 1, UMR 6118 CNRS, 35042 Rennes Cedex, France

<sup>3</sup> IPGS-EOST, UMR 7516, Université de Strasbourg, Strasbourg, France

<sup>4</sup> Service Géologique, Koniombo Nickel SAS, 98883 Voh, Nouvelle Calédonie, France



rich silicates and their possible role in the distribution of Ni in the saprock or in the overlying horizons (yellow limonite) (Wells et al. 2009; Dublet et al. 2012). Thus, nickel is thought to be redeposited after its leaching from rock-forming minerals in the upper laterite horizons, either in the fine-grained laterite where goethite is the main Ni-bearing mineral phase, the so-called “lateritic ore,” or below the laterites, in the rocky saprolite level, where it occurs in several mineral phases including goethite (Chen et al. 2004; Dublet et al. 2012) and silicates (serpentine, talc-like, and sepiolite) (Wells et al. 2009; Villanova-de-Benavent et al. 2014; Cathelineau et al. 2015a; Fritsch et al. 2016). The evolution of goethite, in particular its dissolution/recrystallization, is thought to have a crucial role in the downward Ni redistribution and enrichment (Dublet et al. 2015; Wells and Ramanaidou 2015). In the saprock and the bedrock below, Ni-rich silicate phases occur frequently as successive mineral fillings in fractures.

Although a series of detailed crystal chemistry studies on Ni-serpentine and talc-like phases were performed from the 1970s and 1980s by Brindley and co-authors (Brindley and Hang 1973; Brindley and Wan 1975; Brindley et al. 1979) by XRD and then by Manceau and Calas (1985, 1986) using EXAFS, little is known about the genetic conditions of formation of the Ni silicate occurring in fractures, such as the temperature, the fluid pressure, and the relationships with tectonics. In New Caledonia, the fracture sets filled by garnierite were investigated in several pioneering works such as those from Leguéré (1976) and then Fandeur (2009), at Koniambo, and Cluzel and Vigier (2008) at the scale of the island. In the Koniambo deposit, Cathelineau et al. (2015a) discriminated two main types of Ni silicate occurrences in fractures within the saprock: (i) type 1 ore which represents the veins with several mineral fillings including serpentine, talc-like minerals, and quartz and (ii) type 2 ore, called target-like, which consists of an external rim of green pimelite around an internal zone composed of white kerolite. All these ore types are probably not synchronous, and the long-lived processes may probably explain the confusion establishing the relative timing of mineral crystallization. The vein-hosted Ni concentration represents local very high Ni values, which were exploited at the beginning of the twentieth century but which account only as a few percent of the present-day ores. However, they are of prime interest as they represent a preconcentration which is fault controlled and is redistributed within several other ore types: (i) target-like ores, thought to be related to hydration-dehydration cycles which provoke successive saturation with respect to talc-like phases, also called kerolite, especially the two end members of the solid solution (pimelite ( $\text{Ni}_{100}$ )-kerolite ( $\text{Ni}_0$ )) in joints (Cathelineau et al. 2015a), and (ii) the complex red saprolitic ores, which contain relics of all early Ni silicates (vein hosted and target-like) and a fine-grained material dominated by oxyhydroxides.

The genesis of the ore type 1, localized in fractures, is still poorly understood. Cluzel and Vigier (2008) provide the first

attempt to link tectonics and mineral formation, which emphasized that a part of the vein fillings might be considered as “syntectonic.” However, the relative timing of mineral crystallization in the vein and the physical-chemical conditions of their formation remain insufficiently studied to define a consistent genetic model.

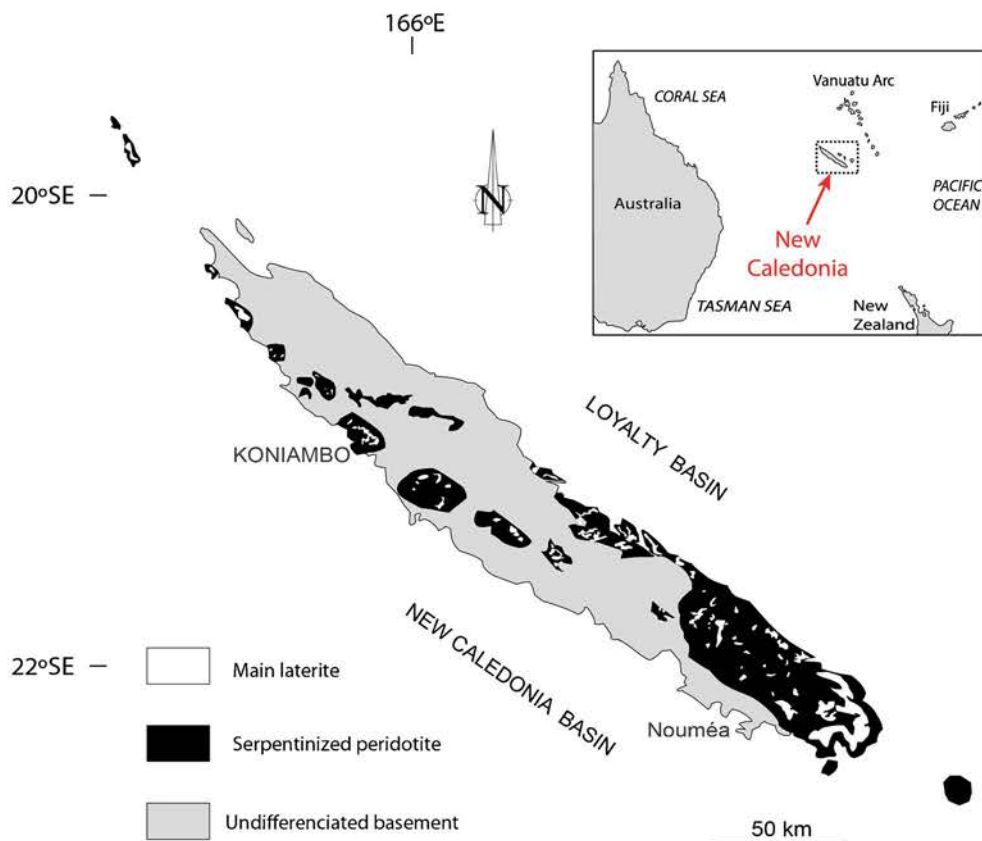
The objective of this paper is therefore (i) to propose a mineral sequence for type 1 veins, especially the spatial and time relationships between silicates: serpentine polymorphs and talc-like minerals, which are the main Ni-bearing silicates and quartz, and (ii) to evaluate the conditions of paleo-fluid circulation, which led to their formation. Exceptional samples preserved from hydrolysis and oxidation were collected in the open pits from the Koniambo massif in order to establish a complete sequence of fracture filling. Detailed in situ mineral determination using a combination of complementary analytical techniques (optical and electron microscopies, Raman spectroscopy, electron microprobe, and laser ablation (LA)-ICP-MS) and a new mineral sequence allow to propose a new genetic model of the Ni silicate vein formation.

## Geology of the site

Ni deposits in New Caledonia (Fig. 1) represent 11 % of the world Ni reserves and 8 % of the nickel production in 2015 (USGS 2016). These deposits are developed on ultramafic massifs, which represent relicts of an obducted peridotite nappe (Fig. 1). The Koniambo massif is one of the klippe occurring along the northwestern coast. The south-westward emplacement of the Peridotite Nappe is considered to have occurred at ca. 35 Ma (Cluzel et al. 2001, 2012; Paquette and Cluzel 2007; Maurizot et al. 2009). Outcropping serpentized peridotites (Fig. 2) were weathered under tropical climate generating a thick lateritic cover (Trescases 1975). The Koniambo massif is characterized by steep slopes and sharp reliefs culminating at around 850 m above sea level. Current enhanced chemical and mechanical erosion, through the constant water runoff and hydrolysis of the peridotite minerals (olivine and pyroxene) predominates, in particular, on the highest topographic levels (Chardon and Chevillotte 2006). Laterite facies occur as relicts, sometimes preserved and perched at the highest altitudes, and in other cases as collapse or creep sediments in the slopes, following the models from Chardon and Chevillotte (2006). Paleomagnetic ages (around 25 Ma) obtained on lateritic duricrust from Tiebaghi area, north of the Koniambo area, suggest that the main laterite formation has taken place rather early, from the late Oligocene to the Miocene, but was then successively dismantled (Chardon and Chevillotte 2006; Sevin et al. 2012).

The Koniambo massif has been exploited intermittently since the end of the nineteenth century, and at the end of the

**Fig. 1** a Simplified geology map of the New Caledonia modified after Cluzel et al. (2001). The laterites are compiled from Paris (1981).



twentieth century by Société minière du Sud Pacifique (SMSP), and is now exploited by SMSP-XSTRATA Nickel (Koniambo Nickel SAS). The deposit hosts around 158.6 million tons of saprolite that grades 2.47 % Ni at around the 2 % cutoff grade (XStrata 2012). It offers good outcrops, e.g., a series of open pits, old ones, such as the so-called “Carrière des anciens” (“elders” open pit) or the test pit, and new ones, such as Pit Cagou, and other open pits covering from south-east to north-west a great part of the ore deposit (Fig. 2), including the south-eastern locality named Trazy. Open pits offer a good vertical cross section from bedrock to saprock, with the possibility to observe and sample veins preserved from the supergene alteration and oxidation in the bedrock below the saprock. The most representative fractures, in particular those from the elders and Cagou pits, exhibit either monomineral fillings (Fig. 3) or series of various Mg(Ni)-hydrous silicates (Fig. 4) corresponding to a succession of cracking and sealing events. These fractures belong to ore type 1 and are different from joints, so-called target like with a rim of pimelite around Mg-kerolite (Cathelineau et al. 2015a).

### Analytical methods

Structural description and measurements of most Ni silicate joints and fractures were carried out in the open pits along

measurement lines, which are the main walls of the open pits. The wall being oriented at random, there is no bias in the measurement lines, such as preferential counting of specific directions. Representative samples were taken in oriented fractures. Minerals were identified on polished thin sections using a multi-analytical characterization. Raman spectroscopy was used to identify the serpentine and kerolite series as well as SiO<sub>2</sub> polymorphs; scanning electron microscopy (SEM) and transmission electron microscopy (TEM) were used to examine the textures and chronological relationships between the minerals. The in situ chemical analyses were performed using wavelength-dispersive X-ray spectroscopy (WDS SEM) analysis and quantitative electron microprobe analysis. LA-ICP-MS was used to measure trace elements in quartz.

### Microscopy

After careful examination of the samples by optical microscopy using a transmitted and reflected light microscope, SEM analyses were carried out on polished thin sections with a JEOL SEM, equipped with an energy-dispersive spectrometer using a Si (Li) semiconductor detector and a HITACHI S-4800 SEM at Service Commun de Microscopies Electroniques et de Microanalyses X (SCMEM) (Nancy, France), in order to establish the mineral paragenesis.

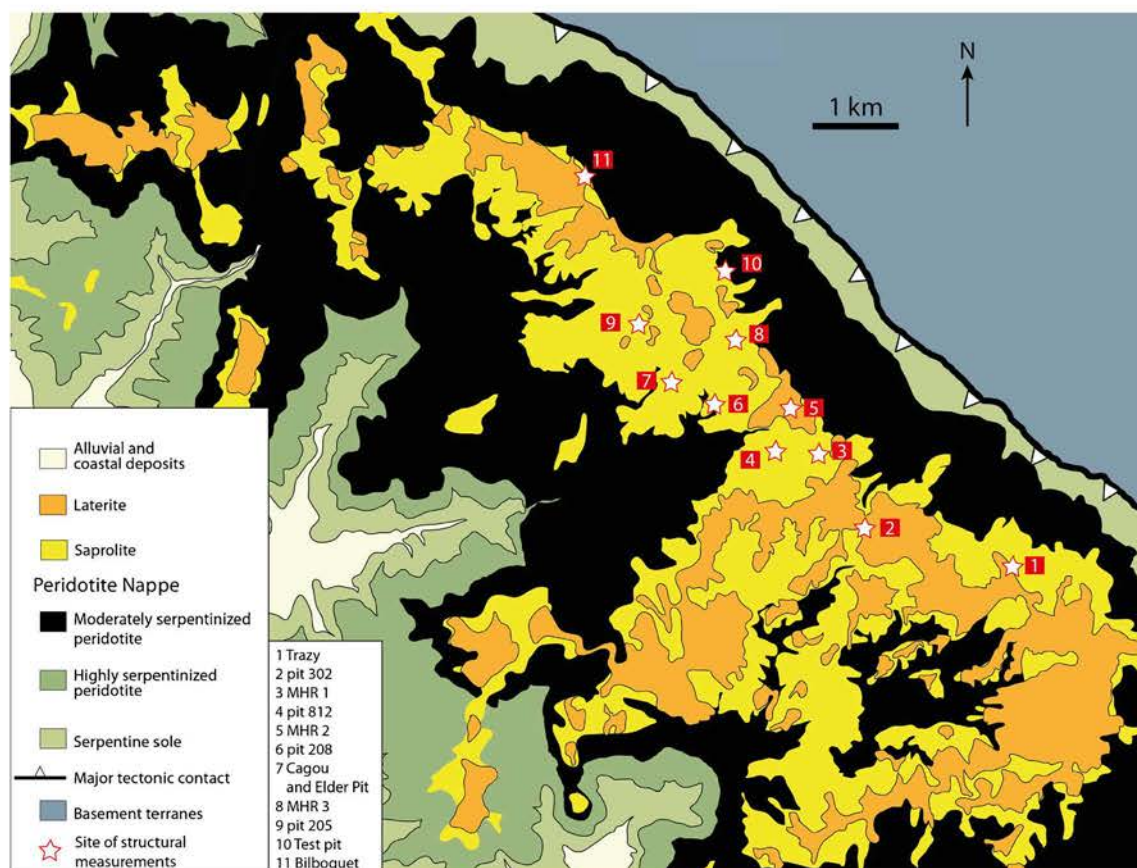


**Fig. 2** Geological map of the Koniambo massif modified after Maurizot et al. (2002)

### Major and trace element quantification

Electron probe microanalyses (EPMA) of kerolite were performed using a CAMECA SX100 instrument equipped with a WDS at SCMEM (Nancy, France). Si, Al, Fe, Mn, Mg, Co, Ni, and Na were calibrated using natural and synthetic oxides albite (Si, Na),  $\text{Al}_2\text{O}_3$  (Al), olivine (Mg), hematite (Fe),  $\text{MnTiO}_3$  (Mn), Co (Co), and NiO (Ni). The analytical conditions were the following: a current of 12 nA, an accelerating voltage of 15 kV, and a counting time of 10 s (and 30 or 60 s for Ni in Ni-poor kerolite). The analyses have a spatial resolution of 1  $\mu\text{m}$ . The total Fe is presented as FeO. Structural formulae were calculated on the basis of an  $\text{O}_{10}(\text{OH})_2$  base, in the case of talc-like minerals, and an  $\text{O}_5(\text{OH})_4$  base, in the case of serpentine. The tetrahedral sheets were assumed to be filled with Si. The octahedral sheets were composed of Ni and Mg.

Trace element analyses in quartz were carried out at the GeoRessources Laboratory (Vandoeuvre-lès-Nancy, France) using a LA-ICP-MS composed of a 193 nm MicroLas Pro ArF Excimer coupled with the Agilent 7500c quadrupole ICP-MS. Analytical settings for laser ablation are detailed by Leisen et al. (2012) and Lach et al. (2013). Laser ablation was performed with a constant 5-Hz pulse rate, with an ablation crater of 60  $\mu\text{m}$  in diameter. The ablated material is transported using a constant He flow and mixed with Ar in a cyclone coaxial mixer

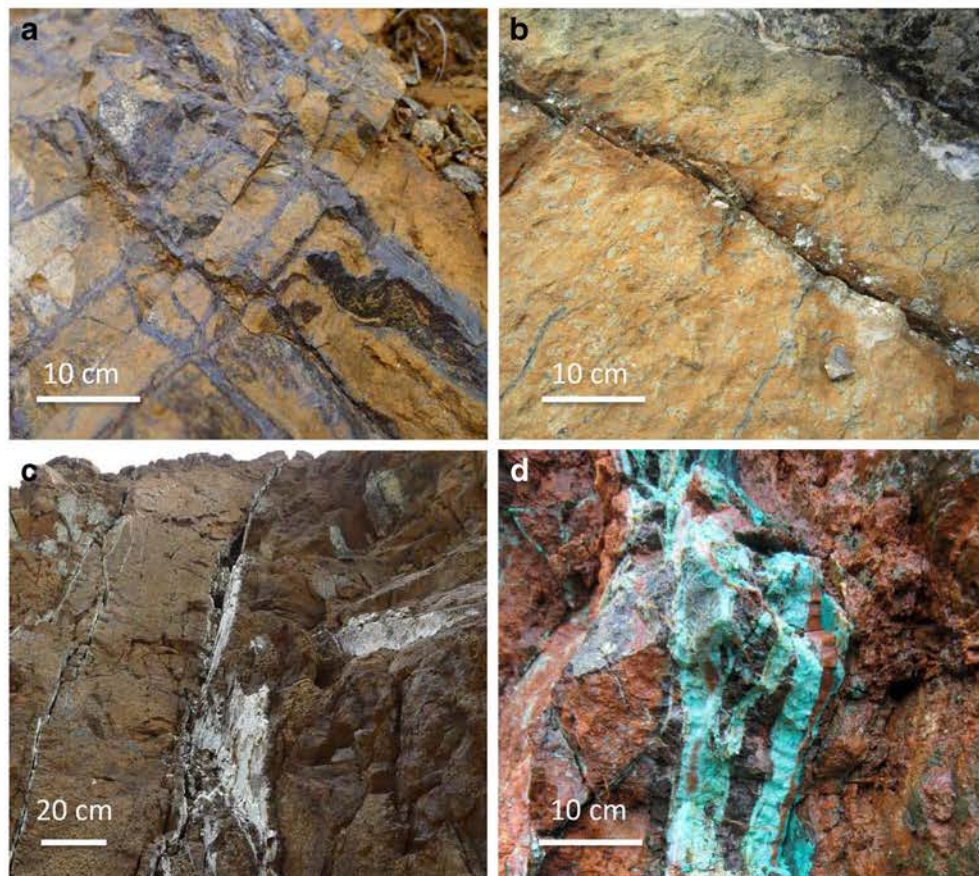
prior to entering the ICP torch and being ionized. The ions are then sampled, accelerated, and focused before being separated and analyzed in the quadrupole mass spectrometer. The following isotopes were monitored:  $^{24}\text{Mg}$ ,  $^{27}\text{Al}$ ,  $^{53}\text{Cr}$ ,  $^{55}\text{Mn}$ ,  $^{57}\text{Fe}$ ,  $^{59}\text{Co}$ ,  $^{60}\text{Ni}$ ,  $^{64}\text{Cu}$ , and  $^{66}\text{Zn}$ . Data reduction was carried out following the standard methods of Longerich et al. (1996) and using Si content—known from prior EPMA analyses—as an internal standard. External standard calibration was performed with the synthetic glass (NIST 610–612, Pearce et al. 1997).

### Raman spectroscopy

The nature of the serpentine polymorphs and other silicates was determined by Raman spectroscopy performed on rock sample and thin and polished section. The Raman spectra were recorded using a LabRAM HR spectrometer (Horiba Jobin Yvon). The acquisition was performed using a grating of 1800 lines/mm, a slit width of 50  $\mu\text{m}$ , and a confocal hole of 500  $\mu\text{m}$  providing a spectral resolution of 0.5 to 1  $\text{cm}^{-1}$ . The excitation beam was provided by an  $\text{Ar}^+$  laser (Stabilite 2017, Spectra Physics, Newport Corporation) at 514.53 nm, and a power of 200 mW focused on the sample using a  $\times 50$  objective. The spot size was  $< 1 \mu\text{m}$ . Acquisition time, limited by a weak luminescence, ranged between 2 and 6 s. The number of accumulations was set between 10 and 30 to optimize the signal-to-noise ratio within a reasonable



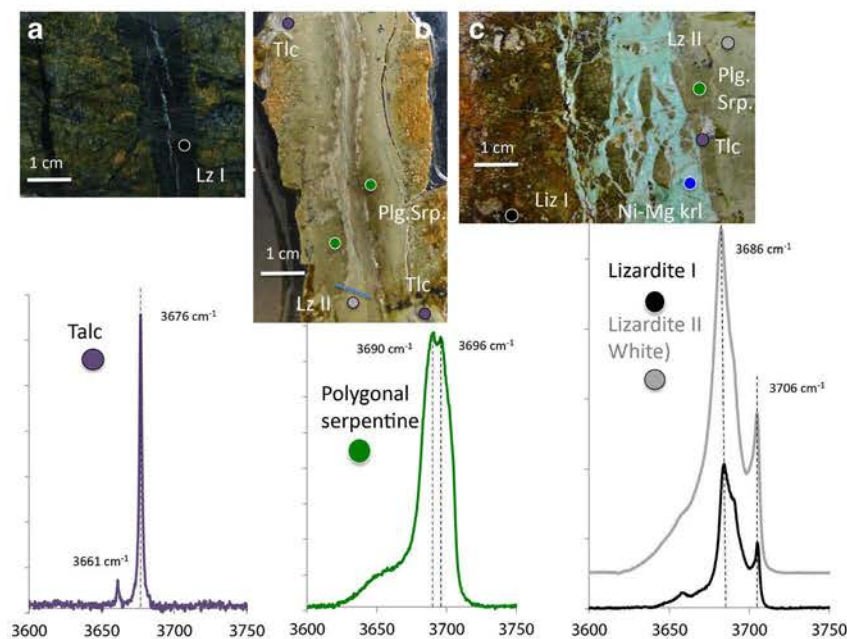
**Fig. 3** Representative examples of field occurrence of vein fillings at Koniambo: **a** lizardite (test pit); **b** lizardite with talc (Cagou pit); **c** polygonal serpentine (Trazy), generally green, but here bleached (whitish surface color) due to recent supergene alteration in open pit; and **d** fractures by filled kerolite and hematite-goethite microcrystalline quartz (lowest part of the test pit).



acquisition time. All Mg-Ni hydrous silicates were analyzed in two regions, the low wave number ( $100\text{--}1200\text{ cm}^{-1}$ ) and the high wave number regions ( $3550\text{--}3750\text{ cm}^{-1}$ ). The main discriminating bands are those corresponding to the OH stretching within the high-frequency region. In the region of OH stretching vibrations,

the four serpentine polymorphs are distinguished (Lemaire 2000; Auzende et al. 2004), as well as the talc-like minerals (kerolite-pimelite series) (Cathelineau et al. 2015b): (i) serpentines: the OH stretching bands for lizardite are at  $\sim 3690$  and  $\sim 3706\text{ cm}^{-1}$ ; for the polygonal serpentine as defined by Baronnet and Devouard

**Fig. 4** Macroscopic features of vein fillings and representative Raman spectra of the different silicates: **a** lizardite vein (test pit); **b** lizardite with talc, replaced partially into polygonal serpentine and lizardite II (vein corresponding to that of Fig. 3B, Cagou Pit); and **c** lizardite vein partially replaced by polygonal serpentine and lizardite II, re-cracked, and sealed by kerolite (elder pit (sample KON-207-H)). Colored dots indicate the location of Raman analyses. *Lz* lizardite, *Tlc* talc, *Plg. Serp.* polygonal serpentine, *Ni-Mg krl* Ni-Mg kerolite. The blue line corresponds to the location of polygonal and lizardite II microprobe analyses from Table 1



(1996), at  $\sim 3690$  and  $\sim 3698\text{ cm}^{-1}$ ; for chrysotile at  $\sim 3689$  and  $\sim 3701\text{ cm}^{-1}$ ; and finally, for antigorite, two main bands are centered at  $\sim 3661$  and  $\sim 3698\text{ cm}^{-1}$  and (ii) talc: the major OH stretching band is around  $3675\text{ cm}^{-1}$  and (iii) talc-like (kerolite-pimelite series): the shape of the OH stretching vibration band shows a strong evolution with increasing Ni content (noted from 0 to 100), with a shift toward lower wave number and an evolution to a complex band structure displaying several maxima with increasing the Ni content (Cathelineau et al. 2015b). In the middle of the substitution range (around Ni50) of the kerolite-pimelite series, the spectrum is a complex band cluster between  $3620$  and  $3700\text{ cm}^{-1}$  with three major peaks at  $3649$ ,  $3670$ , and  $3700\text{ cm}^{-1}$ .

### Breccia texture

A few representative examples of breccias were described quantitatively using four parameters: (1) clast morphology, (2) particle size distribution, (3) composition of matrix, and (4) dilation ratio. The clast morphology is related to the complexity of shape of individual clasts, while particle size distribution was applied to all plurality of fragments found in each samples. The shape of the fragments and their size distribution were described using fractal analysis techniques. There are several methods to characterize a clast shape by their boundary fractal dimension: box counting, structured walk, dilation, and Euclidean distance mapping (Bérubé and Jébrak 1999). In this study, the boundary fractal dimension of fragment morphology,  $D_r$ , was quantified using the box-counting method, developed specifically for computerized fractal analysis and implemented in the plugin “FracLac” (Karperien 1999–2013) for ImageJ (Rasband 1997–2014). Fractal dimension of particle size distribution,  $D_s$ , was calculated using a cumulative distribution curve of the fragment sizes assuming the validity of a power law (Turcotte 1986; Blenkinsop 1991) over a certain range of scale where the curve can be fitted by a straight line. Note that the calculation of local slopes on the graph, following Bonnet et al. (2001), leads to the same estimate of the fractal dimension  $D_s$ . Processing was carried out on Digital Microscope VHX-2000 (© Keyence), whereby the clasts and their geometrical sizes were identified. The dilation ratio was calculated as the volume ratio of matrix and fragments. These quantitative analyses were then compared with results of review of the main brecciation processes (Jébrak 1997).

## Results

### Mineralogical and chemical characterization of mineral fillings

Fractures are characterized by a succession of mineral fillings that always follows the same order from edge to center: black lizardite ( $\pm$  talc), polygonal serpentine, white lizardite, kerolite, red-brown microcrystalline quartz, and, finally, clear

quartz (Figs. 3, 4, 5, 6, and 7). The whole sequence corresponds thus to a centripetal crystallization from wall rock to the center of the vein. There is no occurrence of similar succession crosscutting this mineral sequence, which indicates that the whole sequence represents a single series of fluid events. Some veins show breccia textures, the most common having a red microcrystalline quartz cement (e.g., Fig. 5b). In some instances, the fractures exhibit partial mineral sequence: (i) Fig. 4a, b shows a serpentine filling, which was not reopened during the Ni stage, and (ii) Fig. 4c presents a fracture filled by serpentine and affected by microfractures filled by Ni-kerolite, but not by red microcrystalline quartz. Complete successions are, however, frequently found such as that shown in Fig. 6. The fracture width varies from a few millimeters up to a few centimeters, rarely reaching a few decimeters. Filled fractures can be observed spread over several meters both in the horizontal and in the vertical directions of the fracture plane.

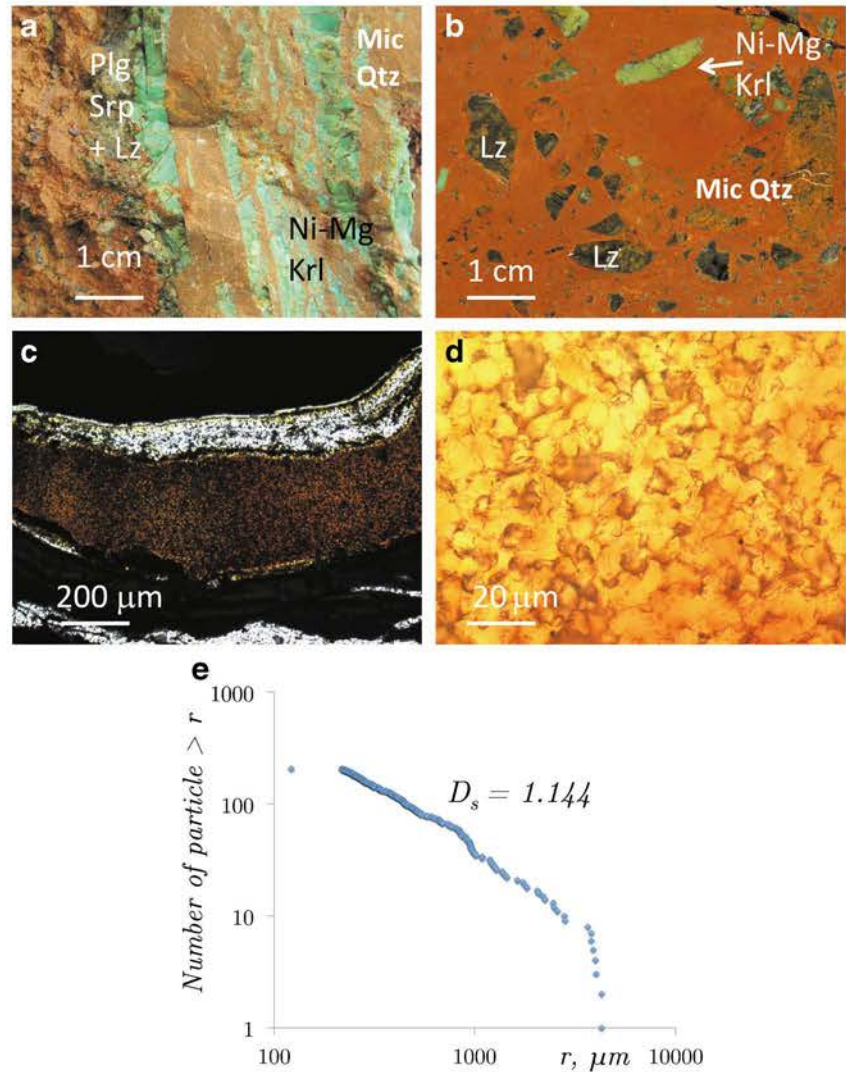
*The early filling: the serpentine stage (lizardite, polygonal serpentine)*

**The lizardite-talc stage** Along the edges of the fractures occurs black lizardite, as recognized by Raman spectroscopy, resulting of the pervasive transformation of the peridotite by localized fluid circulation in the fracture. This distinctive feature is related to both the color of the lizardite itself (Figs. 3a and 4a) and the presence of tiny magnetite crystals, which are less than tens of microns in size. In the harzburgite, millimetric to centimetric crystals of talc are formed after pyroxene, within the wall rocks replaced by lizardite on both sides of the fractures, as shown in Figs. 3b and 4b. The formation of lizardite affects the edges of the fracture on a few centimeters when fractures are metric in length. At the bottom of the ophiolite nappe close to the main deformation of the sole, fractures are pluridecamic in length, and the width of lizardite alteration zone can reach more than  $0.5\text{ m}$ , and movements on fractures attest to local shearing. In the upper part of the massif at around  $800\text{ m}$  of altitude, regular sets of fractures are plurimetric to decamic in length and centimetric in width. These observations are coherent with the structural model of Quesnel et al. (2016b), which discriminates two main distinct structural levels with two deformation styles, e.g. the sole, highly serpentinized, characterized by pervasive shearing and major faults, and the upper part of the massif, less serpentinized, with more brittle sets of subparallel fractures.

**The polygonal serpentine stage** Polygonal serpentine is generally dark to light green in color (Fig. 4b) and replaces lizardite. Polygonal serpentine has the following: (i) a typical Raman spectra characterized at high frequency by a large peak composed of two bands centered at  $3690$  and  $3696\text{--}3700\text{ cm}^{-1}$ ; (ii) textures under SEM reveal radiating sector boundaries as described by Baronnet and Devouard (1996);



**Fig. 5** Breccia and fracture fillings. **a** Fracture with polygonal serpentine (lower part of test pit) filled with Ni-Mg kerolite and later microcrystalline quartz. **b** Breccia with a microcrystalline quartz cement and clasts of lizardite and Ni-Mg kerolite. **c** Veinlet of goethite-hematite microcrystalline quartz (sample KON-207-H, see Fig. 6). **d** Detail of **c**. **e** Fractal dimension of clast size distribution,  $D_s$ , of breccia



and (iii) under TEM, a typical texture of short cylinders, which are empty in their center and when observed perpendicular to the cylinder axis, displays typical rolled sheet silicate such as chrysotile. The main difference with chrysotile is the very short length, with typical length/width ratio being around 2 to 4, compared to that of chrysotile which reaches values higher than 100.

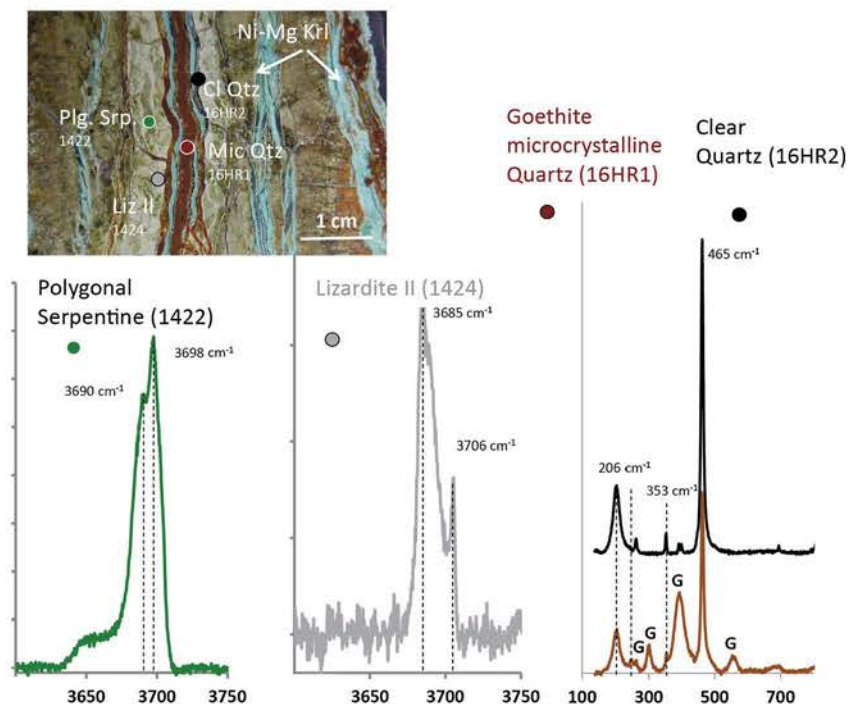
**The white lizardite stage** Along the main fractures, clasts of light green polygonal serpentine are then cemented by a whitish lizardite serpentine (Figs. 4b, c, 6, and 7c).

**The Ni-Mg kerolite** The bluish-greenish Ni-rich minerals (Figs. 3d, 4c, and 5) are talc-like (kerolite) as defined by Brindley and Wan (1975) and Brindley et al. (1979). They are characterized by a d spacing of  $9.5 \text{ \AA}$  in the TEM data. The Raman spectra are sometimes difficult to obtain on Koniambo kerolites due to fluorescence, regardless of the used wavelength. In the best cases, they display a complex series of nine bands in the OH

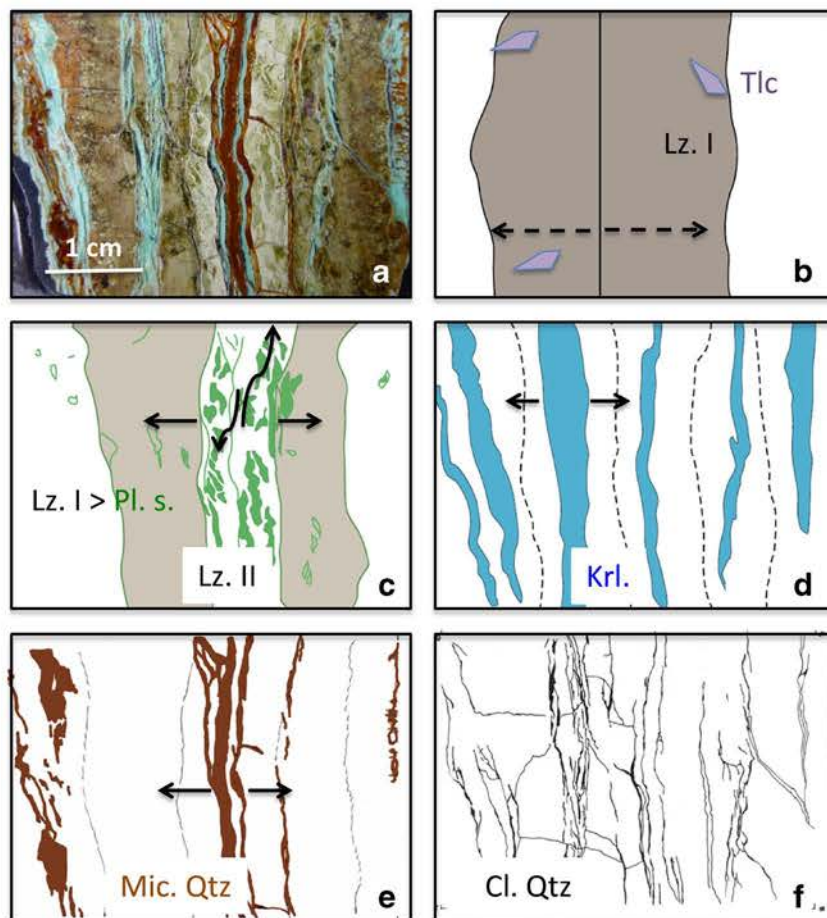
region in between  $3620$  and  $3700 \text{ cm}^{-1}$  as already described by Cathelineau et al. (2015b).

The low content of Ni of serpentine group minerals and the large Ni/Mg ratio of kerolites are shown in Fig. 8. Lizardite, polygonal serpentine, and white lizardite are chemically close to the Mg-serpentine end member (Table 1, Fig. 8). FeO content varies around  $5.7 \pm 0.5 \%$  for lizardite and is slightly lower in the polygonal and white lizardite (4 to 4.5 % FeO) (Table 1). Ni content is generally very low in lizardite and polygonal serpentine from samples taken away from Ni ores, but it may reach a few percent in kerolite-bearing samples. In the latter veins (Fig. 4c), the two serpentines (polygonal and white lizardite) display homogeneous content of 2 to 3 wt% NiO (Fig. 10). The main Ni silicate, Ni-Mg kerolite (talc-like), is characterized by a strong chemical zonation, with a NiO content varying from 10 wt% NiO to 27 wt% NiO. It is noted that all kerolites show a significant stoichiometric deviation from talc, with an excess in octahedral Ni (+Mg) occupancy observed in

**Fig. 6** Succession of lizardite (talc)–polygonal serpentine–Mg–Ni kerolite–hematite microcrystalline quartz and clear quartz fillings along subparallel fissures (elder pit, KON-207-H), with representative Raman spectra of the different silicates. Same abbreviations as in Fig. 4; *Mic Qtz* goethite microcrystalline quartz



**Fig. 7** Schematic reconstruction of the succession of mineral fillings in a typical vein in which complete mineral succession is observed (elder open pit; sample KON-207-H)



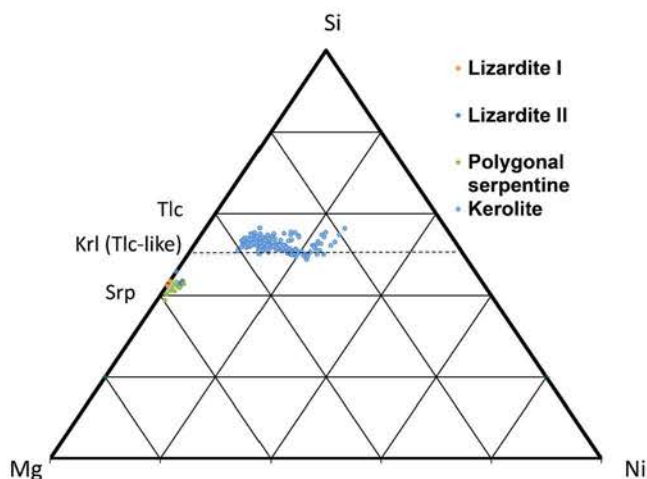


**Fig. 8** Si-Mg + Fe-Ni triangular diagram (electron probe microanalyses) for lizardite, polygonal serpentine, and kerolite from the vein (sample KON-207-H). Same abbreviations are in Fig. 4

correlation with a deficiency in the tetrahedral occupancy. Kerolites have a  $\text{Si}/(\text{Si} + \text{Mg} + \text{Ni})$  ratio around  $0.52 \pm 0.02$  distinct of talc (0.4) and serpentine (0.4–0.43) (Fig. 8).

### Quartz stages

**Red-brown quartz and breccia** The kerolite veins, in almost all samples, are fractured and cemented by microcrystalline quartz characterized by an intense red-brown color due to abundant microparticles of iron oxyhydroxides (Fig. 5d). In the Raman spectra presented in Fig. 6, the iron oxyhydroxide shows bands around 240, 300, 390, and  $550 \text{ cm}^{-1}$ , close to those of goethite, but rather wide. The large band around  $400 \text{ cm}^{-1}$  frequently found in brown quartz has more similarities with that obtained on  $\delta\text{-FeOOH}$  than the band of well-crystallized goethite (de Faria et al. 1997), indicating that the iron oxyhydroxide is probably poorly crystallized. The main bands typical of hematite at 404 and  $1310 \text{ cm}^{-1}$  were not found. The XRD pattern of bulk red-brown quartz and that of the finest grain fraction extracted from the red-brown quartz show only reflections of quartz and indicate that quartz has a high crystallinity at variance with the iron oxyhydroxide, which is either not sufficiently abundant or crystalline to be detected. The texture of quartz grains is very fine grained, but its high crystallinity is revealed by the well-defined and fine Raman bands at 465 and around  $205 \text{ cm}^{-1}$  (Fig. 6).

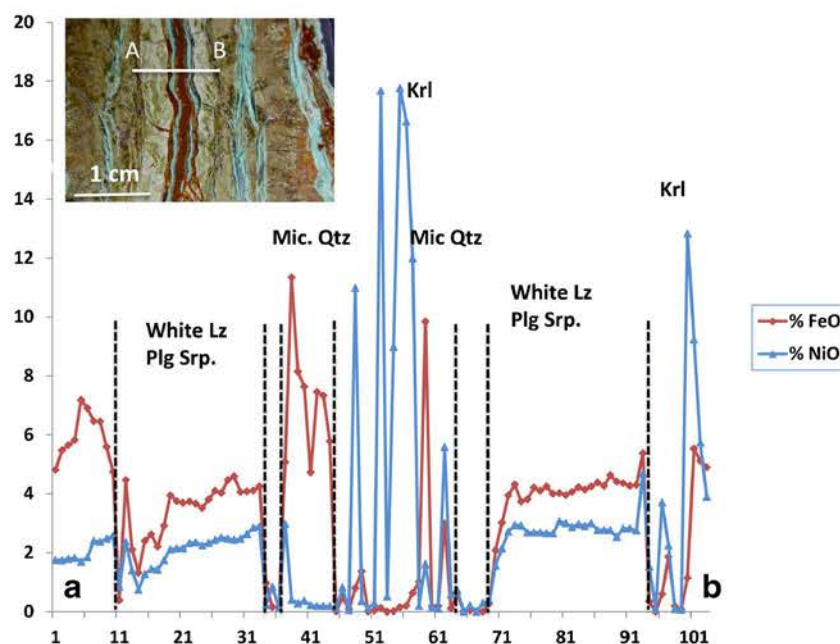
**Table 1** Electron probe microanalyses and structural formulae for the main silicates forming the fracture cements: lizardite, polygonal serpentine, kerolite, and microcrystalline quartz

| Sample                    | Lizardite<br>KON-low test<br>pit<br>$n = 3$ |          | Polygonal<br>serpentine<br>KON-207-H<br>$n = 18$ |          | Ni-Mg<br>kerolite<br>KON-207-H<br>$n = 22$ |          | Microcrystalline<br>quartz<br>Si-BR-4<br>$n = 19$ |          | Microcrystalline<br>quartz<br>KON-207-H<br>$n = 9$ |          |
|---------------------------|---|----------|--|----------|--|----------|---|----------|--|----------|
|                           | $m$   | $\sigma$ | $m$  | $\sigma$ | $m$  | $\sigma$ | $m$   | $\sigma$ | $m$  | $\sigma$ |
| % $\text{Na}_2\text{O}$   | 0.01  | 0.01     | 0.01   | 0.01     | 0.00                                       | 0.00     | 0.03  | 0.02     | 0.01   | 0.01     |
| % $\text{MgO}$            | 37.68                                       | 0.38     | 36.04  | 1.07     | 18.57                                      | 3.71     | 1.12  | 0.81     | 0.51   | 0.27     |
| % $\text{Al}_2\text{O}_3$ | 0.15  | 0.09     | 0.12   | 0.04     | 0.18                                       | 0.22     | 0.84  | 0.85     | 0.30   | 0.14     |
| % $\text{SiO}_2$          | 42.07                                       | 1.64     | 43.83  | 0.61     | 52.98                                      | 2.37     | 83.11   | 5.62     | 90.56  | 3.34     |
| % $\text{K}_2\text{O}$    | 0.01  | 0.00     | 0.01   | 0.01     | 0.05                                       | 0.02     | 0.02  | 0.02     | 0.00   | 0.01     |
| % $\text{CaO}$            | 0.02  | 0.01     | 0.07   | 0.19     | 0.00                                       | 0.00     | 0.05  | 0.03     | 0.02   | 0.02     |
| % $\text{Cr}_2\text{O}_3$ | 0.00  | 0.00     | 0.03   | 0.06     | 0.02                                       | 0.05     | 0.15  | 0.07     | 0.11   | 0.06     |
| % $\text{MnO}$            | 0.11  | 0.03     | 0.04   | 0.04     | 0.02                                       | 0.03     | 0.05  | 0.04     | 0.03   | 0.04     |
| % $\text{FeO}$            | 4.55  | 1.00     | 5.72   | 0.56     | 0.19                                       | 0.22     | 10.31   | 4.63     | 6.83   | 3.38     |
| % $\text{CoO}$            | 0.00  | 0.00     | 0.02   | 0.03     | 0.01                                       | 0.03     | 0.02  | 0.04     | 0.01   | 0.02     |
| % $\text{NiO}$            | 0.29  | 0.01     | 1.08   | 0.23     | 20.80                                      | 5.13     | 1.65  | 0.29     | 0.48   | 0.63     |
| Total                     | 84.90                                       |          | 86.96  | 0.75     | 92.82                                      | 1.81     | 96.33   | 1.65     | 98.17  | 0.74     |
| Si                        | 2.03  |          | 2.08   |          | 3.86                                       |          |   |          |  |          |
| Al                        | 0.00  |          | 0.01   |          | 0.02                                       |          |   |          |  |          |
| Fe                        | 0.18  |          | 0.23   |          | 0.01                                       |          |   |          |  |          |
| Mg                        | 2.72  |          | 2.55   |          | 2.01                                       |          |   |          |  |          |
| Mn                        | 0.01  |          | 0.00   |          | 0.00                                       |          |   |          |  |          |
| Ni                        | 0.01  |          | 0.04   |          | 1.23                                       |          |   |          |  |          |
| Fe + Mg + Ni              | 2.91  |          | 2.82   |          | 3.25                                       |          |   |          |  |          |

Structural formulae were calculated on the basis of an  $\text{O}_{10}(\text{OH})_2$  base, in the case of talc-like, and an  $\text{O}_5(\text{OH})_4$  base, in the case of serpentine



**Fig. 9** NiO and FeO profile through the vein shown in Fig. 6 (sample KON-207-H). Same abbreviations are in Fig. 4



At the micron scale, the electron microprobe analyses of the microcrystalline iron oxyhydroxides bearing quartz indicate that the iron content is highly variable at small scale due to the relative abundance of microsize iron oxyhydroxide particles (Fig. 9). The  $\text{Fe}_2\text{O}_3$  content in red microcrystalline quartz varies between 4 and 16 wt% with a mean at 10.3 wt%, indicating that it is a mineral assemblage composed of quartz at more than 85 % and iron hydroxides as minute inclusions of less than 1- $\mu\text{m}$  width, probably with a poor crystallinity (Table 1). In addition to Fe, Ni, Al, and Mg have mean values of 1.65 wt% NiO, 0.84 wt%  $\text{Al}_2\text{O}_3$ , and 1.12 wt% MgO, respectively. In the sample displayed in Fig. 6, Ni has a much lower content around 0.48 wt% NiO (Table 1) and the other metals are also lower in concentration (0.3 wt%  $\text{Al}_2\text{O}_3$ ; 0.5 wt% MgO). LA-ICP-MS analyses of this sample are given in Table 2. The red-brown quartz veins contain significant and rather homogeneous amounts of metals (Al, Mn, Cr), a feature which is never encountered in other quartz types, such as the clear quartz veinlets.

**Late quartz** Sets of subparallel thin veinlets of translucent or milky quartz are parallel to the earlier structures (Fig. 7). Quartz

displays a good crystallinity as shown by thin Raman bands, petrographic features typical of quartz grains of more than tens of microns in width, and is, in most cases, transparent without any solid inclusion. Figure 10 summarizes the mineral succession in veins and highlights the three main stages described previously.

### Structural and textural characterization of veins

**Fracture distribution and orientations** Field observations show that fractures filled only by kerolite are rarely observed, as kerolite is generally sealing reopen serpentine fractures (mainly polygonal serpentine). Two types of fractures have been measured on several sites in the area (Fig. 2). The first one consists of fractures filled only by polygonal serpentine, while the second one consists of fractures where kerolite is present together with polygonal serpentine at the selvage of the kerolite fillings. Many of these fractures can be considered as fault planes. Several polygonal serpentine fillings form accreted slickenfibers and have staircase geometry attesting for their syntectonic formation (Quesnel et al. 2016b). For the kerolite fillings, some evidence of slickensides attests, at least in part, for their syntectonic

**Table 2** LA-ICP-MS analyses of metal contents in the microcrystalline quartz (sample KON-207-H)

| Conc. (ppm)        | Mg   | Al   | Cr   | Mn  | Fe     | Co | Ni   | Cu | Zn |
|--------------------|------|------|------|-----|--------|----|------|----|----|
| KON-207-H-3-1      | 1869 | 1829 | 1285 | 282 | 33,613 | 53 | 2313 | 8  | 54 |
| KON-207-H-3-2      | 1914 | 1926 | 1316 | 301 | 35,066 | 56 | 2415 | 9  | 57 |
| KON-207-H-3-3      | 1970 | 1974 | 1383 | 310 | 36,467 | 60 | 2368 | 8  | 57 |
| KON-207-H-4-1      | 2153 | 1677 | 1178 | 265 | 30,938 | 49 | 2238 | 7  | 47 |
| KON-207-H-4-2      | 1743 | 2000 | 1423 | 320 | 37,243 | 61 | 2404 | 9  | 56 |
| KON-207-H-4-3      | 1743 | 2000 | 1423 | 320 | 37,243 | 61 | 2404 | 9  | 56 |
| Mean               | 1899 | 1901 | 1335 | 300 | 35,095 | 57 | 2357 | 8  | 54 |
| Standard deviation | 155  | 127  | 95   | 22  | 2473   | 5  | 69   | 1  | 4  |

Location of analyses close to that of the Raman spectrum from Fig. 6

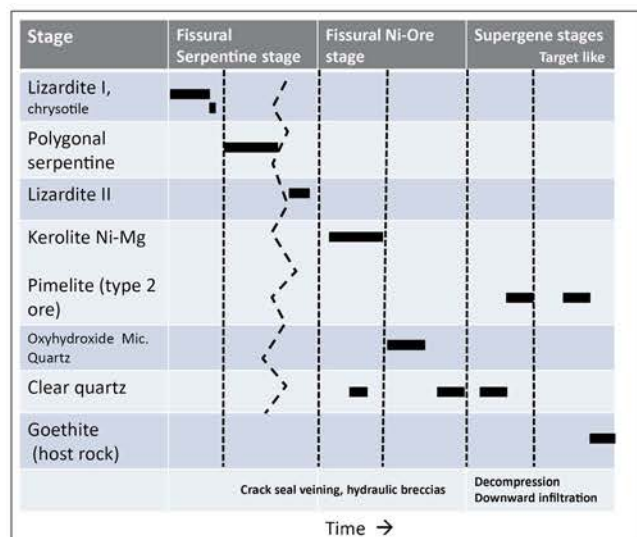


**Fig. 10** Paragenetic sequence showing the three main stages of fracture filling

formation (Cluzel and Vigier 2008). To summarize, (i) only few evidence of slickensides associated to kerolite is observed on the field and (ii) this type of structure does not provide kinematic criteria on the fault plane. Consequently, the stereograms presented in Fig. 11 only present the orientations of the fractures associated with polygonal serpentine and with kerolite, without kinematic interpretation. The two stereograms show a large overlap in the distribution of the poles associated to polygonal serpentine and kerolite. Kerolite fractures display predominant directions in between N170 and N20. For the polygonal fractures, the predominant directions are in between N180 and N30, and fractures show a regular spacing. The two populations of fractures are steeply dipping between 70° and 90°.

For the kerolite population, two clusters of poles differ from the overlap area. They are located in the 0°–45° and

180°–225° quarter of the stereogram and correspond, in part, to the fracture filled by kerolite with no polygonal serpentine.

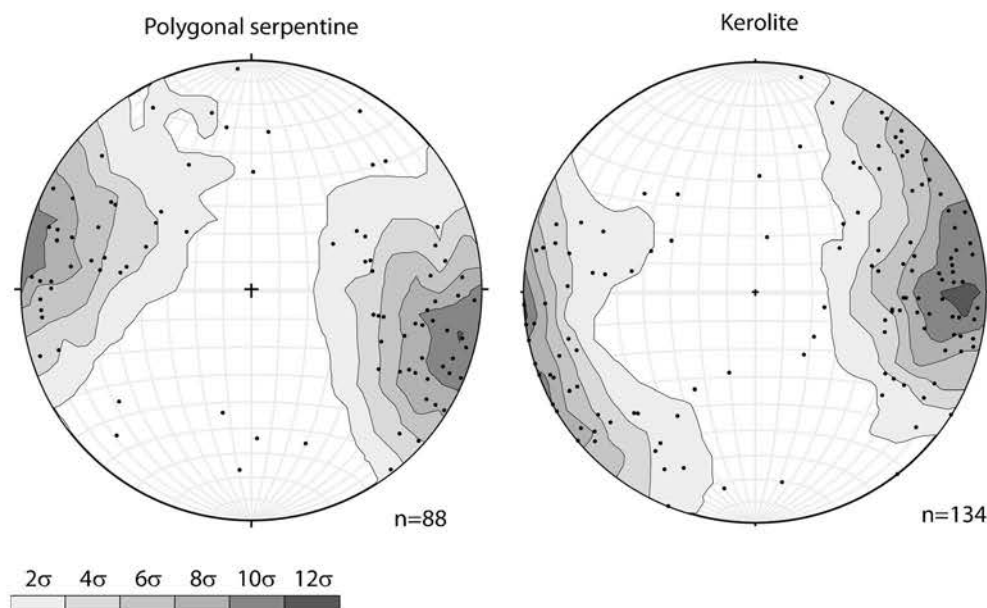
**Characterization of breccia** Breccia samples (Fig. 5) are composed of broken, angular-shaped fragments of (i) serpentine (lizardite, partially to totally converted to polygonal serpentine) and (ii) bluish green Ni-Mg talc-like, cemented together by a reddish-brown microcrystalline quartz-goethite matrix. The dilation ratio of the samples is high: the matrix is abundant and represents more than 80 % of the breccia. Jigsaw textures are locally recognized at grain scale: fragments still match along adjacent surfaces and show that they are former parts of larger clasts. The matrix of the breccia samples is characterized by simple and homogeneous filling material that consists of two co-precipitated minerals: (i) microcrystalline quartz and (ii) microparticles of goethite.

Fragments from the breccias have an angular, nearly Euclidean shape, with a fractal dimension  $D_r = 1.034$ . The particle size distribution (PSD) of 209 clasts is described by a power law relationship. The slope of best-fit line on a log-log plot of  $N(>r)$  vs.  $r$  is equivalent to the fractal dimension,  $D_s$ , of the PSD (Turcotte 1986) and found to be 1.144 (Fig. 5e). Particles larger than 2834  $\mu\text{m}$  deviate from the power law relationship because of censoring effects (Bonnet et al. 2001). These effects imply that fragments with sizes comparable to the sampled region tend to deviate from the power law distribution.

## Discussion

The mineral sequence determined on main Ni silicate fractures follows always the same order: (i) serpentine stage: lizardite > polygonal serpentine > white lizardite, (ii) Ni stage: Ni-Mg

**Fig. 11** Stereograms (lower hemisphere, equal-area projection) showing the orientation of the main fractures characterized by **a** polygonal serpentine after lizardite and **b** veins with kerolite infilling using the Stereonet software (Allmendinger et al. 2013). Data were collected on seven localities (Fig. 2). Shades of gray vary as a function of the probability for the presence of the poles following the Kamb method



kerolite followed by red-brown microcrystalline quartz, and (iii) later stages including the formation of the target-like ores, as joint fillings, and milky to translucent quartz. The goethite-rich microcrystalline quartz corresponds to the last event of the Ni stage and constitutes also the main cement of breccia. This microcrystalline quartz stage is thus of primary importance for understanding the sequence of fracture fillings, as it represents an excellent proxy to infer the conditions of the associated talc-like formation. Several indications can be deduced from the microcrystalline quartz stage closely associated with the talc-like: (i) the geometric distribution of fractures and conditions of breccia formation, (ii) redox conditions, and (iii) temperature of precipitation based on stable isotope data on quartz. The following paragraphs therefore examine these three main points in order to provide new insights into the Ni silicate vein formation and by extension into the genetic model of Ni ore formation.

### Fracture opening and brecciation

Two types of deformation textures have been found: (i) widespread series of fractures where successive fillings are nearly parallel to the previous one resulting of successive cracking and sealing and (ii) fracture opening with subsequent brecciation, found locally.

For the cracked and sealed fractures, the main observations are the following: kerolite-filled small fractures which post-date those of the polygonal serpentine generally correspond to the new cracking of a fractured zone containing serpentines. This suggests a strong influence of the inherited fracture network on the fluid circulation pathway at the origin of kerolite formation. The dip and strike of kerolite and polygonal serpentine fractures show that their mean orientations are close (Fig. 11). Moreover, kerolite occurrences are locally striated (Cluzel and Vigier 2008). Cracking of inherited fractures could be the result of their tectonic reactivation under a compatible stress field. A recent study shows that in the case of weak veins, typically the case of serpentine and kerolite veins, the reactivation of the fracture occurred even if the vein orientation is highly unfavorable relative to the stress field (Virgo et al. 2014). As shown previously, there are also fractures filled by kerolite but with no evidence of polygonal serpentine. These fractures differ, at least in part, in orientation from the mean common orientation of polygonal serpentine and kerolite fractures and could be considered newly formed. However, it appears difficult to provide a kinematic analysis for the kerolite fractures given that kerolite do not provide good kinematic criteria.

In addition of the tectonic influence, the effect of local fluid overpressure cannot be excluded. Indeed, occurrences of silica breccia are consistent with fluid-assisted deformation following Sibson's model (Sibson 1986). Taking a reasonable value of tensile strength for the wall rock (50 bars, Etheridge 1983), Sibson considers that for a depth

$z < 0.5$  km, no implosion of fracture sidewalls should occur and there is no hydrothermal precipitation in extensional veins. As a deeper depth is required for brecciation, it is permissive that the processes occurred at more than 0.5 km depth. The tectonic context favored fracture opening and subsequent upward fluid migration, which in turn enhanced inherited fracture opening and brecciation under local fluid overpressures.

Concerning the breccia samples, the following conclusions may be made:

- The boundary fractal dimension of the clasts, defined as  $Dr = 1.034$ , falls in the range of values typical for a physical (mechanical) breccia formed when the amount of stress exceeds the brittle resistance of the material (Griffith mode) (Jébrak 1997).
- The variation in fragment size approximates a power law distribution with corresponding value of fractal dimension  $Ds = 1.144$ . Such a low PSD value is often observed in hydraulic breccias or in those where transportation caused a size classification (Jébrak 1992; Jébrak 1997; Blenkinsop 1991).
- The brecciation process generated in situ fragmentation with a jigsaw puzzle pattern and absence of significant rotation of the fragments, which are typical features of hydraulic fracturing (Jébrak 1997).
- The matrix of the breccia is homogeneous and represents only two co-precipitated minerals: microcrystalline quartz and microparticles of goethite. The lack of several mineral assemblages as well as lack of banding is usual for fluid-assisted brecciation, since (i) the pressure fluctuation provokes rapid mineral precipitation and (ii) hydraulic fracturing has typically a shorter duration in comparison with tectonic activity, throughout which the mineral deposition conditions may vary (Jébrak 1997).

Thus, breccia samples have all the typical features of hydraulic fracturing (Jébrak 1997). This process is generally caused by differences of pressure between aquifers and the sudden connection between aquifers during seismic events. The increase in fluid pressure may have several origins, including a decrease in fault permeability (due to mineral deposition or fault slip). The breccias occur at specific stages of the vein filling, as attested by the different types of hydraulic breccias: (i) breccia with serpentine cement (polygonal serpentine) around serpentine clasts (lizardite), indicating hydrothermal activity started within the stability field of serpentine; (ii) breccia with kerolite cements and serpentine (all polytypes) clasts; and, finally, (iii) breccia with a reddish microcrystalline quartz cement and clasts of all types (serpentine, kerolite). The time evolution of the cement breccia mineralogy always follows the same sequence, which is also similar to the fracture cement chronology: (i) serpentine, (ii) kerolite, and (iii) red-brown quartz.



## Conditions of red-brown quartz precipitation

The inferred model of Ni-kerolite + red quartz formation relies on the following observations and considerations: (i) Ni-Mg kerolite is intimately associated in space and time with red quartz indicating similar conditions during fracturing and deposition and (ii) trivalent iron in iron oxyhydroxides that co-precipitate with quartz is poorly soluble under oxidizing conditions. According to Stumm and Morgan (1996), the rate law for oxidation of  $\text{Fe}^{2+}$  at 20 °C is first order with respect to both  $\text{Fe}^{2+}$  and  $\text{fO}_2$  and second order for  $[\text{OH}^-]$ . Thus, the time for complete oxidation of iron in an aerated solution is a matter of hours under the pH conditions typical of laterite (waters equilibrated with atmospheric  $\text{CO}_2$  (pH 5.6) and of seconds under saprolite conditions (pH ranging from 7 to 9). The only process accounting for a transport of trivalent iron could be mechanical downward migration of Fe nanoparticles from the above aquifers (Fig. 12). Such a transport might have been partially possible by the formation of fractures due to tectonic activity and downward migration of the ferrihydrite colloid. Alternately, reducing conditions favor iron under the +2 oxidation state in anoxic solution and subsequent iron transport. Such reducing conditions occur below the water table, in the deeper parts of the aquifers (Fig. 13). The co-precipitation of red quartz needs, therefore, the iron oxidation and the syncrystallization of quartz (Fig. 12). Such a process is commonly used in industry to obtain silica-iron hydroxide co-precipitation (Cortez Fernandes et al. 2013; Dyer et al. 2012). Silica precipitation has been shown to be strongly enhanced by adsorption processes on freshly precipitated ferrihydrite, serving as nuclei in oversaturated solutions, with

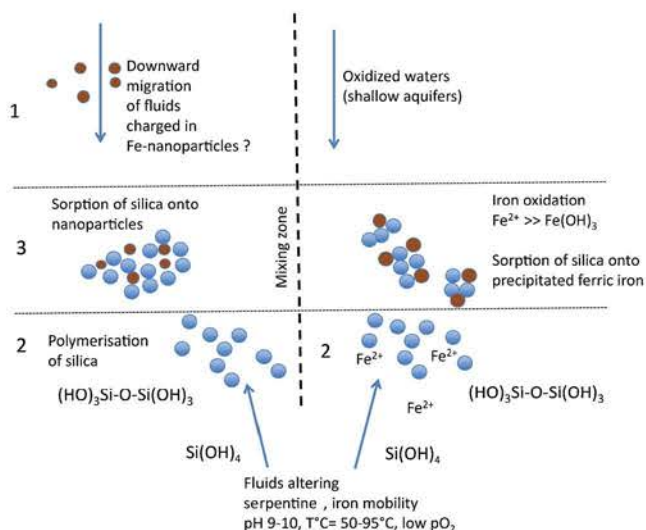


**Fig. 12** Model proposed for the precipitation of the goethite microcrystalline quartz. *Left-hand side:* hypothetical downward transport of trivalent iron as nanoparticles. *Right-hand side:* upward circulation of reduced water transporting divalent iron and co-precipitation of silica and iron hydroxides during mixing with oxidizing surface waters

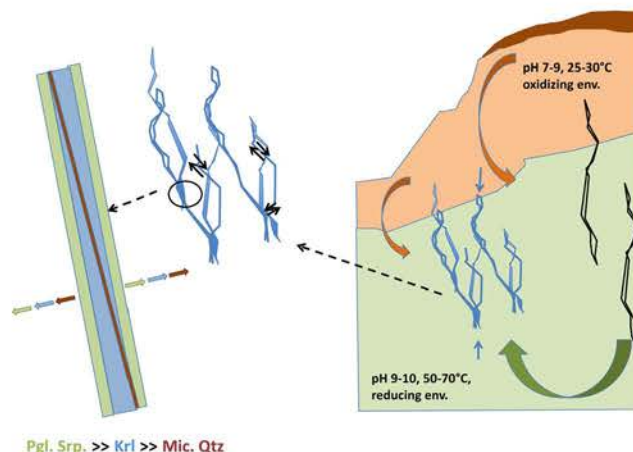


**Fig. 13** Conceptual modeling of the hydrothermal cell at the origin of the vein infillings

maximum sorption attained at pH 7.25–9.5 (Davis et al. 2001, 2002; Swedlund et al. 2011). Under the typical pH values of waters at equilibrium with ultrabasic rocks, i.e., around 9 to 10, it is likely that silica is mostly polymeric (Dyer et al. 2012) (Fig. 12) and, therefore, should strongly bind to iron. Thus, the formation of numerous germs of iron oxyhydroxides causes the co-precipitation of  $\text{SiO}_2$ . The oversaturation of the fluid with respect to silica is also favored by a temperature drop and/or a pH decrease, since silica and quartz solubilities decrease with decreasing temperature and pH. As the red-brown microcrystalline quartz represents a single event and as all other quartz types are free of oxyhydroxide particles, especially those found close to surface in the silicified bedrocks, the hypothesis of upward migration of reduced waters seems the most probable for this stage, in contrast to the other quartz stages.

## Crystallization temperatures of red-brown quartz

During the Ni stage, the late microcrystalline red quartz is a distinctive feature of the kerolite fractures and hydraulic breccia. Microcrystalline quartz always postdates kerolite precipitation, but it seems to be related to the same cycle of fracture cracking and sealing, being geometrically associated to kerolite, and containing variable but significant amount of Ni. The oxygen isotopic composition of microcrystalline quartz from Koniombo ranges from 23.9 to 27.6 ‰ (Quesnel 2015; Quesnel et al. 2016a). These values correspond to calculated temperatures in the range of ~50 to 95 °C (using  $\delta^{18}\text{O}_{\text{Fluide}} = -2.5$  ‰; Quesnel et al. 2016a). Therefore, talc-like formed at a temperature between that of the latest serpentines and a minimum temperature of about 50 °C for quartz. Such medium-range temperature was already proposed by Ducloux et al. (1993) for Bou Azzer kerolite although their temperature range is poorly constrained.

## A model of low-to-medium-temperature fluid circulation for the formation of the Ni silicate veins

Since the microcrystalline quartz ends the main stage of formation of Ni-Mg kerolite, this may indicate that a great part of Ni silicate fracture fillings formed during a series of hydrolic fracturing, which cracks previous fractures, opens new ones, or causes brecciation. Fractures are well oriented and form subparallel sets striking N-S to NE-SW. Upward hydrothermal fluid migration of moderate temperature is inferred for these stages of fracture sealing (Fig. 13). The successive precipitation of talc-like followed by microcrystalline quartz is interpreted to occur when upward ascending fluids encounter more oxidizing waters near the surface. Such a model of medium-temperature upward circulation of reduced waters, as well as the high pressure necessary for hydraulic fracturing or brecciation in relation with tectonics, constitutes an alternative to classic metallogenic models developed for New Caledonian deposits. Thus, a unique downward infiltration of cold oxidizing meteoric water under hydrostatic or infra-hydrostatic pressure cannot explain all the features of the Koniambo deposit. In the proposed model, fluids are considered to transfer quickly from surface (meteoric water), are heated at depth, and then advect within the nappe. The fluids are interpreted to mix during their upward migration with meteoric, oxidized water potentially charged in nickel from the surface water-rock interactions. Therefore, the nickel is unlikely to be dissolved from the deepest part.

## Conclusion

Most of the veins sealed by Ni-Mg kerolite and quartz-hematite correspond to stages of cracking and sealing of preexisting fractures probably formed by fluid overpressure. The tectonic regime at that stage was compatible with the reopening of earlier fractures previously cemented by lizardite, which was then partially to entirely converted to polygonal serpentine.

The systematic occurrence of a main Ni silicate stage marked by the presence of Ni-Mg kerolite, formed in between the latest stage of serpentine and the oxyhydroxide microcrystalline stage, provides a strong argument in favor of a moderate-temperature hydrothermal event. The microcrystalline quartz, formed under temperatures of 50–95 °C during the last stage of the hydrothermal system, provides thus a good estimate of the minimum temperature conditions driving the preceding stages. It is also a good marker of divalent iron migration in a reduced environment, as it appears unlikely that iron could have been transported from surface as nanoparticles. Such Fe-hydroxides could have been formed by the oxidation of  $\text{Fe}^{2+}$ , transported by reduced water from underlying aquifers.

The sequence of fracture filling is therefore interpreted as the result of a hydrothermal system evolution from medium to low temperature under fluctuating fluid pressure and depth >0.5 km. Data from Koniambo massif Ni-mineralized fractures allow us to propose a new genetic model that includes fluid advection driven with tectonic stress. This model is different from the supergene model generally accepted for the formation of Ni silicate ores. The clusters of fractures closely linked to reopening of former serpentine fractures indicate that a Ni preconcentration occurred in relation with tectonics and/or hydraulic processes. Although frequently described as the result of a single downward redistribution of Ni and Mg leached in the upper part of the regolith, the Ni silicate veins appear to have formed as a result upward of fluid flow.

At the scale of mineralized massif, the succession of fluid flow events produced local enrichment in nickel to account for part of the heterogeneity in the distribution of nickel in present-day regolith. Fracture fillings are affected then by dissolution-recrystallization processes within the water table movement zone, a process yielding to the formation of target-like ores, and finally by the downward migration of the oxidation-dissolution front which forms saprolitic ore. The pristine Ni-rich fracture distribution therefore controls partially the geometry of the secondary Ni distribution. The present-day distribution of minerals appears thus as the result of complex superimposed processes and not only as the result of simple downward migration of a nickel front during the main stage of laterite formation.

**Acknowledgments** This work has been carried out thanks to the financial and technical help from Koniambo S.A.S. and Labex Ressources 21 (supported by the French National Research Agency through the national program “Investissements d’avenir,” reference ANR-10-LABX-21-LABEX RESSOURCES 21), with analytical contributions from the UMR GeoRessources No. 7356 laboratory platforms. The field work was introduced by a first 1-day visit at Koniambo in 2011 by C. Couteau and E. Fritsch (field trip organized as part of a CNRT project (French National Centre for Technological Research: “Nickel and its environment”), and consisted in 2-week stays both in 2012 and 2013 financed by Koniambo within the framework of the B. Quesnel’s PhD thesis. This work was supervised in the field by C. Couteau and Maxime Drouillet from Koniambo S.A.S. Marie-Camille Caumon is acknowledged for her help during RAMAN analyses. The authors are grateful to M. Jébrak, E. Ramanaidou, and B. Orberger for their detailed and constructive reviews.

## References

- Allmendinger RW, Cardozo NC, Fisher D (2013) Structural geology algorithms: vectors & tensors. Cambridge University Press, Cambridge, 289 pp
- Auzende A, Daniel I, Reynard B, Lemaire C, Guyot F (2004) High pressure behaviour of serpentine minerals: a Raman spectroscopic study. *Phys Chem Miner* 31(5):269–277
- Baronnet A, Devouard B (1996) Topology and crystal growth of natural chrysotile and polygonal serpentine. *J Cryst Growth* 166:952–960

- Bérubé D, Jébrak M (1999) High precision boundary fractal analysis for shape characterization. *Comput Geosci* 25:1059–1071
- Blenkinsop TG (1991) Cataclasis and processes of particle size reduction. *Pure Appl Geophys* 136:59–86
- Bonnet E, Bour O, Odling NE, Davy P, Main I, Cowie P, Berkowitz B (2001) Scaling of fracture systems in geological media. *Rev. Geophys* 39(3):347–383
- Brindley GW, Hang PT (1973) The nature of garnierites—I structures, chemical compositions and color characteristics. *Clay Clay Miner* 21:27–40
- Brindley GW, Wan HM (1975) Compositions, structures, and thermal behaviour of nickel-containing minerals in the lizardite–nepouite series. *Am Mineral* 60:863–871
- Brindley GW, Bish D, Wan HM (1979) Compositions, structures, and properties of nickel-containing minerals in the kerolite–pimelite series. *Am Mineral* 64:615–625
- Butt CRM, Cluzel D (2013) Nickel laterite ore deposits: weathered serpentinites. *Elements* 9(2):123–128
- Cathelineau M, Caumon MC, Massei F, Brie D, Harlaux M (2015b) Raman spectra of Ni-Mg kerolite: effect of Ni-Mg substitution on O-H stretching vibrations. *Proceedings GEORaman 2014* (11th), St Louis (USA). *J Raman Spectrosc* 46(10):933–940
- Cathelineau M, Quesnel B, Gautier P, Boulvais P, Couteau C, Drouillet M (2015a) Nickel dispersion and enrichment at the bottom of the regolith: formation of pimelite target-like ores in rock block joints (Koniambo Ni deposit, New Caledonia). *Mineral Deposita* 51: 271–282
- Chardon D, Chevillotte V (2006) Morphotectonic evolution of the New Caledonia ridge (Pacific Southwest) from post-obduction tectonosedimentary record. *Tectonophysics* 420:473–491. doi:10.1016/j.tecto.2006.04.004
- Chen TT, Dutrizac JE, Krause E, Osborne R (2004) Mineralogical characterization of nickel laterites from New Caledonia and Indonesia. In: *International Laterite Nickel Symposium* (as held during the 2004 TMS annual meeting). p. 79–99
- Cluzel D, Vigier B (2008) Syntectonic mobility of supergene nickel ores of New Caledonia (Southwest Pacific). Evidence from garnierite veins and faulted regolith. *Resour Geol* 58:161–170. doi:10.1111/j.1751-3928.2008.00053.x
- Cluzel D, Aitchison JC, Picard C (2001) Tectonic accretion and underplating of mafic terranes in the Late Eocene intraoceanic fore-arc of New Caledonia (Southwest Pacific): geodynamic implications. *Tectonophysics* 340(1–2):23–59
- Cluzel D, Jourdan F, Meffre S, Maurizot P, Lesimple S (2012) The metamorphic sole of New Caledonia ophiolite: 40Ar/39Ar, U-Pb, and geochemical evidence for subduction inception at spreading ridge. *Tectonics* 31, TC3016, doi: 10.1029/2011TC003085.
- Cortez Fernandes MT, Rivero Garcia RB, Paula Leite CA, Kawachi EY (2013) The competing effect of ammonia in the synthesis of iron oxide/silica nanoparticles in microemulsion/sol–gel system. *Colloids and Surfaces A: Physicochem Eng Aspects* 422:136–142
- de Faria DLA, Venâncio Silva S, de Oliveira MT (1997) Raman spectroscopy of some iron oxides and oxyhydroxides. *J Raman Spectrosc* 28:873–878
- Davis CC, Chen H, Edwards M (2002) Modeling silica sorption to iron hydroxide. *Environmental Science & Technology* 36(4):582–587. doi: 10.1021/es010996t
- Davis CC, Knoke WF, Edwards M (2001) Implications of aqueous silica sorption to iron hydroxide: mobilization of iron colloids and interference with sorption of arsenate and humic substances. *Environmental Science & Technology* 35(15):3158–3162. doi: 10.1021/es0018421
- Dublet G, Juillot F, Morin G, Fritsch E, Fandeur D, Brown GE (2015) Goethite aging explains Ni depletion in upper units of ultramafic lateritic ores from New Caledonia. *Geochim Cosmochim Acta* 160:1–15
- Dublet G, Juillot F, Morin G, Fritsch E, Fandeur D, Ona-Nguema G, Brown GE Jr (2012) Ni speciation in a New Caledonian lateritic regolith: a quantitative X-ray absorption spectroscopy investigation. *Geochim Cosmochim Acta* 95:119–133
- Ducloux J, Boukili H, Decarreau A, Petit S, Perruchot A, Pradel P (1993) Un gîte hydrothermal de garniérites: l'exemple de Bou Azzer, Maroc. *Eur J Mineral* 5:1205–1215
- Dyer LG, Richmond WR, Fawell PD (2012) Simulation of iron oxide/silica precipitation in the paragoethite process for the removal of iron from acidic zinc leach solutions. *Hydrometallurgy* 119–120:47–54
- Etheridge MA (1983) Differential stress magnitudes during regional deformation and metamorphism: upper bound imposed by tensile fracturing. *Geology* 11:231–234
- Fandeur D (2009) *Géochimie et cristalochimie du chrome au cours de l'altération de roches ultrabasiques en Nouvelle-Calédonie* (Massif du Koniambo). Dissertation, Université Paris Diderot–IPGP
- Freyssinet P, Butt CRM, Morris RC (2005) Ore-forming processes related to lateritic weathering. *Econ Geol*: 681–722. 100th Anniversary
- Fritsch EM, Juillot FA, Dublet GA, Fonteneau L, Fandeur D, Martin E, Caner L, Auzende A-L, Grauby O, Beaufort D (2016) An alternative model for the formation of hydrous Mg/Ni layer silicates (“deweylite”/“garnierite”) in faulted peridotites of New Caledonia: I. Texture and mineralogy of a paragenetic succession of silicate infillings. *Eur J Mineral* 28(2):295–311
- Golightly JP (2010) Progress in understanding the evolution of nickel laterite. *Society of Economic Geologists, Inc. Special Publication* 15:451–485
- Jébrak M (1992) Les textures intra-filoniennes, marqueurs des conditions hydrauliques et tectoniques. *Chron Rech Min* 506:55–65
- Jébrak M (1997) Hydrothermal breccias in vein-type ore deposits: a review of mechanisms, morphology and size distribution. *Ore Geol Rev* 12:111–134
- Karperien A (1999–2013) FracLac for ImageJ <http://rsb.info.nih.gov/ij/plugins/fraclac/FLHelp/Introduction.htm>
- Lach P, Mercadier J, Dubessy J, Boiron MC, Cuney M (2013) In-situ quantitative measurement of rare earth elements in uranium oxides by laser ablation-inductively coupled plasma-mass spectrometry. *Geostandards and Geoanalytical Research* 37:277–296
- Leguéré J (1976) Des corrélations entre la tectonique cassante et l'altération supergene des peridotites de Nouvelle-Calédonie. Dissertation, Université du Languedoc, Montpellier, France
- Leisen M, Dubessy J, Boiron MC, Lach P (2012) Improvement of the determination of element concentrations in quartz-hosted fluid inclusions by LA-ICP-MS and Pitzer thermodynamic modeling of ice melting temperature. *Geochim Cosmochim Acta* 90:110–125
- Lemaire C (2000) Application des spectroscopies vibrationnelles à la détection d'amiante dans les matériaux et à l'étude des serpentines. Dissertation, Université de Paris 07.
- Longerich HP, Jackson SE, Günther D (1996) Laser ablation inductively coupled plasma mass spectrometry transient signal data acquisition and analyte concentration calculation. *J Anal At Spectrom* 11:899–904
- Manceau A, Calas G (1985) Heterogeneous distribution of nickel in hydrous silicates from New Caledonian ore deposits. *Am Mineral* 70: 549–558
- Manceau A, Calas G (1986) Nickel-bearing clay minerals: II. Intracrystalline distribution of nickel: an X-ray absorption study. *Clay Miner* 21:341–360
- Maurizot P, Lafoy Y, Poupée M (2002) Cartographie des formations superficielles et des aléas mouvements de terrain en Nouvelle-Calédonie, Zone du Koniambo: Bureau de Recherches Géologiques et Minières, Public Report RP51624-FR, 45 p
- Maurizot P, Vendé-Leclerc M, Collot J (2009) Carte géologique de la Nouvelle-Calédonie au 1/500.000. Service Géologique de la Nouvelle-Calédonie/DIMENC-BRGM

- Paquette JL, Cluzel D (2007) U–Pb zircon dating of post-obduction volcanic-arc granitoids and a granulite-facies xenolith from New Caledonia. Inference on Southwest Pacific geodynamic models. *Int J Earth Sci* 96:613–622. doi:10.1007/s00531-006-0127-1
- Pearce NJG, Perkins WK, Westgate JA, Gorton MP, Jackson SE, Neal CR, Chenery SP (1997) A compilation of new and published major and trace element data for NIST SRM 610 and NIST SRM 612 glass reference materials. *Geostandards and Geoanalytical Research* 21:101–114
- Quesnel B (2015) Altération supergène, circulation des fluides et déformation interne du massif de Koniambo, Nouvelle-Calédonie: Implication sur les gisements nickélifères latéritiques. Dissertation, Rennes Univ., 276 p
- Quesnel B, Boulvais P, Gautier P, Cathelineau M, John CM, Dierick M, Agrinier P, Drouillet M (2016a) Paired stable isotope (O, C) and clumped isotope thermometry of magnesite and silica veins in the New Caledonia Peridotite Nappe. *Geochim Cosmochim Acta* 183: 234–249
- Quesnel B, Gautier P, Cathelineau M, Boulvais P, Couteau C, Drouillet M (2016b) The internal deformation of the Peridotite Nappe of New Caledonia: a structural study of serpentine-bearing faults and shear zones in the Koniambo Massif. *J Struct Geol* 85:51–67
- Rasband WS (1997–2014) ImageJ. US National Institutes of Health, Bethesda, Maryland, USA, <http://imagej.nih.gov/ij/>
- Sevin B, Ricordel-Prognon C, Quesnel F, Cluzel D, Lesimple S, Maurizot P (2012) First palaeomagnetic dating of ferricrete in New Caledonia: new insight on the morphogenesis and palaeoweathering of “Grande Terre”. *Terra Nov.* 24(1):77–85
- Sibson RH (1986) Brecciation processes in fault zones. *Pure Appl Geophys* 124:159–175
- Stumm W, Morgan JJ (1996) *Aquatic chemistry*, 3rd edn. Wiley and Sons, New York, 1022 pp
- Swedlund PJ, Sivaloganathan S, Miskelly GM, Waterhouse GIN (2011) Assessing the role of silicate polymerization on metal oxyhydroxide surfaces using X-ray photoelectron spectroscopy. *Chem Geol* 285: 62–69
- Trescases JJ (1975) L'évolution géochimique supergène des roches ultrabasiques en zone tropicale. *Mem ORSTOM*, 78, 259 p
- Turcotte DL (1986) Fractal and fragmentation. *J Geophys Res* 91:1921–1926
- USGS (US Geological Survey) (2016) Mineral commodity summaries, January 2016. <http://minerals.usgs.gov/minerals/pubs/commodity/nickel/mcs-2016-nicke.pdf>
- Villanova-de-Benavent C, Proenza JA, Galí S, García-Casco A, Tauler E, Lewis JF, Longo F (2014) Garnierites and garnierites: textures, mineralogy and geochemistry of garnierites in the Falcondo Ni-laterite deposit, Dominican Republic. *Ore Geol Rev* 58:91–109
- Virgo S, Abe S, Uria JL (2014) The evolution of crack seal vein and fracture networks in an evolving stress field: insights from discrete element models of fracture sealing. *J Geophys Res* 119:12:8708–8727
- Wells MA, Ramanaidou ER, Verrall M, Tessarolo C (2009) Mineralogy and chemical chemistry of “garnierites” in the Goro lateritic nickel deposit, New Caledonia. *Eur J Mineral* 21:467–483
- Wells MA, Ramanaidou ER (2015) Variability of the Ni content in goethite for New Caledonian lateritic nickel deposits. In: *Proceedings of the 13th Biennial SGA (Society for Geology Applied to Mineral Deposits) meeting*, Nancy, 24–27 August 2015
- XStrata (2012) Mineral resources and reserves at 31 Dec. 2012. *Ann Rep* 50



# CONCLUSIONS

The main objective of this work can be summed up in the desire to enhance our understanding of the formation of New Caledonian nickel ore deposits and in particular to identify the factors governing the behaviour of Ni mineralization as well as its redistribution within the regolith. The work belongs to the part of the Priority Research Action PRA5 of LABEX RESOURCES 21 that is focused on the 3D modelling of the ore geometry and metal transport at various scales to understand the distribution of metals and how ore deposits form over space and time.

First developed model represents a detailed study of the development of the secondary nickel ores upon vertical downward progression of the alteration front. Here, thanks to long-term 1D transport simulations we identified the major mechanism of Ni transfer in between different concurrent retention processes, namely adsorption on a goethite surface, precipitation/dissolution of kerolite/sepiolite as well as incorporation of Ni into the goethite structure, which is most common Ni-bearer in the laterites from New Caledonia. Such a modeling taking into account formation of both most common for New Caledonia oxide and hydrous-silicate ores was first performed in the framework of this thesis and clearly demonstrates that the Ni enrichment and thickening of iron-rich zone are governed by the vertical progression of the pH front. Moreover, the model gives new valuable insights into the strongly debated Ni retention mechanism within the limonite zone. Indeed, often explained as a result of adsorption processes the presence of Ni in this upper horizon was proved to have more complex behaviour where adsorption serves as a transition process in continuous Ni transfer between Ni-rich silicates dissolution and goethite formation. Thus, after its release from silicates due to the decrease in pH, the adsorbed nickel further passes to the lattice of goethite or precipitates with it. The oxides associated with entirely leached silica zones were shown to hold Ni only in its structure while those presented deeper in the profile within the silicate horizon may contain both adsorbed and in-lattice nickel. This distribution is in agreement with EX-AFS data (Dublet et al., 2012) or with sequential extraction (Ambrosi, in 'Nickel project' CNRT report). The latter can be of importance in improvement of ore-processing technics as well as in fast-developing phytomining when choosing a metal-hyperaccumulating plant species. In addition, the mechanism of competitive occupation of the goethite sorption sites



was established, showing a big influence of the other cations released during the ultramafic bedrock alteration on adsorption process, in particular Mg. Therefore, the adsorption of Ni was proven to become important in a restricted range of pH around 8, quickly releasing at lower than neutral pH values to pore water and being minor due to competition with Mg at higher ones.

Direct comparison of Ni distribution obtained after the modelling with its typical distribution in the profiles provided in depth understanding of Ni geochemical behavior during ophiolite weathering as well as revealed the validity of developed reactive transport model. After the detailed study of chemical mechanisms of Ni ore formation and identification of its key controlling parameters this geochemical part was at further step coupled with relevant hydrodynamic system. Such an investigation aimed at proposing a new conceptual mineralization model of Ni redistribution in complex uplifted environments with a specific focus on understanding of distinguished in situ local exceptional Ni enrichments, namely: i) topographically controlled increase of Ni grade in the zone of low relief, as those described by Quesnel et al. (2017), ii) precipitation of Ni-bearing pimelite within the fractures, and iii) formation of concentric Ni-silicate ore under the control of fractures network. The results of the model revealed the critical control of topography and preferential pathways on redistribution and future location of Ni deposits. Remobilized from upper horizons, nickel was found to concentrate in neo-formed silicates in bottom of the saprolite zone. Furthermore, simulations have revealed minor contribution of the laterite horizon (Ni-oxi-hydroxides) into the Ni remobilization. Instead, the remobilized Ni appeared to come mostly from the saprolite due to the redissolution of previously formed Ni-bearing silicates and olivine that still persists in this zone. The latter is explained by the lateral migration of the pH front in the saprolitic formation which triggers dissolution of the silicates with subsequent leaching of mineralizing components (Ni, Mg and Si) in a downslope direction. The lateral infiltration of water with remobilized Ni from areas such as topographic highs to downstream slope areas leads to the formation of richest deposits in this lower part of profile. The manner of redistribution is fully governed by the local topographic features, such as slope, bedrock contact and position of the preferential pathways. It was also established that migration of the mineralizing components from saprolite into the fractures is further enhanced by the dissolution processes that occur within the bedrock horizon. Both of these processes result in a formation of exceptional Ni enrichments within the fractured zone. Moreover, additional investigation of the impact provided by the regular fractures network allowed us to explain the weathering processes that occur within the rocky blocks. Based on the consistency of the

results of modelled mineral paragenesis with in situ observations a new model of concentric ore formation in a fully-saturated media was proposed.

The ore genesis concept tested in this work with aim at explaining metal enrichment in saprolites, laterites and fractured bedrock zone takes into account both the low-temperature 'hydrothermal' history linked to early deformational stages (syntectonic Ni and associated silicates) and the supergene processes. Based on the quantitative analyses of the breccia samples found in faults from bedrocks of New Caledonia as well as on the oxygen isotopic composition of microcrystalline quartz which ends the main stage of formation of Ni-Mg kerolite it was inferred that the great part of Ni-silicate fracture infillings were formed during a series of fluid- assisted fracturing and brecciation process. The defined temperature range of such a formation was suggested to lie within 50 to 90°C which can also be supported by the lack of sepiolite-like minerals in a talc-like and quartz succession. Indeed, as it was demonstrated in Chapter 2 the stability zone of sepiolite minerals disappears at temperatures higher than 50°C, thus, excluding it from the formation. Therefore, the sequence of fracture fillings was interpreted as the result of a hydrothermal system evolution from medium to low temperature under fluctuating fluid pressure. Consequences of these observations are rather important for the inferred models of ore fluid circulations. Such a model complements our understanding of New Caledonian deposits development that, therefore, appears as the result of complex superposition of hydrothermal and supergene processes and can not be interpreted by simple downward migration of a nickel front during the main stage of laterite formation.

Presented in this work models, thus, cover the formation of all the major observed Ni mineralizing distributions in New Caledonia as well as reveal the main keys to understanding both topographic and chemical control of trace elements mobility in ultramafic environment. The latter gives new insights into the Ni distribution in present day profiles and, therefore, may greatly help in mineral prospecting and forecasting the distribution of future resources.

## PERSPECTIVES

Recommendations for future research can be splitted into two parts. First of all, the improvement can be performed at the level of hydrodynamics where Richard's equation should be incorporated for describing processes within the vadose zone. This will allow to reinforce developed 2D model and improve its accuracy by investigation of different position of water table that would have an effect on both darcy velocity field and mass transport of chemical components. In addition, implementation of secondary fractures network into the saprolite

zone would lead to more precise tracing of pH migration front through this part but at the same time requires developing a methodology of implementation the fractures as 1D objects. Indeed, current representation of preferential pathways in 2D greatly restricts their number presented in a profile as it has a drastic effect on calculation time. Such an improvement would also allow incorporation of more realistic fractures network within the bedrock horizon which has been proved to have an important influence on the development of secondary nickel ores. In particular, this can be seen from the Figure 4.1 that demonstrates how different position of the fracture subsequently affects the directions of weathering processes. This point has a direct implications for improvement of mineral prospecting and future construction of Ni distribution maps.

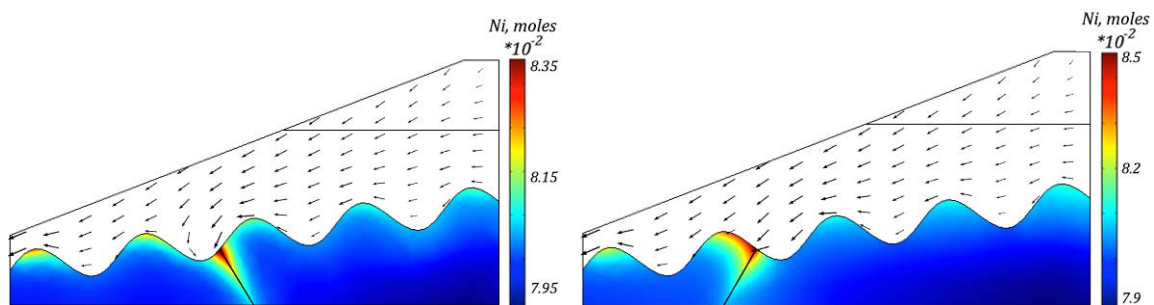


Figure 4.1 – *Development of secondary nickel ores within the bedrock zone after 100 years with two contrasting positions of the fracture*

The second part of perspectives belongs to the development of additional couplings of the presented in this work model with mechanical deformations as well as formation of the preferential pathways. This will allow to carry out an in depth exploration of the proposed per-ascensum concept and to improve the understanding of the existing interactions between the hydro-mechanical phenomena and the mass transport of chemical species, involved in the brecciation and hydraulic fracturing processes observed in New Caledonia. In particular the increase of pressure in veins may lead to the enhanced nickel mobilization process resulting from decrease of solubility of the minerals under the stress. Such a remobilization may partly reconcentrate the veins and provide some valuable insights into the Ni distribution along their length. The parametric study of pressures required to open the fractures can be estimated through the simulation of the hydro-mechanical behavior of peridotite affected by circulations of ascending fluids.

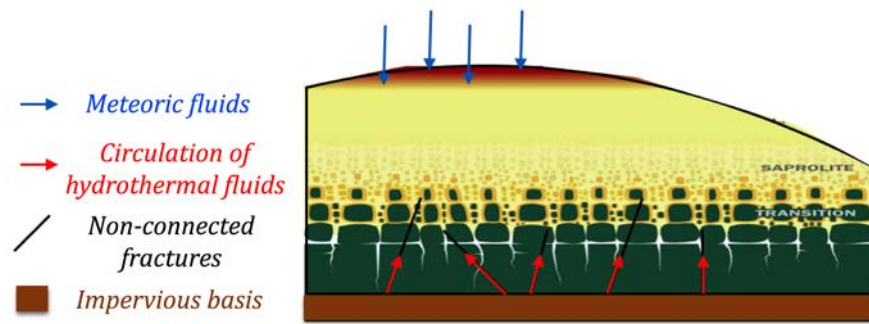


Figure 4.2 – *Conceptual model of fractures reopening due to the circulations of ascending fluids*

The latter can be achieved by using a cohesive zone model of fluid-driven fracture propagation performed in a framework of thesis of Maxime Faivre (Faivre et al., 2016). The representation of proposed model is shown in Figure 4.2. In addition, we propose a thermal coupling that would account for entering of the relatively hot (up to 90°C) hydrothermal fluids into the formation and, thus, will allow to investigate the temperature impact on the paragenesis within the fractures as well as potential elements remobilization and upward mass transfer.



# BIBLIOGRAPHY

- Aghbelagh, Y. B. and Yang, J. (2017). Role of hydrodynamic factors in controlling the formation and location of unconformity-related uranium deposits: insights from reactive-flow modeling. *Hydrogeology Journal*, 25(2):465–486.
- Aitchison, J. C., Clarke, G. L., Meffre, S., and Cluzel, D. (1995). Eocene arc-continent collision in New Caledonia and implications for regional southwest Pacific tectonic evolution. *Geology*, 23(2):161–164.
- Aitchison, J. C., Ireland, T. R., Clarke, G. L., Cluzel, D., Davis, A. M., and Meffre, S. (1998). Regional implications of U/Pb SHRIMP age constraints on the tectonic evolution of New Caledonia. *Tectonophysics*, 299(4):333–343.
- Alcock, R. (1988). The character and resources available to the nickel industry, extractive metallurgy of nickel and cobalt: Proceedings of a symposium, the metallurgical society, cp tyroler and ca landolt ed. In *117th TMS Annual Meeting, Phoenix, Arizona*, pages 67–89.
- Anand, R. R. and Paine, M. (2002). Regolith geology of the Yilgarn Craton, Western Australia: implications for exploration. *Australian Journal of Earth Sciences*, 49(1):3–162.
- Avias, J. (1967). Overthrust structure of the main ultrabasic New Caledonian massives. *Tectonophysics*, 4(4):531–541.
- Avias, J. (1969). Note sur les facteurs contrôlant la genèse et la destruction des gîtes de nickel de la Nouvelle-Calédonie. importance des facteurs hydrologiques et hydrogéologiques. *CR Acad. Sci*, 268:244–246.
- Barry, D. A., Miller, C. T., and Culligan-Hensley, P. J. (1996). Temporal discretisation errors in non-iterative split-operator approaches to solving chemical reaction/groundwater transport models. *Journal of Contaminant Hydrology*, 22(1-2):1–17.
- Brand, N. W., Butt, C. R. M., and Elias, M. (1998). Nickel laterites: Classification and features. *AGSO Journal of Australian Geology and Geophysics*, 17:81–88.

- Brindley, G. (1978). The structure and chemistry of hydrous nickel-containing silicate and aluminate minerals. *Bulletin du BRGM Section II*, 3:233–245.
- Brindley, G. W. and Hang, P. T. (1973). The nature of garnierites-i. structure, chemical compositions and color characteristics. *Clays and Clay Minerals*, 21:27–40.
- Butt, C. R. M. (1975). *Nickel Laterites and Bauxites: A Summary of Observations Made During an Overseas Trip in 1974*. CSIRO Division of Mineralogy, Minerals Research Laboratories.
- Butt, C. R. M. (2007). The weathering of nickel sulfide deposits and implications for geochemical exploration. *Special Publication-Society Of Economic Geologists*, 13:139.
- Butt, C. R. M. and Cluzel, D. (2013). Nickel laterite ore deposits: Weathered serpentinites. *Elements*, 9:123–128.
- Carrayrou, J., Mosé, R., and Behra, P. (2004). Operator-splitting procedures for reactive transport and comparison of mass balance errors. *Journal of Contaminant Hydrology*, 68(3):239–268.
- Cathelineau, M., Caumon, M. C., Massei, F., Brie, D., and Harlaux, M. (2015). Raman spectra of ni–mg kerolite: effect of ni–mg substitution on o–h stretching vibrations. *Journal of Raman Spectroscopy*, 46(10):933–940.
- Cathelineau, M., Myagkiy, A., Quesnel, B., Boiron, M. C., Gautier, P., Boulvais, P., Ulrich, M., Truche, L., Golfier, F., and Drouillet, M. (2016a). Multistage crack seal vein and hydrothermal ni enrichment in serpentinitized ultramafic rocks (koniombo massif, new caledonia). *Mineralium Deposita*, pages 1–16.
- Cathelineau, M., Quesnel, B., Gautier, P., Boulvais, P., Couteau, C., and Drouillet, M. (2016b). Nickel dispersion and enrichment at the bottom of the regolith: formation of pimelite target-like ores in rock block joints (Koniombo Ni deposit, New Caledonia). *Mineralium Deposita*, 51 (2):271–282.
- Chevillotte, V., Chardon, D., Beauvais, A., Maurizot, P., and Colin, F. (2006). Long-term tropical morphogenesis of New Caledonia (Southwest Pacific): Importance of positive epeirogeny and climate change. *Geomorphology*, 81(3):361–375.
- Cluzel, D., Aitchison, J., Clarke, G., Meffre, S., and Picard, C. (1994). Point de vue sur l'évolution tectonique et géodynamique de la Nouvelle-Calédonie. *C. R. Acad. Sci. Paris*, 319:683–688.

- Cluzel, D., Aitchison, J. C., and Picard, C. (2001). Tectonic accretion and underplating of mafic terranes in the late eocene intraoceanic fore-arc of new caledonia (southwest pacific): geodynamic implications. *Tectonophysics*, 340(1):23–59.
- Cluzel, D. and Vigier, B. (2008). Syntectonic mobility of supergene nickel ores of New Caledonia (Southwest Pacific). Evidence from garnierite veins and faulted regolith. *Resource Geology*, 58(2):161–170.
- Collot, J. Y. and Missègue, F. (1986). Extension de la formation des basaltes de la côte ouest et de la zone d’enracinement des péridotites dans le Grand Lagon Nord de la Nouvelle-Calédonie: données géophysiques. *Comptes Rendus de l’Académie des Sciences. Série 2: Mécanique*, 303(16):1437–1442.
- Crawford, A., Meffre, S., and Symonds, P. (2003). 120 to 0 Ma tectonic evolution of the southwest Pacific and analogous geological evolution of the 600 to 220 Ma Tasman Fold Belt System. *Geological Society of America Special Papers*, 372:383–403.
- De Vletter, D. R. (1955). How Cuban Nickel ore was formed: a lesson in laterite genesis. *Engineering and Mining Journal*, 156(10):84–87.
- De Vletter, D. R. (1978). Criteria and problems in estimating global lateritic nickel resources. *Mathematical Geology*, 10(5):533–542.
- Domènech, C., Galí, S., Villanova-de Benavent, C., Soler, J. M., and Proenza, J. A. (2017). Reactive transport model of the formation of oxide-type ni-laterite profiles (punta gorda, moa bay, cuba). *Mineralium Deposita*, pages 1–18.
- Dublet, G. (2013). *Relation entre spéciation et distribution du nickel dans les couvertures d’altération latéritique des roches ultrabasiques de Nouvelle-Calédonie*. PhD thesis, Paris 6.
- Dublet, G., Juillot, F., Morin, G., Fritsch, E., Fandeur, D., and Brown, J. G. (2015). Goethite aging explains Ni depletion in upper units of ultramafic lateritic ores from New Caledonia. *Geochim Cosmochim Acta*, 160:1–15.
- Dublet, G., Juillot, F., Morin, G., Fritsch, E., Fandeur, D., Ona-Nguema, G., and Brown, J. G. (2012). Ni speciation in a New Caledonian lateritic regolith: A quantitative X-ray absorption spectroscopy investigation. *Geochim Cosmochim Acta*, 95:119–133.
- Dzombak, D. A. and Morel, F. M. M. (1990). *Surface Complexation Modeling:Hydrous Ferric Oxide*. New York, John Wiley and Sons.



- Elias, M. (2001). Global laterite resources. *Aust. J. Mining*, 16(174):64–65.
- Faivre, M., Paul, B., Golfier, F., Giot, R., Massin, P., and Colombo, D. (2016). 2d coupled hm-xfem modeling with cohesive zone model and applications to fluid-driven fracture network. *Engineering Fracture Mechanics*, 159:115–143.
- Faust, G. T. (1966). Hydrous nickel-magnesium silicates-garnierite group. *American Mineralogist*, 51(3-4):279.
- Freyssinet, P., Butt, C. R. M., Morris, R. C., and Piantone, P. (2005). Ore-forming processes related to lateritic weathering. *Economic Geology*, 100th Anniversary Volume:681–722.
- Fridleifsson, I. B., Bertani, R., Huenges, E., Lund, J. W., Ragnarsson, A., and Rybach, L. (2008). The possible role and contribution of geothermal energy to the mitigation of climate change. In *IPCC scoping meeting on renewable energy sources, proceedings, Luebeck, Germany*, volume 20, pages 59–80. Citeseer.
- Fritsch, E., Juillot, F., Dublet, G., Fonteneau, L., Fandeur, D., Martin, E., Caner, L., Auzende, A. L., Grauby, O., and Beaufort, D. (2016). An alternative model for the formation of hydrous Mg/Ni layer silicates ("deweylite" / "garnierite") in faulted peridotites of new caledonia: I. texture and mineralogy of a paragenetic succession of silicate infillings. *European Journal of Mineralogy*, 28(2):295–311.
- Golightly, J. P. (1981). Nickeliferous laterite deposits. *Economic Geology*, 75th anniversary volume:710–735.
- Golightly, J. P. (2010). Progress in understading the evolution of nickel laterites. *Society of Economic Geologists Special Publication*, 15:451–485.
- Guilbert, J. M. and Park, C. F. (1986). *The geology of ore deposits. 4th ed.* New York : W.H. Freeman.
- Guillon, J. H. (1975). *Les massifs péridotitiques de Nouvelle-Calédonie: type d'appareil ultrabasique stratiforme de chaîne récente.* Number 76. IRD Editions.
- Hobbs, B. E., Zhang, Y., Ord, A., and Zhao, C. (2000). Application of coupled deformation, fluid flow, thermal and chemical modelling to predictive mineral exploration. *Journal of Geochemical Exploration*, 69:505–509.
- Jacques, D., Simunek, J., Mallants, D., and Van Genuchten, M. T. (2006). Operator-splitting errors in coupled reactive transport codes for transient variably saturated flow and contaminant transport in layered soil profiles. *Journal of contaminant hydrology*, 88(3):197–218.

- Johnson, J., Anderson, G., and Parkhurst, D. (2000). Database from thermo.com.v8.r6.230 prepared at lawrence livermore national laboratory. (Revision: 1.11).
- Klingelhoefer, F., Lafoy, Y., Collot, J., Cosquer, E., Geli, L., Nouze, H., and Vially, R. (2007). Crustal structure of the basin and ridge system west of New Caledonia (southwest Pacific) from wide-angle and reflection seismic data. *Journal of Geophysical Research: Solid Earth*, 112(B11).
- Kroenke, L. W. and Rodda, P. U. (1984). *Cenozoic tectonic development of the Southwest Pacific*. Number 6. Technical Secretariat of CCOP/SOPAC c/o Mineral Resources Department.
- Latham, M. (1986). *Altération et pédogenèse sur roches ultrabasiques en Nouvelle-Calédonie: genèse et évolution des accumulations de fer et de silice en relation avec la formation du modelé*. IRD Editions.
- Leguere, J. (1976). Des corrélations entre la tectonique cassante et l'altération supergène des péridotites de Nouvelle Calédonie. (*PhD Thesis*). University of Montpellier.
- Lelong, F., Tardy, Y., Grandin, G., Trescases, J. J., and Boulange, B. (1976). Pedogenesis, chemical weathering and processes of formation of some supergene ore deposits, in Wolf K.H., ed., supergene and surficial ore deposits. Texture and fabrics. *Handbook of strata-bound and stratiform ore deposits: Amsterdam, Elsevier*, v. 3:93–133.
- Meffre, S. (1995). The development of island arc-related ophiolites and sedimentary sequences in New Caledonia.
- Mudd, G. M. (2009). Nickel sulfide versus laterite: the hard sustainability challenge remains. In *Proc. 48th Annu. Conf. of Metallurgists, Canadian Metallurgical Society, Sudbury, Ontario, Canada, 23–26 August 2009*.
- Myagkiy, A., Truche, L., Cathelineau, M., and Golfier, F. (2017). Revealing the conditions of Ni mineralization in the laterite profiles of New Caledonia: Insights from reactive geochemical transport modelling. *Chemical Geology*, 466:274–284.
- Nahon, D. and Tardy, Y. (1992). The ferruginous laterites. *Regolith exploration geochemistry in tropical and subtropical terrains*, pages 41–55.
- Nardi, A., Idiart, A., Trinchero, P., de Vries, L. M., and Molinero, J. (2014). Interface COMSOL-PHREEQC (iCP), an efficient numerical framework for the solution of coupled multiphysics and geochemistry. *Computers & Geosciences*, 69:10–21.

- Norton, S. A. (1973). Laterite and bauxite formation. *Economic Geology*, 68(3):353–361.
- Nriagu, J. O. (1975). Thermochemical approximation for clay minerals. *American Mineralogist*, 60:834–839.
- Ober, J. A. (2017). Mineral commodity summaries 2017. Technical report, US Geological Survey.
- Orloff, O. (1968). *Etude géologique et géomorphologique des massifs d’ultrabasites: Compris entre Houailou et Canala (Nouvelle-Calédonie)*. (PhD Thesis). Université de Montpellier.
- Paris, J. P. (1981). *Géologie de la Nouvelle-Calédonie*. Number 113-114. BRGM.
- Parkhurst, D. L. and Appelo, C. A. J. (2013). Description of input and examples for PHREEQC version 3-A computer program for speciation, batch-reaction, one-dimensional transport, and inverse geochemical calculations. *U.S. Geological Survey Techniques and Methods*, book 6, chap. A43, 497 p., available only at <http://pubs.usgs.gov/tm/06/a43/>.
- Pelletier, B. (1996). Serpentine in nickel silicate ore from New Caledonia. *Nickel’96: Mineral to market*, pages 197–205.
- Pelletier, B. (2003). Les minerais de nickel de Nouvelle-Calédonie. *GEOLOGUES-PARIS-*, pages 30–37.
- Pokrovsky, O. S. and Schott, J. (2000). Kinetics and mechanism of forsterite dissolution at 25°C and pH from 1 to 12. *Geochim. Cosmochim. Acta*, 64:3313–3325.
- Quesnel, B., Boulvais, P., Gautier, P., Cathelineau, M., Cédric, M. J., Dierick, M., Agrinier, P., and Drouillet, M. (2015). Formation of silica and magnesite veins in the Massif of Peridotite of Koniambo: Geometric and stable isotopes data. *13th SGA Biennial Meeting 2015. Proceedings*, 3:1189–1192.
- Quesnel, B., Boulvais, P., Gautier, P., Cathelineau, M., Cédric, M. J., Dierick, M., Agrinier, P., and Drouillet, M. (2016). Paired stable isotopes (o, c) and clumped isotope thermometry of magnesite and silica veins in the new caledonia peridotite nappe. *Geochimica et Cosmochimica Acta*, 183:234–249.
- Quesnel, B., de Veslud, C. L. C., Boulvais, P., Gautier, P., Cathelineau, M., and Drouillet, M. (2017). 3d modeling of the laterites on top of the Koniambo Massif, New Caledonia: refinement of the per descensum lateritic model for nickel mineralization. *Mineralium Deposita*, pages 1–18.

- Saaltink, M. W., Carrera, J., and Ayora, C. (2001). On the behavior of approaches to simulate reactive transport. *Journal of Contaminant Hydrology*, 48(3):213–235.
- Schellart, W. P., Lister, G. S., and Toy, V. G. (2006). A late cretaceous and cenozoic reconstruction of the southwest pacific region: tectonics controlled by subduction and slab rollback processes. *Earth-Science Reviews*, 76(3):191–233.
- Sevin, B., Ricordel-Prognon, C., Quesnel, F., Cluzel, D., Lesimple, S., and Maurizot, P. (2012). First palaeomagnetic dating of ferricrete in New Caledonia: new insight on the morphogenesis and palaeoweathering of Grande Terre. *Terra Nova*, 24(1):77–85.
- Springer, G. (1974). Compositional and structural variations in garnierites. *The Canadian Mineralogist*, 12(6):381–388.
- Stoessell, R. K. (1988). 25°C and 1 atm dissolution experiments of sepiolite and kerolite. *Geochimica et Cosmochimica Acta*, 52:365–374.
- Thornber, M. R. (1992). The chemical mobility and transport of elements in the weathering environment. *Regolith Exploration Geochemistry in Tropical and Subtropical Terrains. Handbook of Exploration Geochemistry*, 4:79–96.
- Thorne, R. L., Roberts, S., and Herrington, R. (2012). Climate change and the formation of nickel laterite deposits. *Geology*, 40:331–334.
- Trescases, J. J. (1973). Weathering and geochemical behaviour of the elements of ultramafic rocks in New Caledonia. *Bureau Mineral Res Geol Geophys Dep Mineral Energy Canberra Bull*, 141:149–161.
- Trescases, J. J. (1975). *L'évolution géochimique supergène des roches ultrabasiques en zone tropicale: Formation des gisements nickélifères de Nouvelle-Calédonie: Mémoires ORSTOM (Office de la Recherche Scientifique et Technique Outre-Mer)*. PhD thesis.
- Troly, G., Esterle, M., Pelletier, B., and Reibel, W. (1979). Nickel deposits in New Caledonia: some factors influencing their formation. *International Laterite Symposium, New Orleans*,, pages 85–119.
- Ulrich, M. (2010). *Péridotites et serpentinites du complexe ophiolitique de la Nouvelle-Calédonie*. PhD thesis, Université de la Nouvelle-Calédonie et Université de Grenoble.
- Villanova-de-Benavent, C., Proenza, J. A., Galí, S., García-Casco, A., Tauler, E., Lewis, J. F., and Longo, F. (2014). Garnierites and garnierites: Textures, mineralogy and geo-

- chemistry of garnierites in the Falcondo Ni-laterite deposit, Dominican Republic. *Ore Geology Reviews*, 58:91–109.
- Whattam, S. A., Malpas, J., Ali, J. R., and Smith, I. E. (2008). New SW Pacific tectonic model: Cyclical intraoceanic magmatic arc construction and near-coeval emplacement along the Australia-Pacific margin in the Cenozoic. *Geochemistry, Geophysics, Geosystems*, 9(3).
- Windley, B. F., Razafiniparany, A., Razakamanana, T., and Ackermann, D. (1994). Tectonic framework of the precambrian of madagascar and its gondwana connections: a review and reappraisal. *Geologische Rundschau*, 83(3):642–659.
- Zhang, Y., Schaubs, P. M., Zhao, C., Ord, A., Hobbs, B. E., and Barnicoat, A. C. (2008). Fault-related dilation, permeability enhancement, fluid flow and mineral precipitation patterns: numerical models. *Geological Society, London, Special Publications*, 299(1):239–255.

## TITLE

Mineralization of Nickel in saprolitic ore of New Caledonia: Dynamics of metal transfer and modeling of coupled geochemical and hydrodynamic processes

## ABSTRACT

New Caledonia hosts significant lateritic nickel reserves, and presently became the fifth largest Ni producer in the world. These deposits are generally thought to be closely associated with the intense chemical and mechanical weathering of peridotite bedrock that is a principal source of nickel. Thus, the main ore genesis model for Ni ores in New Caledonia is based on a single per descensum model where most elements (Mg, Ni, and Si) are leached from the surface, particularly, during lateritic soil development. Nickel is then concentrated either in the fine-grained laterite where goethite is the main Ni bearer, the so-called 'lateritic ore', or below the laterites, in the saprolite level, where nickel occurs as goethite and several types of Mg-Ni silicates, in particular kerolite. Recent mineralogical and structural observations together with mining data have revealed a lot of different types of heterogeneities associated with the distribution and mineralogy of Ni bearing minerals. Therefore, in depth investigations of Ni mobility, its retardation processes along with its governing chemical and hydrodynamic parameters are of big importance for understanding and subsequent prediction of Ni distribution in profiles of New Caledonia. Such an investigation is an objective of the present work. The concept is based on the development of i) a powerful 1D model with particular emphasis on Ni geochemical behavior during ophiolite weathering, its comparison with in situ observations, and detailed understanding of trace elements mobility, and ii) 2D hydro-geochemical model coupled with complex hydrodynamics, that would additionally provide new insight into the structural control on Ni redistribution and mineralization. While the 1D simulations provide a remarkable result for understanding the chemical features that drive Ni retention processes in a profile, 2D model appears to be a powerful tool for understanding how local Ni-enrichments may form. The results of this model show the reactivation of Ni from upper horizons and its concentration in neo-formed silicates in bottom of the saprolite. The reactivated Ni comes mostly from the saprolite horizon due to the redissolution of previously formed Ni-bearing silicates and still persisting in this olivine zone. Modeling has revealed minor contribution of the laterite horizon (Ni-oxi-hydroxides) into the Ni remobilization. The lateral infiltration of water with remobilized Ni from areas such as topographic highs to downstream slope areas leads to the formation of richest deposits in

this lower part of profile. The manner of redistribution is fully governed by the topographic slopes, orientation and position of the fractures. Presented models appear to be of importance in attempt of explanation of Ni mineralization processes, revealing the main keys to understanding the control of trace elements mobility in ultramafic environment. The latter gives new insights into the Ni distribution in present day profiles and, therefore, may greatly help in mineral prospecting and forecasting the distribution of future resources.

## KEYWORDS

Laterite, Transport Modelling, Hydrodynamics, Kinetics, Water-rock interactions

## TITRE

La minéralisation du nickel dans le minerai saprolitique de Nouvelle-Calédonie: étude de la dynamique de transfert des métaux et modélisation couplée des processus géochimiques et hydrodynamiques.

## RÉSUMÉ

La Nouvelle-Calédonie détient d'importantes réserves de nickel latéritique et est devenue, en 2017, le cinquième producteur mondial de Ni. Ces dépôts sont habituellement considérés comme résultant d'altération latéritique intense de la péridotite, qui constitue la principale source de nickel. Ainsi, le principal modèle conceptuel de la formation des minerais de nickel latéritique en Nouvelle-Calédonie est un modèle *per descensum* où la plupart des éléments (Mg, Ni et Si) ont été lessivés depuis la surface, en particulier lors du développement du sol latéritique. Le nickel est ensuite reprécipité, soit dans la goethite de la latérite fine, soit au niveau de la saprolite, sous forme de goethite et de silicates Mg-Ni, dont des talc-like ou kéro-lite. Les observations minéralogiques et structurales récentes ainsi que les données minières ont cependant mis en évidence de nombreux types d'hétérogénéités dans les concentrations, et la distribution des porteurs de Ni. Comprendre les facteurs la mobilité de cet élément, ses mécanismes de piégeage ainsi que les paramètres chimiques et hydrodynamiques à l'origine de ce piégeage, est essentiel afin de prévoir la distribution du nickel dans les profils latéritiques en Nouvelle-Calédonie, et constitue l'objectif de cette thèse. Ce travail est basé sur le développement (i) d'un modèle 1D s'intéressant en particulier au comportement géochimique du nickel lors de l'altération de l'ophiolite, sa comparaison avec les observations *in situ* et une compréhension détaillée de la mobilité des éléments traces pendant le processus, et

(ii) d'un modèle 2D hydro-géochimique couplé avec l'hydrodynamique complexe des profils latéritiques, améliorant ainsi la connaissance du contrôle structural sur la redistribution et la minéralisation du nickel. Tandis que les simulations 1D permettent de mieux comprendre les aspects chimiques contrôlant les processus de rétention du nickel au sein d'un profil, le modèle 2D se révèle être un outil puissant pour la compréhension de la formation des dépôts locaux les plus riches en nickel. Les résultats du modèle 2D montrent une remobilisation du nickel depuis les horizons supérieurs puis sa reprécipitation sous forme de silicates dans la saprolite. Le nickel remobilisé provient principalement de la zone saprolitique à cause de la dissolution des silicates de nickel formés précédemment ainsi que de l'olivine résiduelle de cette zone. Ce modèle a également révélé que l'horizon latéritique (et en particulier les oxyhydroxydes de nickel) avait un faible impact dans la remobilisation du nickel. L'infiltration latérale de l'eau contenant le nickel dissout issu des formations surincombantes est à l'origine de la formation des zones les plus riches dans les parties inférieures du profil. Cette redistribution est entièrement contrôlée par l'hydrodynamique locale, la topographie ainsi que l'orientation et la position des fractures. Les modèles présentés permettent d'expliquer les processus de formation des minerais de nickel latéritique saprolitique, améliorant ainsi la compréhension des paramètres contrôlant la mobilité des éléments traces dans un environnement ultramafique. Ceci donne une nouvelle clé de distribution du nickel dans les profils actuels, qui peut devenir un outil pour la prospection minière, et la recherche de nouvelles ressources exploitables.

## MOTS-CLÉS

Latérite, Modélisation des Transports, Hydrodynamique, Cinétiques, Interactions Eau-Roche







